공학박사 학위논문

Stochastic Security-Constrained Generation Scheduling with Wind Power Generation based on Dynamic Line Rating

풍력발전을 포함한 계통에서 동적송전용량을 고려한 확률론적 발전계획 수립 방안

2016년 8월

서울대학교 대학원

전기·컴퓨터공학부

박 현 곤

Stochastic Security-Constrained Generation Scheduling with Wind Power Generation based on Dynamic Line Rating

지도 교수 박 종 근

이 논문을 공학박사 학위논문으로 제출함
2016년 6월

서울대학교 대학원
전기·컴퓨터공학부
박 현 곤

박현곤의 공학박사 학위논문을 인준함
2016년 6월

위 원 장 문 승 일 (인)

부위원장 박 종 근 (인)

위 원 윤 용 태 (인)

위 원 김 재 철 (인)

위 원 이 병 준 (인)

Abstract

Stochastic Security—Constrained Generation Scheduling with Wind Power Generation based on Dynamic Line Rating

Hyeongon Park
School of Electrical Engineering and Computer Science
The Graduate School
Seoul National University

The penetration of renewable energy resources is strongly on the rise worldwide. However, difficulty in accurately forecasting the power output, which is an unavoidable and inherent nature of renewable energy resources such as wind power, is expected to cause short-term scarcity events in the operation of power system. Consistently increased loads and limited transmission line resources also impose issues to power system operation, such as transmission congestion, re-dispatch of generators, and wind power spillage. Accordingly, operating reserve requirements must be revised in order to maintain a desired system reliability level in an uncertain operating environment, and the effective employment of network resources must be developed.

This dissertation proposes day-ahead generation scheduling that utilizes demand-side resources (DSR) and wind power generation (WPG) itself as a reserve

for managing increased uncertainty. When optimizing the scheduling process, dynamic line rating (DLR) is employed as a power flow limit for the transmission line rather than static line rating (SLR). However, when incorporating DLR into the generation scheduling problem, it should not be overlooked that new uncertain factors arise with regard to the determined DLR. Hence, a stochastic problem is suggested to properly manage the newly introduced uncertainty that originates from DLR.

The uncertainty in load is expressed using a time series model after analyzing real data in-depth. In order to reflect the tendency of time sequential change in uncertainty, an autoregressive integrated moving average (ARIMA) model is adopted. After the diagnostic check, i.e., Q-Q plot, autocorrelation function (ACF), and partial autocorrelation function (PACF) of residuals, it is confirmed that the model fits the real data well enough. Wind speed forecast error is also designed as a time series model. Because this dissertation aims for security-constrained generation scheduling, equipment failures in power systems are also considered, from which the probability distribution model is determined based on a Markov chain.

All the constraints and objective functions of the generation scheduling problem with DLR are converted into mixed integer linear forms in order to solve the optimization problem by applying mixed integer linear programming (MILP) generally adopted in practical system operation. Heat balance equations related to DLR are expressed as a linear form with reasonably acceptable assumptions. On the other hand, because the common simplified decoupled power flow model cannot be used for various reasons, in this study, relatively less approximated power flow equations are proposed for the generation scheduling problem.

The optimization problem is designed by a two-stage decision model where the objective function is to minimize the expected operating cost that comprises the generation, reserve, DSR, and load-shedding costs. The problem is constrained by individual generation constraints (e.g., ramping up and down, minimum up and down time, and power generation limits) and by system constraints (e.g., system active/reactive power balance, reserve requirement, and transmission flow limit). The expected energy not supplied at each bus is also calculated to assess reliability.

The performance of the proposed generation scheduling was verified using a six-bus system and modified IEEE 118-bus system integrated with wind power units. The simulation results clearly demonstrate that with DLR, a system operator (SO) can significantly reduce the expected operating cost. This advantage stems from the sufficient utilization of the existing transmission line, which leads to an optimal commitment of the generating units and dispatched volume, and efficient use of harvested wind energy. The expected energy that is not served also drastically decreases by means of incorporating DLR. In other words, the proposed method is more reliable in terms of reduced load-shedding amount.

The simulation results also show that additional cost savings can be achieved with demand-side participation and deloaded control of the wind power generator. It can be interpreted that DSR and the reserve from WPG are clearly capable of managing the increased uncertainty due to wind power integration with the desired reliability. The effects are remarkable, especially at higher wind power penetration levels. The computational time, a crucial factor for short-term generation-scheduling tools, increases with multiple scenarios and newly inserted constraints, but it is not excessive owing to the reduced non-linearity of the mathematical formulation.

Keyword: Dynamic Line Rating, Generation Scheduling, Operating Reserve, Wind Power, Uncertainty, Power System Operation

Student Number: 2011-20848

Contents

List of Tables

List of Figures

Chapter 1 Introduction

1.1 Background

Currently, power system load is increasing consistently and a large volume of wind power generation (WPG) has recently been introduced into the power system. Wind energy is expected to provide 15–30% of US generation additions by 2024. When the support of production tax credit for renewable energy is available, the wind market share is expected to increase continuously [1]. Because of the inherent variability and uncertainty of WPG, system operator (SO) has confronted a challenge of operating their systems with managing the resulting increased uncertainty [2]. On the other hand, consistently increased load and WPG with finite transmission line resources also impose concerns to power system operation, namely, transmission congestion.

However, construction of new transmission lines has been affected negatively by many issues recently, such as environmental problems and delayed completion of new lines; accordingly, the efficient utilization of existing network assets without expansion of a new electric network is highly addressed. Traditionally, maximum transmitted power limits have been calculated based on the "worst-case scenario" condition in static line rating (SLR). These conservative ratings lead to inefficient transmission operation, such as wind power spillage, re-dispatch of generators, and load shedding [3-5]. Meanwhile, in order to enhance the capability of the transmission line, SO can determine the transfer limit of transmission lines in real time, called "dynamic line rating (DLR)," "ambient-adjusted rating," or "electrothermal coordination rating." In these approaches, the flow limits are calculated through the heat balance equation where all the parameters in the

equation vary, and do not remain static, under different circumstances.[1] Figure 1.1 shows a comparison between DLR and SLR. As shown in the figure, SLR is calculated seasonally.

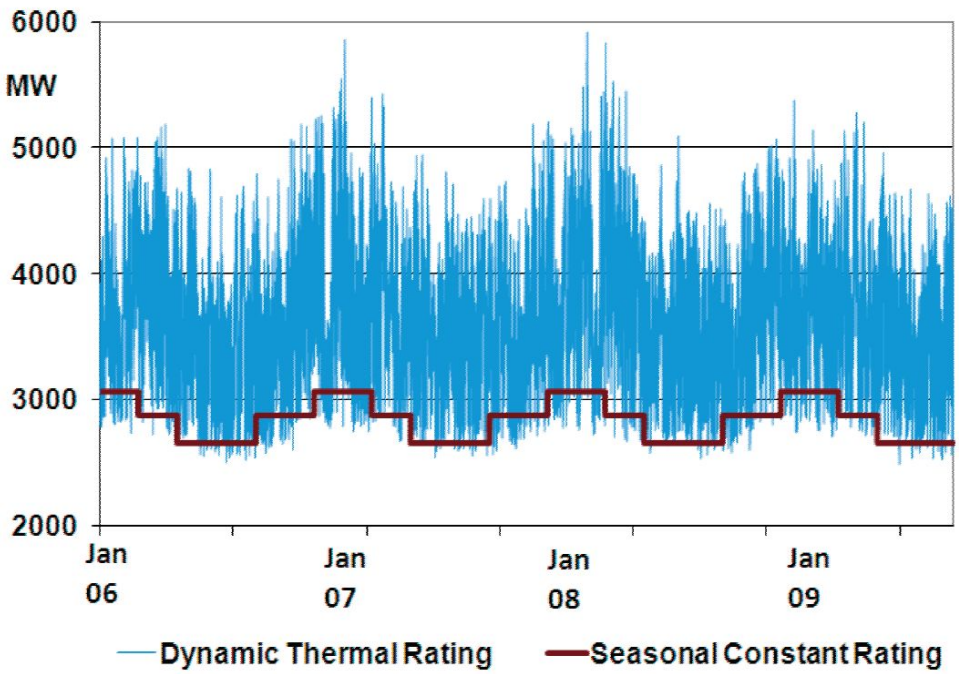

Figure 1.1 DLR and SLR for the Transmission Line [6]

For stable system operation, a power balance must be maintained under all circumstances, and hence SO must adjust the power output of dispatchable (controllable) generating resources in order to match the variations in the net demand. The increased uncertainty due to wind energy integration raised not only the operating cost of maintaining the short-term power balance, but also the frequency of short-term scarcity events caused by ramping capability shortages [7] . The key to solve this problem is generation flexibility, which depends on the

[1] In this dissertation, the first terminology, DLR, is used to place emphasis on a comparison with SLR.

generating resources (flexible resources and energy storage) and/or demand-side resources (DSR). The reserve from WPG in itself is also considered owing to the development of control schemes [8].

In general, SO exploits unit commitment (UC) to determine appropriate on/off states and dispatch for each conventional generating unit in order to meet the predicted system load in consideration of uncertain changes. Generation scheduling[2] is an important optimization task in centralized power system operations in terms of system reliability and economics. The objective of generation scheduling is to minimize the total operating cost of maintaining a power balance over a specific short-term period under given system and unit constraints, such as generator power output limits, system spinning reserve, ramp rate limits, and minimum up and down times of the units. Existing generation scheduling must be revised in order to accommodate wind power uncertainty, which makes power systems highly unpredictable and vulnerable.

[2] Generation scheduling is a comprehensive term that covers UC and economic dispatch. Because the other type of generating resources (i.e., wind power generator and participants of demand-side) are also considered for the schedule in this study, the generation scheduling term is also used.

1.2 Previous Studies

Numerous studies of wind power integration have been conducted for defining, investigating, and understanding uncertainty issues, and for finding UC solutions. Various technical approaches have been suggested to determine the optimal generation scheduling in a wind-integrated power system at an allowable reliability level [9-11].

A fundamental approaches to prepare for the uncertain nature of WPG and load demand is to add reserve requirements in the UC formulation, which is known as deterministic UC. In this straightforward approach, the appropriate required amount of reserve margin should be carefully optimized because it is related to both the reliability and economics. A larger operating reserve margin provides greater ability to accommodate unexpected generator losses or demand increases. However, a larger reserve margin also leads to higher generation costs of the reserve generators. Because operating reserve should be available at all times, an excessive operating reserve margin can lead to significant additional costs.

In addition to the uncertain nature that comes from load and/or generator outages [12-14], much has been written on the effect of WPGs on generation scheduling. In [15] and [16], determination of the reserve amount based on scenarios was suggested for reducing the expected cost with equal system reliability. In [17] , the authors drew a comparison between the cost of providing reserve and the benefit from reducing the expected energy not supplied in order to determine the optimal reserve. Using the deterministic UC method is advantageous in that it is consistent with current operating practices. Nonetheless, intertemporal variations are not explicitly considered in the deterministic UC method, which can lead to either a too conservative or too risky generation schedule [18].

Another approach for managing uncertainty in power systems is stochastic UC. In this method, rather than including the reserve constraint to manage the uncertainty, the optimization problem is solved by considering several scenarios that could capture the uncertainty in the system operation [19]. In [20], a two-stage stochastic UC is suggested where a commitment decision is made at the first stage, whereas the economic dispatch is completed at the second stage. As verified in [21] and [22], stochastic UC has the merit in the aspect of the operating cost compared with that of deterministic UC. However, because the computational time becomes burdensome with the stochastic approach, a scenario reduction technique is typically utilized, which means that a limited number of scenarios are chosen to represent the entire generated scenarios in order to achieve computational tractability.

The aforementioned techniques consider only generation and exclude DSR or the reserve from deloaded control of WPG. In [23] and [24], the interruptible load that is one of the representative DSRs was considered in the UC problem. Although the effect of interruptible load on the reserve was directly investigated in [23], the authors in [24] proposed a method for indirectly determining the optimal required amount of interruptible load. Modeling of WPG participation in automatic generation control (AGC) was illustrated in [25], and it was shown that deloading the wind power for the reserve could be used effectively in the generation scheduling stage in [26] and [27].

When great attention has been shown to the question of the supply and demand balance problem imposed by WPG uncertainty, there have been several studies that have indicated the integration of WPG in consideration of DLR. [6] analyzed the impact of DLR when WPG is integrated through sensitivity analysis

and constraint cost. In [28], the advantages of using DLR with WPG were investigated; in particular, the study showed that the wasted production of WPG could be reduced if DLR were considered. Electrothermal coordination for the power system operation has been suggested with theoretical basis and implementation scheme [29] and numerical studies [30]. The integration of DLR in UC was proposed and security analysis was conducted in [31], but the study did not consider the effect of WPG on DLR and neglect the uncertainty of DLR determination.

1.3 Dissertation Objective

As mentioned before, the majority of studies concerned with generation scheduling have focused on finding the optimal reserve that is supposed to manage the uncertainties in the power system. In recent years, there have been considerable efforts to utilize newly introduced reserve resources, such as DSR and/or energy storage. However, few have attempted to treat deloaded wind power as a reserve, even though installed capacity of wind power has continuously increased in the power system and it has become more important to secure a sufficient reserve. The correlation of WPG as reserve with DLR is vastly underexplored.

Prior studies have performed DLR with a view toward WPG integration, but have not focused on the generation scheduling of conventional generators. Although there has been scant research on UC with DLR, no definitive interpretation has been given to the uncertainty that would arise when DLR is applied to the scheduling problem. In other words, the factors that establish DLR should not be neglected in the scheduling process because they undoubtedly have uncertainty as well, similar to WPG or load forecast.

In this dissertation, a generation scheduling method is investigated considering wind power as a reserve resource along with DSR. In order to reflect the uncertainty in power systems, sophisticatedly generated scenarios that use time series analysis are placed into the optimization problem. For a network security-constrained scheduling solution, equipment-failure scenarios are also reflected in the problem. A new stochastic generation scheduling method that could manage its uncertainty is proposed to compensate for the problems related to the uncertainty of DLR. The applicability of the proposed method is verified with the case study that uses a simple six-bus system and modified IEEE 118-bus system.

1.4 Dissertation Overview

The remainder of this dissertation is organized as follows. Chapter 2 introduces DLR in detail. The factors that determine the power flow limit of the transmission line are: 1) thermal constraint, 2) voltage constraint, and 3) stability constraint. Each of the factors is described in a subchapter. The heat balance equation that governs the thermal constraint of the power flow limit is analyzed, and linearization of the equation is discussed in the end of Chapter 2.

Chapter 3 elaborates the probabilistic modeling of uncertainty in load and wind speed forecasts evaluated via time series analysis. A model based on a Markov chain is used to represent the failure of the generator and transmission line.

Chapter 4 describes generation scheduling that considers DLR. The general formulation of stochastic UC is introduced and compared with the proposed method. The method to approximate the power flow equations in order to readily combine this with the existing generation scheduling is provided in the subsection. Spinning reserve procurement methods from wind power and DSR are also included. In the last part of Chapter 4, the mathematical formulation of stochastic security-constrained generation scheduling is provided and discussed.

Chapter 5 presents a case study for the proposed method. First, a simple six-bus system is used to scrutinize the numerical results of generation scheduling when the proposed method is applied to the optimization problem. In the interest of testing the scalability of this dissertation's approach, the generation scheduling problem is also performed in the modified IEEE 118-bus system.

Chapter 6 summarizes the conclusion, and future extensions related to this dissertation are provided.

Chapter 2 Dynamic Line Rating

In the day-ahead of an operating day, SO should determine the generation scheduling; in other words, SO should indicate when the generators need to turn on/off, or how much electricity to provide at each hour in advance. In this procedure, system constraints (e.g., the power balance between supply and demand, system spinning reserve, and power flow limit) and each generating unit constraint (e.g., generator power output, ramp rate, and minimum up and down times) should be satisfied.

In this chapter, a comprehensive explanation associated with the power flow limit is provided.[3] The heat balance equation is crucial for calculating the power transfer limit, and elements of the equation, such as 1) convective heat loss, 2) radiated heat loss, 3) rate of solar heat gain, 4) conductor electrical resistance, and 5) Joule heating, are sequentially described. The linearization method for the heat balance equation is included at the end of the chapter. This linearization is essential for solving the optimization problem of a large-scale power system.

2.1 Power Flow Limit for Transmission Line

Transmitting power from one point to another is restricted by various limits. The first is the stability limit, which is related to the loss of synchronism between the machines in the power system. The second is the voltage limit, which is linked to the dielectric limit. The last is the thermal limit, which is how much power can be transferred within the allowable conductor temperature.

[3] The other constraints are described in the Chapter 4.

2.1.1 Stability Constraint on Power Flow Limit

It is said that the power system is transient stable for the fault if the system possesses the inherent strength to withstand a severe disturbance and eventually reach its prefault condition [32]. Figure 2.1 illustrates a system considered as transient stable (case I) and transient unstable (case II).

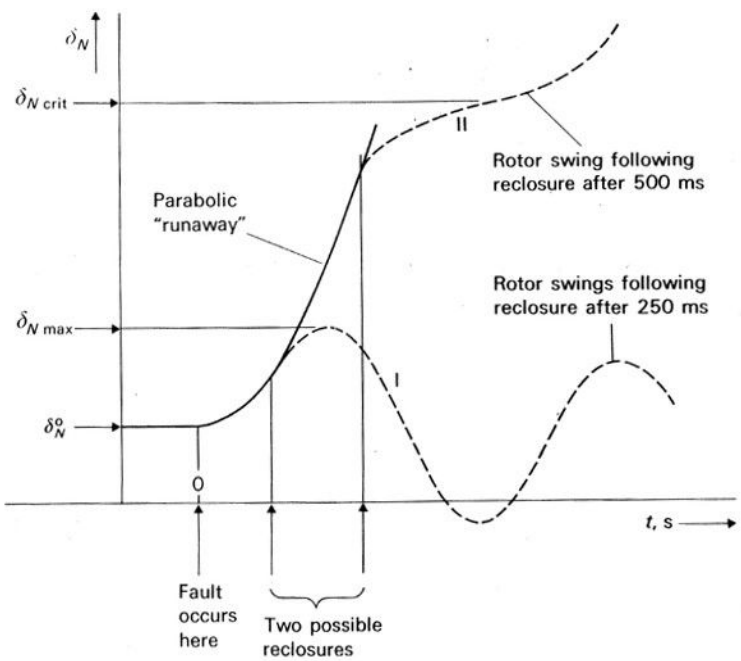

Figure 2.1 Power angle graph after generation trip and machine reclosure [32]

On the other hand, compared with transient stability, a small signal stability is defined as the ability of the system to maintain its synchronism when subjected to a small disturbance [33]. Here, the small disturbances imply the load variations or small changes that result from the operation of switching devices. One of the most important equation in the power system dynamics is the swing equation:

$$P_T - P_G = \frac{H}{\pi f^0}\frac{d^2\delta}{dt^2} \tag{2-1}$$

where P_T and P_G represent the turbine power and generator bus power, respectively, and δ indicates the power angle. H represents the inertia constant defined as system kinetic energy W_{kin}^0 divided by generator rating P_r. When conducting stability analysis, it is interesting to note that the swing equation is not only affected by an operating point (P_T^0, P_G^0, δ^0), but also by the impedance of the transmission line incorporated in the P_G term. Hence, the maximum allowable power flow limit with regard to stability constraint is associated with the line length. This is not the case for a thermal constraint, which is considered in a later subchapter 2.1.3.

2.1.2 Voltage Constraint on Power Flow Limit

Because the two most critical limits that restrict the power flow limit are thermal effect and stability [34], the voltage limit is briefly described in this dissertation. In order to ensure a secure power system operation, neither a high or low voltage level, compared with the nominal values, is acceptable. High voltage that exceeds the dielectric limit can result in insulation failure, which could trigger a short circuit. At the same time, a low voltage level should also be avoided because it requires a more reactive power supply that could incur current increases and resultant increased losses. In other words, the voltage deviation is managed within a plus/minus (±) specific predetermined value.

2.1.3 Thermal Constraint on Power Flow Limit

The last limitation imposed on the transmission line is the thermal constraint. The temperature of the conductors is increased when there are more current flows along the line. A related equation is I^2R, known as Joule, resistive, or ohmic heating. If heat I^2R is increased, the temperature of the conductors is also increased, which could lead to sag of the transmission line; in other words, the clearance between the transmission line and ground is reduced. Hence, an excessive temperature rise should be restrained, and this is expressed as the thermal constraint on the power flow limit.

In addition to the amount of current in the line, a characteristic of the conductor (e.g., material or diameter of the conductor) and the ambient condition of the line (e.g., speed of air at conductor, solar radiation, air temperature, etcetera) also affect the thermal limit. The effect of these and the current-temperature relationship is formulated through the heat balance equation, which is the subject of the next subchapter.

The heat balance with regard to the transmission line is sustained in every segment of the line. Accordingly, the entire length of the line is not the factor that determines the thermal limit of the line. Figure 2.2 shows a comparison of the stability and thermal limits on power flow. For the short lines, the thermal limit is strict, whereas the stability limit dominates for the long lines [34]. In general, SO of most countries considers the thermal limit as a constant line rating during each season or even the entire year, namely, SLR. The thermal limit is calculated based on harsh conditions, which is a fairly conservative approach, and it causes excessive equipment investment and underutilized installed facilities.

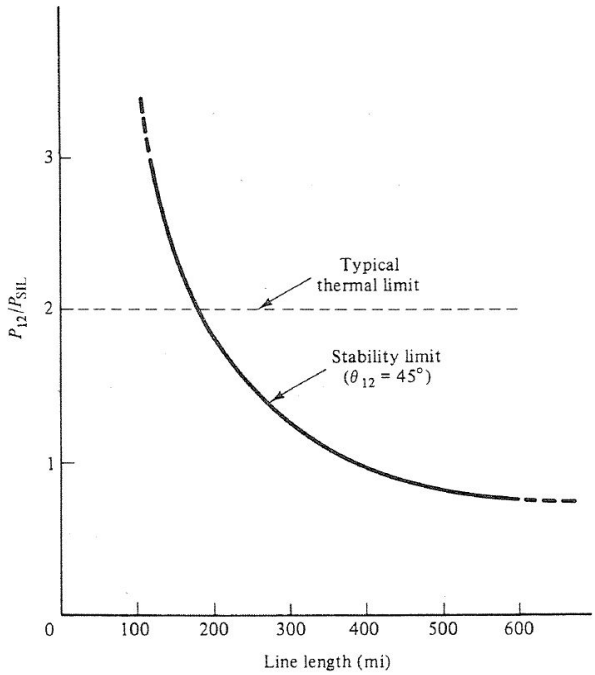

Figure 2.2 Stability limit and typical thermal limit on transmission line [34]

In this study, the thermal limit is determined on an hourly forecasted value instead of the worst-case scenario in order to take advantage of the DLR, rather than the SLR. Means to determine the thermal limit and resultant constraint changes in the optimization formulation are discussed in the following subchapter and Chapter 4, respectively.

2.2 Heat Balance Equation

The temperature of the transmission line is related to the electrical current and ambient weather conditions, and the representative formulation is the heat balance equation. The relevant documents were proposed by IEEE (Std. 738, 2012) [35] and CIGRE (Technical Brochure 601, 2014) [36]. Although several studies, such as [37] and [38], supported the fact that both standards are closely analogous, the formulas discussed in the IEEE standard are used in this dissertation.

Two types of heat balance equations are derived, and each is applied to the "Non-steady-state Case:"

$$q_c + q_r + mC_p \frac{dT_{avg}}{dt} = I^2 R(T_{avg}) + q_s \tag{2-2}$$

and "Steady-State Case:"

$$q_c + q_r = I^2 R(T_{avg}) + q_s \tag{2-3}$$

where q_c and q_r represent the convective and radiated heat loss rates, respectively. $I^2 R(T_{avg})$ is Joule heating, and the heat gain rate from the sun is expressed as q_s. The equation for the "Non-steady-state case" has an additional term that represents the conductor heat capacity mC_p times the first order differential equation. This term indicates how much of the conductor temperature deviation goes up/down with time. Worth noting is the net value of the heating and cooling terms; in other words, the sum of heat gain terms (q_c, q_r) minus the sum of heat loss terms (I^2R, q_s) governs the direction of the temperature variation. This can be apparently shown with a rearrangement of equation (2-3).

$$mC_p \frac{dT_{avg}}{dt} = I^2 R(T_{avg}) + q_s - q_c - q_r \quad (2\text{-}4)$$

However, in this dissertation, the heat balance equation for the steady-state case, rather than non-steady-state case, is used for the following reasons:

1) Generation scheduling for the conventional generators and WPG is conducted for every hour of the next operating day. Meanwhile, if the time constant of the solution for the differential equation is much shorter than one hour, it seems quite reasonable to assume that all the variables "settle down" to the desired steady state at every hour. In the worst weather condition, this is the same condition in the SLR calculation: the time constant is equal to 14 min when 848A of the electric current (the exact allowable value of SLR) is injected as a step input in the ACSR transmission line [39]. In other words, the temperature goes up to 63.2% of the final value within 14 min. This could also be interpreted as the temperature going down to 36.8% of the final value if the heat loss is greater than the heat gain. Because 42 min are required to reach 95% of the final value, in this work, it is assumed that 1 hour is sufficient time for the temperature to settle down to the new steady state value.
2) There are concerns with regard to excessive temperatures that could exceed the thermal limit during the intra-hour condition if the dynamic term in the heat balance equation is neglected during generation scheduling [31]. However, similar to the way in which deploying a reserve capacity could manage the intra-hour variation in supply and demand [22, 40, 41], the extreme case could be covered by the margin implicitly

acquired when generation scheduling is performed. The reason for the belief that the margin, which is the counterpart of the reserve, could be secured is based on the generated scenarios that result after consideration of the factors in the heat balance equation.

In the followings, heat balance equation elements are described sequentially. In order to calculate the convective heat loss, the Reynolds number should be determined as follows:

$$N_{\mathrm{Re}} = \frac{D_0 \cdot \rho_f \cdot s_t}{\mu_f} \tag{2-5}$$

D_0 is outside the conductor diameter, and ρ_f and μ_f represent the air density and absolute viscosity, respectively. s_t is the wind velocity that drastically changes for different situations. The conductor diameter does not vary based on changed circumstances because it is a fixed value; however, air density and viscosity can fluctuate mostly based on the temperature.

In general, convective heat loss q_c is divided into two categories: forced and natural convection. As is obvious from the name, forced convection occurs when the wind takes the heated air away from the conductor. To calculate the forced convection heat loss, the larger value between q_{c1} and q_{c2} is chosen. Each of the values can be calculated as follows:

$$q_{c1} = K_{angle} \cdot [1.01 + 1.35 \cdot N_{\mathrm{Re}}^{0.52}] \cdot k_f \cdot (T_c - T_a) \tag{2-6a}$$

$$q_{c2} = 0.754 \cdot K_{angle} \cdot N_{\mathrm{Re}}^{0.6} \cdot k_f \cdot (T_c - T_a) \tag{2-6b}$$

The angle between the transmission and wind direction affects convection

heat loss. This factor is represented as K_{angle}, which is included in equations (2-6a) and (2-6b), The coefficient of thermal conductivity of air k_f is also multiplied by the difference of the conductor temperature (T_c) and ambient air temperature (T_a). A detailed method for calculating the figure of K_{angle}, ρ_f, μ_f, and k_f is included in the Appendix A.

On the other hand, natural convection is applied when there is zero speed of air stream at the conductor. The related formula is given as

$$q_{cn} = 3.645 \cdot \rho_f^{0.5} \cdot D_0^{0.75} \cdot (T_c - T_a)^{1.25} \tag{2-7}$$

When determining convective heat loss, the larger value between forced convective heat and natural convection is used. It should be certainly indicated that equation (2-7) is nonlinear with the conductor temperature term (T_s), whereas equations (2-6) are linear functions of the conductor temperature.

The second heat loss factor in the heat balance equation is radiated heat loss rate, represented as q_r. Thermal radiation means the transfer of energy by the emission of electromagnetic waves that could propagate through the vacuum of space. When there is a difference in temperature between the conductor and ambient air, heat transfer in the form of radiation must occur. The quantity of radiated heat loss can be calculated as the following equation:

$$q_r = 17.8 \cdot D_0 \cdot \varepsilon \cdot \left[\left(\frac{T_c + 273}{100} \right)^4 - \left(\frac{T_a + 273}{100} \right)^4 \right] \tag{2-8}$$

The effect of the surface condition of the transmission line is symbolized as ε, called “emissivity.” Radiated heat loss is governed by the Stefan-Boltzmann law: accordingly, the energy radiated is related to the fourth power of the

temperature. Because this nonlinearity burdens the computational time, it is necessary to linearize the formula, and the related method is to be precisely delineated in the next subchapter.

The first component to be introduced that raises the temperature is solar heat gain. The amount of energy originated from the sun is subject to the heat flux density of total solar and sky radiation (Q_s), elevation of the sun's position, and effective incidence angle of the sun's rays (θ'). The surroundings of the transmission line also impact the solar heat gain, which could be represented as a combination of the projected area of the conductor (A') and absorptivity (α). If we consider the heat flux density value corrected for the elevation (Q_{se}), the corresponding solar heat gain could be determined as follows:

$$q_s = \alpha \cdot Q_{se} \cdot \sin(\theta') \cdot A' \tag{2-9}$$

The relationship between Q_{se} and Q_s, and how to compute the value of each component, is discussed in the Appendix A. As counterpoint to all other heat/loss components of the heat balance equation, the solar heat gain bears no relation to the conductor temperature itself. That is to say, the solar heat gain is a predetermined value, not a resultant value of the generation scheduling optimization problem. Figure 2.3 shows the average measured hourly solar radiation with respect to a different month [42].

In the heat balance equation, Joule heating $I^2R(T_{avg})$ is the only component that contains the electrical current term. Similar to Joule heating, the aforementioned conductor temperature variable is indissolubly linked to the electrical variable. Conductor resistance, represented by $R(T_{avg})$, is affected by

temperature.

$$R(T_{avg}) = \left[\frac{R(T_{high}) - R(T_{low})}{T_{high} - T_{low}}\right] \cdot (T_{avg} - T_{low}) + R(T_{low}) \qquad (2\text{-}10)$$

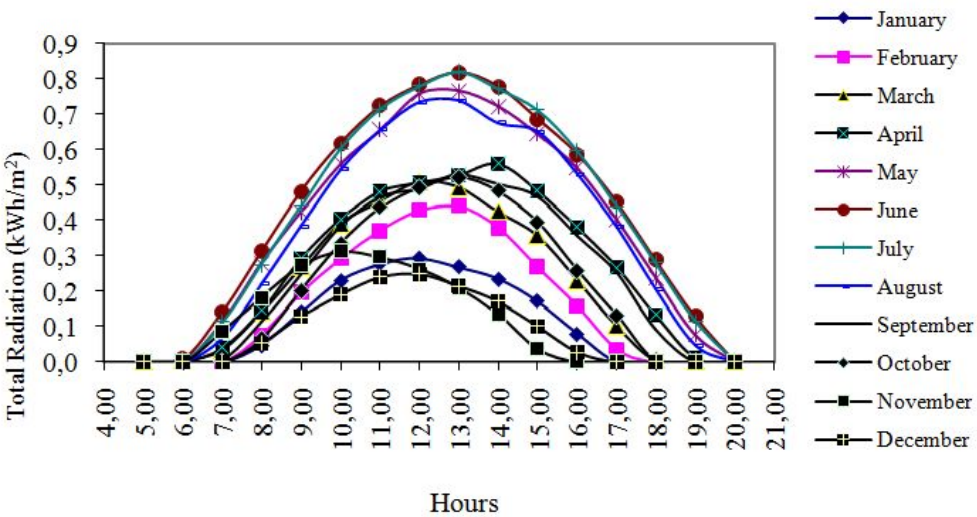

Figure 2.3 Average hourly solar radiation (measured data) [42]

Conductor resistivity tends to increase linearly as the conductor temperature increases. However, in this dissertation, it is assumed that resistance is a fixed value that does not vary with temperature, whose value is calculated at the maximum allowable temperature. Although this assumption provides conservative results when the temperature of the transmission line is below the maximum temperature limit, the very same conclusion could be drawn when the transmission is operated close to its acceptable thermal limit.

Although resistance is assumed to be a constant, Joule heating is still a quadratic equation. Since the generation scheduling problem is supposed to be resolved by mixed integer linear programming (MILP) in this study, the quadratic form should be linearized. This is discussed in the next subchapter.

2.3 Linearization of Heat Balance Equation

Among the components included in the heat balance equation, heat loss from convection (q_c), radiation (q_r), and Joule heating ($I^2R(T_{\max})$) need to be linearized, as mentioned before. The larger value between forced and natural convection is elected to be the convection heat loss. The forced convection that can be estimated with equations (2-6a) and (2-6b) is already expressed in linear form. Only the natural heat loss equation needs to be linearized, and this can be done by setting apart linear term of the difference between conductor and ambient temperature from the original term of which the difference is raised to the five-fourths power. The remainder term, that is, the difference raised to the one-fourth power, can be substituted with predetermined representation value. Then each of the equations is expressed as the product of a multiplier and the difference term. The most dominating convective heat loss can be easily determined by comparing multipliers of each equations, because the largest value of multipliers will give the largest convective heat loss.

Radiation heat loss and Joule heating terms are similarly modified into the linear function. Because the MILP technique is adopted for solving the generation scheduling problem, the integer variable can also be used in the equation modification. In other words, the nonlinear function can be linearized using both continuous and discrete binary variables. The newly introduced binary variables allow the nonlinear function to be separated into several Heaviside step functions. The approach that employs binary variables has the merits of a reduced number of constraints and related constants calculation; however, the computational time drastically increases, especially when a large number of step functions are provided

for accurate approximation. On the other hand, using only continuous variables to construct a piecewise linear function generates more constraints, but its computational complexity increments are not as severe as those of the formal function. Because the advantages of using only continuous variables outweigh the disadvantages in this study setting, the heat loss function (equation (2-9)) and Joule heating are linearized using piecewise linearization, as shown in Figure 2.4.

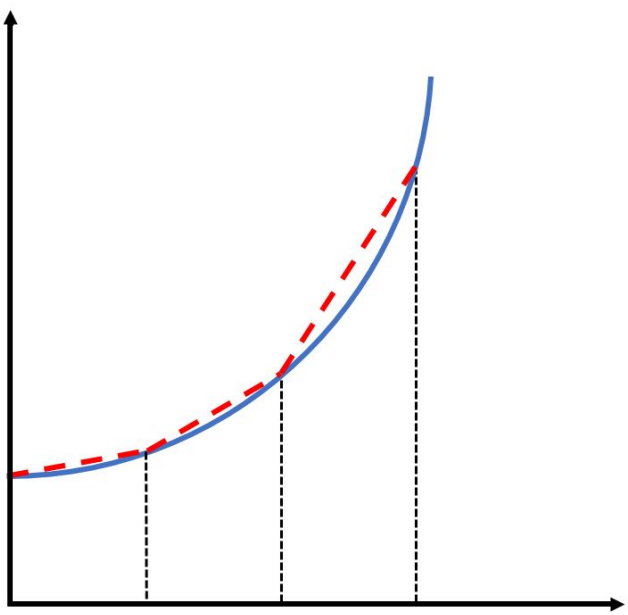

Figure 2.4 Piecewise linearization of nonlinear function

Chapter 3 Uncertainty Model

The expected operating cost that considers uncertainties is computed with a given probabilistic distribution function for forecasting errors. Although the forecasted amount of wind power output and load are treated as given in the generation scheduling problem, uncertainty modeling is required when assessing the expected operating cost. When generating the scenarios that will be used as an input to the stochastic UC problem, the uncertainty modeling has a noticeable impact on the results in several ways, such as commitment states of the conventional generators, dispatch volume of each turned-on generator, and operating point of wind power.

In this dissertation, three types of uncertainty are considered: the first and second are related to the load and WPG forecasts, respectively. The last represents equipment failure, such as generator outages and transmission line faults. Two uncertainty sources, load and wind generation, are modeled via the time series analysis. Load forecast uncertainty is represented with the autoregressive integrated moving average (ARIMA) model. The general ARIMA (p, d, and q) model can be formulated as a model with an autoregressive order p and moving average (MA) term q. Parameter d is the degree of differencing. Because the difference parameter is redundant in the wind uncertainty modeling, the ARMA model is applied instead of ARIMA. The reason for adopting the time series model is that it can consider the tendency of the time sequential change.

The probability distribution model of the generator and transmission outages are calculated using the forced outage rate (FOR) per equipment, which is defined as the probability of the unit being unavailable.

3.1 Load Forecast

For dynamic load L_t modeling, the following equation, where FL_t is the forecasted load and UL_t represents uncertainty in the load, is used in the mathematic formulation:

$$L_t = FL_t + UL_t \tag{3-1}$$

Hourly forecasted load value FL_t is a constant that does not vary based on the scenarios. The deviation between actual and forecasted load, namely uncertainty in load UL_t, is designed by the ARIMA model after analyzing the historical time series data [43].

In order to determine the appropriate model that represents uncertainty in the load, the Box-Jenkins model selection methodology is used, where the entire procedure is shown as a flowchart in Figure 3.1. As shown in the diagram, the model selection is terminated after confirming that the obtained model is valid. Each step is discussed in more detail below.

Step 1. Load data

Before analyzing the time series data, uncertainty in load UL_t is set apart from the Pennsylvania-New Jersey-Maryland Interconnection (PJM) actual load data.[4] There is a difference in the peak level of the load data, whether it is a weekday, weekend, or holiday. However, because there is not much difference between the patterns of uncertainty in the load, all the raw data are loaded without sorting. The uncertainty in load according to time is plotted in Figure 3.2.

[4] The metered load data investigated in this study is for the period January–February 2016.

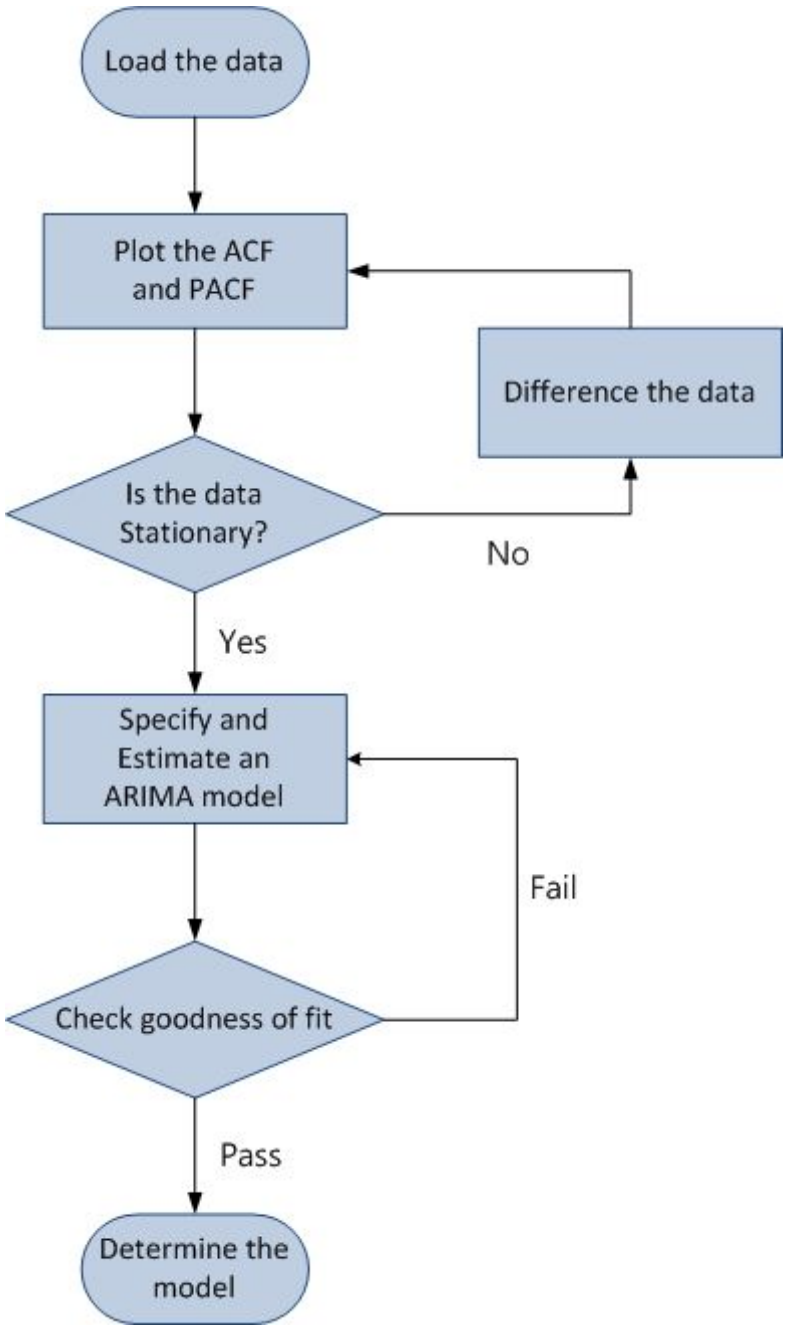

Figure 3.1 Flowchart for ARIMA model selection

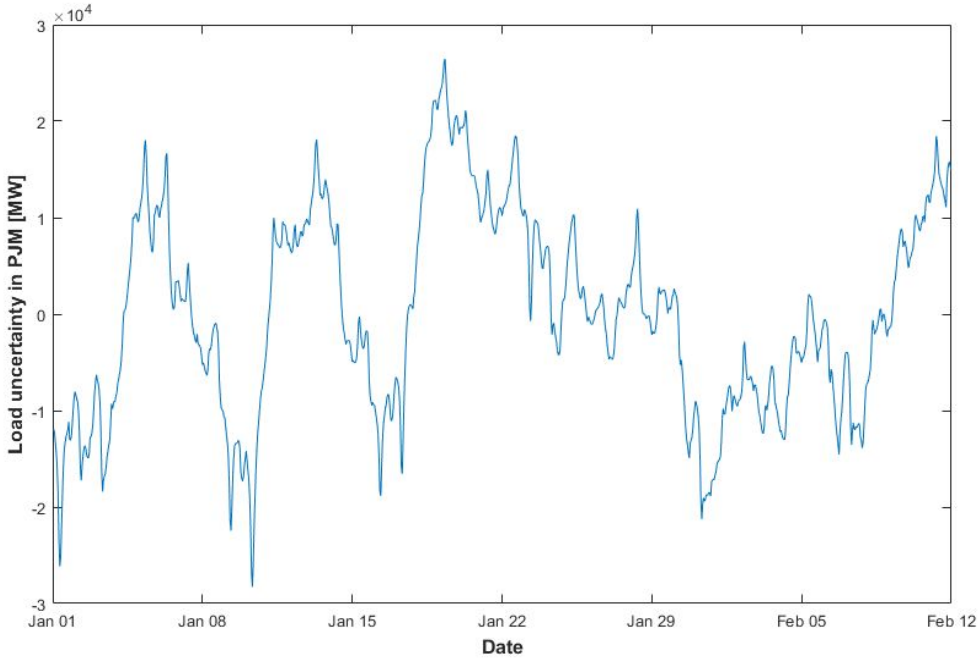

Figure 3.2 Load uncertainty in PJM

Step 2. Plot autocorrelation function and partial autocorrelation function for data

Identifying whether the uncertainty data is stationary or nonstationary using only the plot in the time domain is difficult. Hence, the autocorrelation function (ACF) and partial autocorrelation function (PACF) are used. ACF yields a clue with regard to the dependence order when the analyzed data have a MA component. More specifically, ACF for the MA q model has a nonzero value for lags that are less than or equal to q, whereas ACF is zero for the range of lags that is greater than q. The characteristics of PACF are similar to those of ACF, but PACF contains information on auto-regressive (AR) models. Displaying the ACF and PCAF for the data found in the previous step can indicate whether the process is stationary. The results of the plot are shown in Figure 3.3.

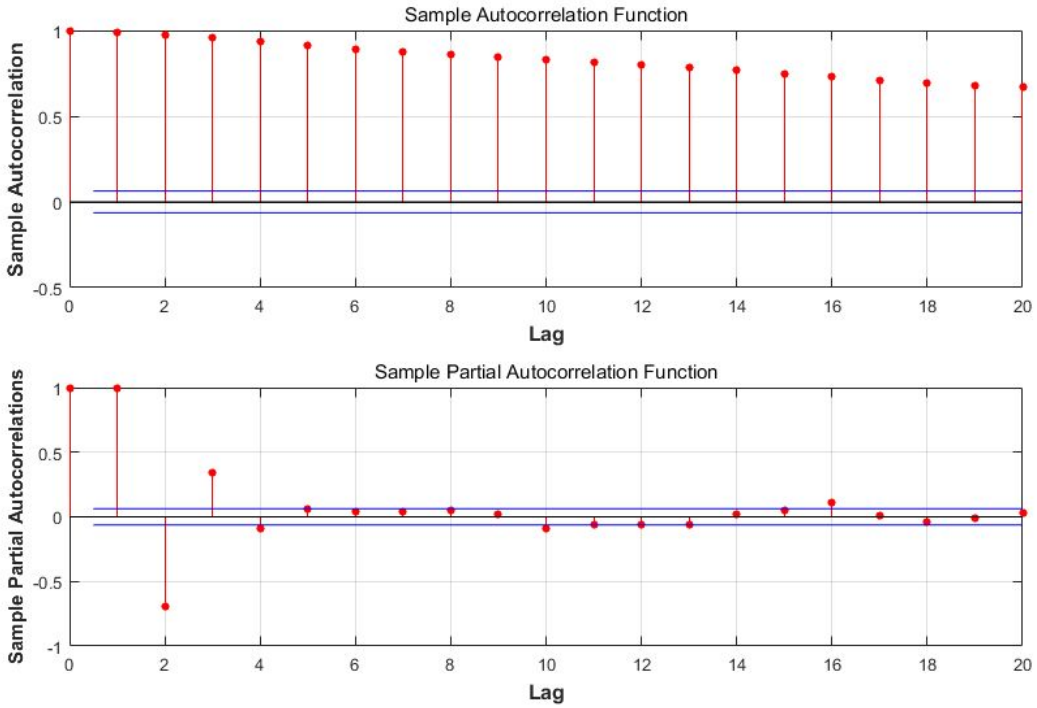

Figure 3.3 ACF and PACF for load uncertainty data

Step 3. Differenced data

It can be interpreted that load uncertainty is not stationary by noting that the sample ACF is clearly linearly decayed. Generating a stationary process, rather than a nonstationary process, is required before ARMA model estimation. In order to lead to a stationary process, a first difference of the data has been taken in this dissertation.[5] The differenced data is defined as y_t in the following equations:

$$UL_t = UL_{t-1} + y_t \tag{3-2}$$

$$\nabla UL_t = UL_t - UL_{t-1} = y_t \tag{3-3}$$

The next step is to check that y_t can satisfy the stationary property. This can

[5] Second differencing, or logarithm of raw data also can be used to transform nonstationary signals to stationary.

also be confirmed through ACF and PACF as implemented in step 2.

Step 4. Plot ACF and PACF of differenced data

Figure 3.4 shows the raw data of uncertainty in load UL_t (upper figure) and differenced data y_t (bottom figure) for the comparison of stationariness. The differenced series appears comparably stationary. ACF and PACF of the differenced are plotted to further demonstrate a stationary process, as shown in Figure 3.5. As expected, ACF of the differenced data declines exponentially.

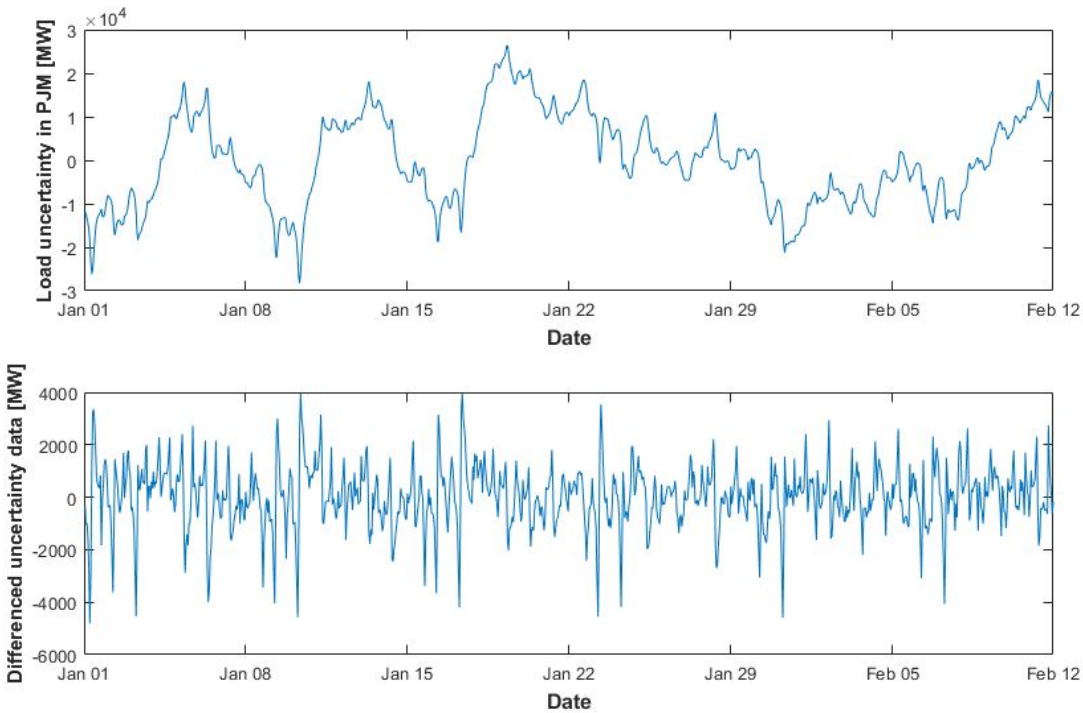

Figure 3.4 Raw data versus differenced data of load uncertainty

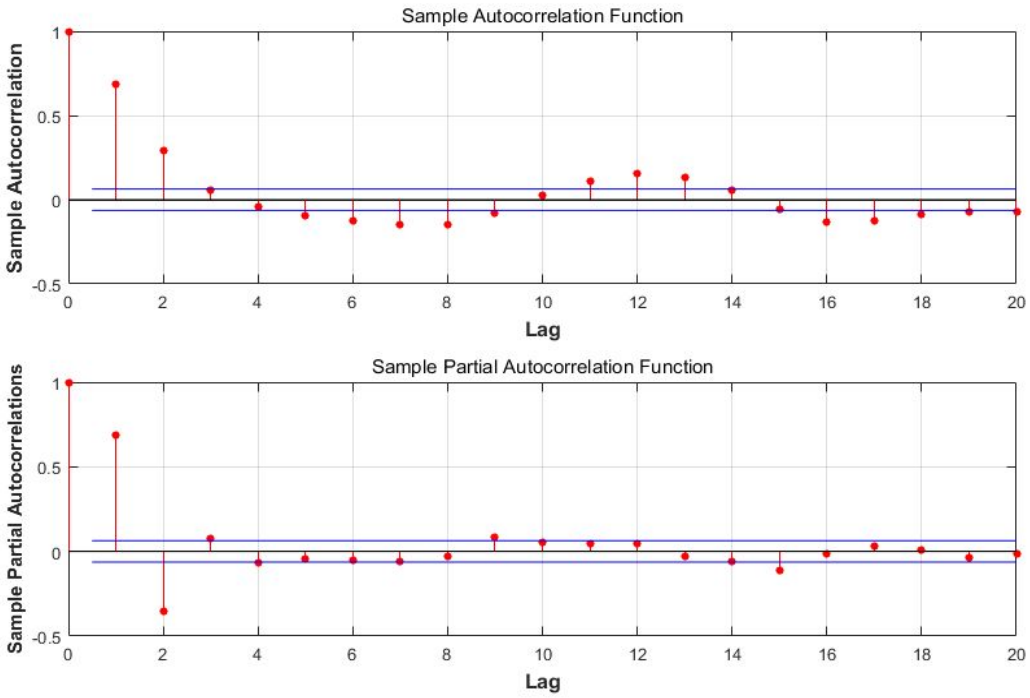

Figure 3.5 ACF and PACF of differenced data

Step 5. Specify and estimate an ARIMA model

Although ACF for the adjusted data tails off, it appears that PACF cuts off after lag 2. In the PACF graph, with the exception of the first three points, the points fall within the threshold limits (dashed line that corresponds to 95% confidence). In other words, it can be deduced that the model follows a second degree autoregressive model, or AR(2) model, according to the summary in Table 3.1 [43]. Now that the first differencing process has been performed, and PACF for the differenced data follows the behavior of the AR(2) model, uncertainty in load UL_t can be specified as the integrated ARMA or ARIMA (2, 1, 0) model. The estimation process of unknown parameters can be performed under the assumption that the time series data follows the ARIMA model. Table 3.2 is the consequence of

the model estimation. As revealed in Table 3.2, both AR coefficients are significant at the 0.05 significance level. The ARIMA (2, 1, 0) model with estimated coefficients can be written as the equation below, where innovation distribution ε_t is assumed to be a Gaussian function with constant variance.

$$\begin{aligned} y_t &= \phi_1 y_{t-1} + \phi_2 y_{t-2} + \varepsilon_t + \mu \\ &= 0.9342 y_{t-1} - 0.3558 y_{t-2} + \varepsilon_t + 11.1705 \end{aligned} \tag{3-4}$$

Table 3.1 Behavior of ACF and PACF

	AR (p)	MA (q)	ARMA (p, q)
ACF	Tails off (Exponentially decay)	Cuts off After lag q	Tails off (Exponentially decay)
PACF	Cuts off After lag q	Tails off (Exponentially decay)	Tails off (Exponentially decay)

Table 3.2 Estimation of ARIMA (2, 1, 0) model

Parameter	Value	Standard Error	t - Statistic
Constant	11.1705	26.0191	0.429317
AR 1 (ϕ_1)	0.93426	0.019993	46.8744
AR 2 (ϕ_2)	-0.355803	0.02118	-16.7977

Step 6. Check goodness of fit

The next step after identification of a time series model is to check the goodness of fit of the model. A diagnostic check is made in order to verify that the model is reasonable. Asymptotic tests (e.g., Box-Ljung, Sign, Rank, and Q-Q plot), in addition to ACF, PACF, AIC, and BIC, are usually applied. The residuals are inferred from the fitted model and tested for large N cases in the asymptotic tests, whereas AIC and BIC statistics provide the theoretical predictive power of the estimated model with numerically calculated values. In this dissertation, the Q-Q plot that represents the asymptotic tests, and ACF and PACF for the residuals are conducted. The results can be seen in Figures 3.6 and 3.7, respectively.

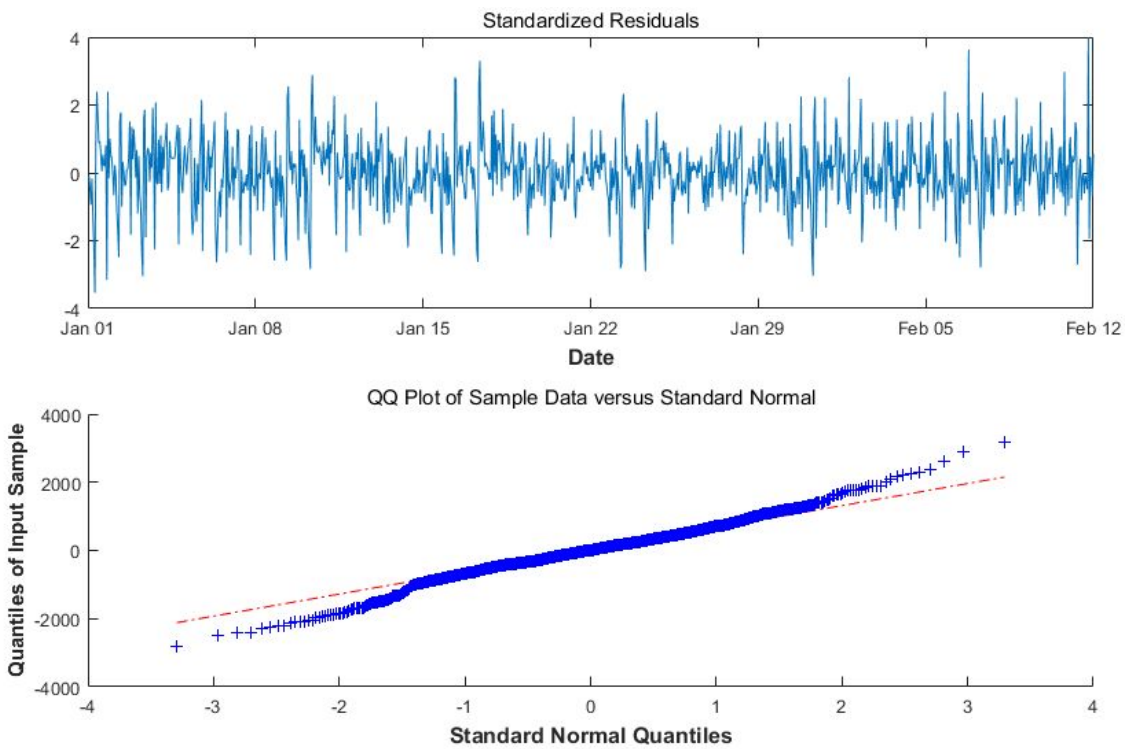

Figure 3.6 Standardized residuals graph and Q-Q plot

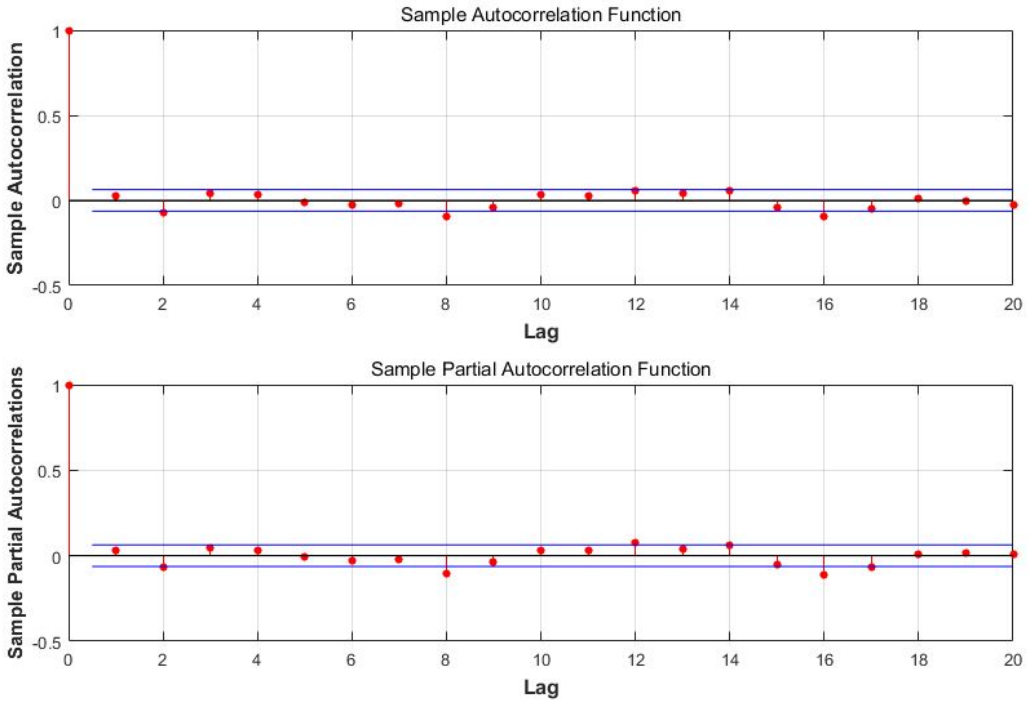

Figure 3.7 ACF and PACF for residuals

The residuals resemble white noise (upper figure) and the form of the Q-Q plot (bottom figure) is linear, as shown in Figure 3.6. It can be concluded that the residuals follow a normal distribution; moreover, the ARIMA (2, 1, 0) model with estimated parameters indicated in Table 3.2 is appropriate for the data. Figure 3.7 consistently justifies that the residuals are normally distributed and uncorrelated, considering that the correlation coefficient is negligible.

Step 7. Determine model

After investigating the time series data along with the Q-Q and residual diagnostic plots, the model to be used for generating scenarios is finally determined.

3.2 Wind Speed Forecast

It is generally acknowledged that the wind speed in a given location closely follows a Weibull or Rayleigh distribution. However, generated wind speed that uses a Weibull distribution might not properly reflect the correlation in the time domain [44], which could significantly affect the generation scheduling results. The ARMA model can consider the characteristic where the wind speed tends to be close to the immediately previous wind speed at any time; in other words, there are no sudden changes in wind speed.

In this dissertation, the ARMA (3,2) model is adopted to generate hourly wind speed in accordance with [45]. The authors established the ARMA (3,2) model after computing the actual hourly wind speed for three years and the standard deviation of the wind speeds by the least squares method. This model is given by

$$ds_t = \phi_1 ds_{t-1} + \phi_2 ds_{t-2} + \phi_3 ds_{t-3} + e_t + \theta_1 e_t + \theta_2 e_t \tag{3-5}$$

As shown in Figure 3.8, WPG is less than the available power contained by the wind stream. This is because of the non-stationary characteristic of the wind on the downwind side of the rotor [46]. The available wind power energy from the kinetic energy of air in motion is represented by power coefficient C_p. Power coefficient is affected by tip speed ratio and blade pitch angle, where the tip speed ratio is defined as the blade tip speed divided by the wind speed, as expressed in the following equation [47]:

$$\lambda_{tip} = \frac{\omega_r \cdot R}{s_t} \tag{3-6}$$

In summary, the active power output of the wind turbine can be computed by equation (3-7), whose wind speed s_t arise generated using the aforementioned

ARMA model.

$$P_{w,t}(v) = \frac{1}{2} \cdot \rho \cdot A \cdot s_t^3 \cdot C_p(\lambda_{tip}, \theta) \tag{3-7}$$

In order to derive WPG, in addition to wind speed s_t and power coefficient C_p, information on air density (ρ) and the swept area of the wind turbine (A) are required. The swept area of the wind turbine is determined by the rotor diameter of the wind turbine. In the interest of simplicity, it is assumed that air density (ρ) and power coefficient (C_p) are constant values in this dissertation. All the parameter values used are indicated in Chapter 5.

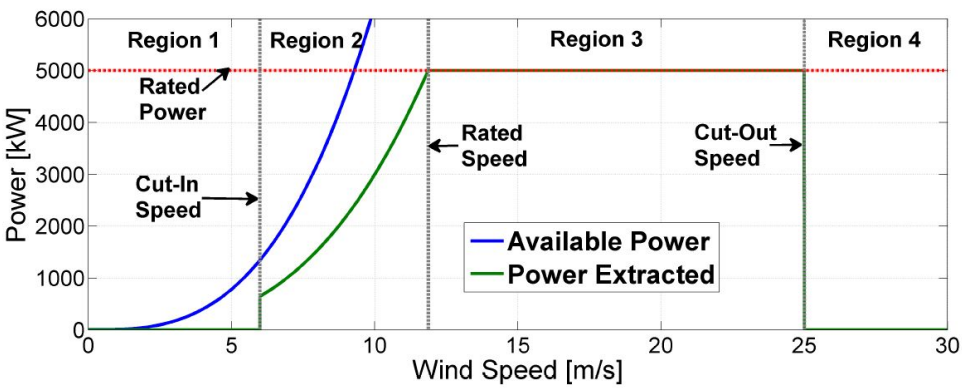

Figure 3.8 Available power of wind stream and power extracted by turbine [46]

3.3 Generator and Transmission Line Failure

Because this dissertation aims to establish security-constrained generation scheduling, the probability model with regard to generator and transmission line failure should be chosen before producing the scenarios to be used as an input to the stochastic optimization problem. A model based on a Markov chain, as shown by the state transition diagram in Figure 3.9, is adopted to represent the failure of the generator and transmission line.

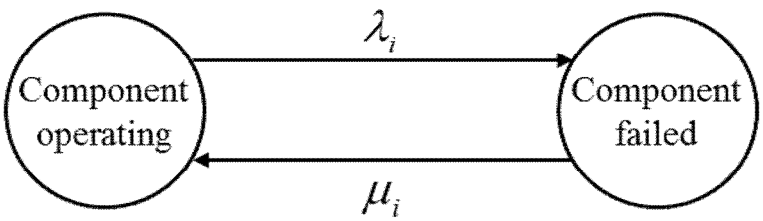

Figure 3.9 State space diagram for generator and transmission line

The probability distribution model for generator outages could be calculated using FOR for each generator [48]. Because the probability distribution model is calculated hourly, FOR for each generator is defined as the probability of the generator not being available within that hour. Therefore, the probability of the generator being available within that hour is given by 1 – FOR. That is, the probability of the generator being operable and failing at specific time t of specific unit i could be expressed as the following equations [49]:

$$P_{o,i}(t) = \frac{\mu_i}{\lambda_i + \mu_i} + \frac{\mu_i}{\lambda_i + \mu_i} e^{-(\lambda_i + \mu_i)t} \tag{3.8a}$$

$$P_{f,i}(t) = \frac{\lambda_i}{\lambda_i + \mu_i} + \frac{\lambda_i}{\lambda_i + \mu_i} e^{-(\lambda_i + \mu_i)t} \\ = 1 - P_{o,i}(t) \tag{3.8b}$$

Parameters λ_i and μ_i are known as the failure and repair rates, respectively. The rate values could also be found by equations (3.9) that indicate the relationship between the mean up/down time and failure/repair rate.

$$Mean\ Up\ Time(h) = m = \frac{1}{\lambda} \tag{3.9a}$$

$$Mean\ Down\ Time(h) = r = \frac{1}{\mu} \tag{3.9b}$$

The scenarios for the transmission line failure for the stochastic security-constrained problem could be treated with the same procedure as that for generators. It is assumed that the failed components might not be repaired or replaced during the operation period. The rates for each component used in this study are indicated in Chapter 5.

Chapter 4 Generation Scheduling with Dynamic Line Rating

Generation scheduling can be determined with the modeling of the uncertain factors in power systems that has been discussed so far. There are two types of approach to the generation scheduling of the power system for managing uncertainty. One is deterministic UC that manages uncertainties by imposing the predetermined reserve level or reliability index, and the other is stochastic UC, where the schedule is established based on various scenarios.

Network security should be checked when attempting to find the optimal commitment states and dispatched volume of generating units. Accordingly, the power flow equations are also given in the optimization problem. The UC problem that includes the power flow equations is a nonlinear and nonconvex mixed integer problem that is difficult to solve. Similar to the equations related to the heat gain/loss of the line, the power flow equations should be linearized before being incorporated into the generation scheduling problem.

The essential description of UC is provided in the following subchapters. At first, because the existing decoupled power flow equations cannot properly provide the resistive element for the transmission line, a new method is proposed for the linearization of AC power flow equations. Secondly, the spinning reserve procurement method from wind power generators and DSR is given. New types of reserve providers not confined to the conventional generator are important because the reserve requirements become larger as a result of newly integrated variable generators to the power system. In the last part of the chapter, the generation scheduling of the dissertation is formulated. It discusses all the factors considered in this study.

4.1 Unit Commitment of Conventional Generators

In order to manage the uncertainties in power system operation, such as load forecasting errors and equipment failure, SO must determine the commitment states of the units to provide robustness and flexibility to the system. The most common method used by operators is to commit sufficient generators to provide a total capacity above the firm system demand and maintain a spinning reserve. In the purpose of procuring a spinning reserve in UC, the optimization problem can be formulated as follows:[6]

$$\min \sum_{t=1}^{NT} \sum_{i=1}^{NG} C_{G,i}(P_{G,i,t}, U_{i,t}) \tag{4-1}$$

subject to

$$\sum_{i=1}^{NG} P_{G,i,t} = P_{D,t} \tag{4-2}$$

$$\sum_{i=1}^{NG} u_{i,t} P_{G,i}^{\max} \geq \overline{P}_{D,t} \tag{4-3}$$

Cost function $C_{G,i}$ measures the fuel cost, where operating unit i generates power output level $P_{G,i,t}$ during time period t. The commitment state of a unit is represented by binary variable $U_{i,t}$. Generator i is online at time t if $U_{i,t} = 1$ and it is off if $U_{i,t} = 0$. $P_{D,t}$ is the forecasted load during period t. As shown in the formula, in addition to the supply and demand balance constraint of equation (4-2), the spinning reserve constraint represented as equation (4-3) is inserted into the optimization problem, where $P_{G,i}^{\max}$ is the maximum operating level of unit i,

[6] In order to facilitate a comparison between deterministic and stochastic UC, detailed system and generator constraints are omitted. A further explanation of the constraints is provided in subchapter 4.4.

and $\overline{P}_{D,t}$ is the peak load for each time period that can be obtained from the worst-case scenario. In other words, SO can be ready for an uncertain situation with sufficient reserve margin procured from this reserve constraint. An excess system capacity is called "spinning reserve" [50], and the spinning reserve of the power system is fully explained in subchapter 4.3. The mathematical formulation of the above described model is deterministic UC. As the name implies, a predetermined level of reserve constraint is explicitly included in the optimization problem.

Unlike deterministic UC, the stochastic UC formulation is given as follows:

$$\min \sum_{s=1}^{NS} \pi_s \sum_{t=1}^{NT} \sum_{i=1}^{NG} C_{G,i}(P_{G,i,t}^s, U_{i,t}) \tag{4-4}$$

subject to

$$\sum_{i=1}^{NG} P_{G,i,t}^s = P_D^s \tag{4-5}$$

Instead of representative peak demand, a range of possible scenarios is generated to exemplify the uncertainty of load forecast. π_s indicates the probability of each scenario, and the weighted sum of each scenario's cost function is minimized in stochastic UC. It should be noted that the power output of each generating unit $P_{G,i,t}^s$ and load P_D^s appear clearly different depending on the scenarios, whereas the state of a unit must be the same for all corresponding scenarios.[7] Although only the supply and demand equality constraint is introduced in this formulation, all other constraints related to the UC problem surely have to

[7] Commitment decisions of fast starting units can be regarded to be similar to economic dispatch; that is, it can be changeable between scenarios, but this type of generator is not considered in this study.

be satisfied throughout every scenario.

The deterministic UC method with reserve requirements is consistent with current operating practices. However, it lacks the ability of capturing intertemporal variations. Consequently, the resulting deterministic UC solution can be either too conservative or too risky. On the other hand, although the stochastic UC approach has the major limitation of computational complexity, it was demonstrated that stochastic UC could be more cost effective than deterministic UC with reserve requirements. In addition, if the proper reserve requirement is additionally combined into the stochastic formulation, the weakness of stochastic programming can be minimized. Thus, stochastic formulation is used in this dissertation.

The optimization techniques for efficiently solving UC problems are highly important because the problems are large-scale and nonlinear. The solution procedure directly affects the convergence and computational time. Various mathematical programming methods and optimization techniques have been applied to UC problems, including priority-list, branch-and-bound, dynamic programming (DP), Lagrangian relaxation (LR), and MILP [51-54]. The priority-list method is fast, but the quality of the solution is too coarse for practical application. Application of the branch-and-bound method is limited to small-scale power systems because of the dimensionality curse. Although DP is a flexible technique for solving UC problems, it can still result in high-dimensionality problems when applied to modern power systems because of the large number of generating units. The LR method provides a fast solution, and it is a reasonably efficient and realistic technique for large-scale problems. However, it has limitations in the quality of the solution; in other words, it is expected that the operating cost is high compared with that of MILP. Although the MILP method is

somewhat burdensome to manage UC problems for very large power system due to scalability limitations [55], it provides more efficient generation scheduling results than all the techniques described above [54]. Given that a commitment decision is made in advance of the operating day, the MILP approach is adopted in this dissertation for accentuating economic importance in compensation of computational time.

4.2 Approximations to the Power Flow Equation

Contingency analysis is conducted for the purpose of assessing how severely a possible contingency can affect power systems. Currently, a bulk power system consists of several buses with hundreds of machines and thousands of transmission lines, which can lead to computational issues related to contingency analysis. Therefore, several studies have contributed to the methodology of seeking the power flow solutions that must be obtained for security analysis [56-58].

The method frequently applied in generation scheduling is usage of decoupled power flow equations. As the name indicates, the active power flow is governed mostly by the difference in the voltage phasor angle, whereas the reactive power flow is governed mostly by the difference in the voltage phasor magnitudes. In other words, there are decoupling features between the equations for real and reactive power, which is not in the case for normal power flow equations [34]. Such decoupled power flow equations are established based on the following observations:[8]

1) Resistance of the transmission line is much smaller than the reactance component, and thus the transmission lines are mostly reactive. For example, the average X/R ratio in the power system of South Korea is 7.59, 15.03, and 27.72 for 154 kV, 345 kV, and 765 kV, respectively.
2) Under normal operating conditions, the difference in angles of the bus voltage is fairly small, generally less than 10° [34]. This makes

[8] This approximation can only be applied to electric high voltage systems. Unlike high voltage transmission lines, the X/R ratio is between 1 and 3 for distribution network systems.

reasonable approximations regarding the sine/cosine of a small angle.

3) The magnitudes of bus voltage are very close to 1.0 when it is represented in per unit value.

With the three observations, the complex power flow equations (4-6) and (4-7) can be approximated to equations (4-8) and (4-9).[9]

$$P_k = \sum_{j=1}^{N} |V_k||V_j|\left(G_{kj}\cos(\theta_k - \theta_j) + B_{kj}\sin(\theta_k - \theta_j)\right) \tag{4-6}$$

$$Q_k = \sum_{j=1}^{N} |V_k||V_j|\left(G_{kj}\sin(\theta_k - \theta_j) - B_{kj}\cos(\theta_k - \theta_j)\right) \tag{4-7}$$

$$P_k = \sum_{\substack{j=1 \\ j\neq k}}^{N} B_{kj}(\theta_k - \theta_j) \tag{4-8}$$

$$Q_k = -b_k + \sum_{\substack{j=1 \\ j\neq k}}^{N} |b_{kj}|\left(|V_k| - |V_j|\right) \tag{4-9}$$

$|V_k|$ indicates the voltage magnitude of bus k, and θ_k is the angle of the voltage phasor. G_{kj} and B_{kj} are the conductances and susceptances, respectively. The term b_{kj} in equation (4-9) is a negative value of susceptances, and it can be expressed as $B_{kj} = -b_{kj}$. The term b_k indicates the shunt element that satisfies the relationship $B_{kk} = b_k + \sum_{\substack{j=1 \\ j\neq k}}^{N} b_{kj}$. It should be noted that the conductances terms G_{kj} are omitted in the decoupled power flow equations, which means that the resistive values are assumed to be zero. As shown in the approximated equations

[9] The magnitude of the power flow varies with respect to time, but subscript time t is excluded for notational simplicity.

(4-8) and (4-9), active power and reactive power equation is a simple linear function of voltage magnitude and angle, which allows efficient computation. In particular, the formulations can be readily incorporated with the existing generation scheduling problem represented in MILP.

Nonetheless, decoupled power flow equations cannot be used in this study because the first observation conflicts with the Joule heating gain $I^2R(T_{avg})$ calculation. More specifically, observation 1) assumes that resistive component R is equal to zero for the entire network, that is, lossless transmission lines, whereas there is a definite nonzero value in the Joule heating term involved in the heat balance equation.

Hence, relatively less approximated power flow equations are suggested with observations 2) and 3), and then employed in the optimization problem. Owing to the small degree of difference in the voltage angles,[10] typical power flow equations (4-6) and (4-7) can be approximated as the following equations:

$$\begin{aligned} P_k &= \sum_{j=1}^{N} |V_k||V_j| \left(G_{kj}\cos(\theta_k - \theta_j) + B_{kj}\sin(\theta_k - \theta_j) \right) \\ &= \sum_{j=1}^{N} |V_k||V_j| \left(G_{kj} + B_{kj}(\theta_k - \theta_j) \right) \\ &= \sum_{j=1}^{N} |V_k||V_j| G_{kj} + \sum_{j=1}^{N} |V_k||V_j| B_{kj}(\theta_k - \theta_j) \\ &= |V_k|^2 G_{kk} + \sum_{\substack{j=1 \\ j\neq k}}^{N} |V_k||V_j| G_{kj} + \sum_{j=1}^{N} |V_k||V_j| B_{kj}(\theta_k - \theta_j) \end{aligned} \tag{4-10}$$

[10] Observation 2)

$$
\begin{aligned}
Q_k &= \sum_{j=1}^{N} |V_k||V_j| \left(G_{kj} \sin(\theta_k - \theta_j) - B_{kj} \cos(\theta_k - \theta_j) \right) \\
&= \sum_{j=1}^{N} |V_k||V_j| \left(G_{kj}(\theta_k - \theta_j) - B_{kj} \right) \\
&= \sum_{j=1}^{N} |V_k||V_j| G_{kj}(\theta_k - \theta_j) - \sum_{j=1}^{N} |V_k||V_j| B_{kj} \\
&= \sum_{j=1}^{N} |V_k||V_j| G_{kj}(\theta_k - \theta_j) - |V_k|^2 B_{kk} - \sum_{\substack{j=1 \\ j \neq k}}^{N} |V_k||V_j| B_{kj}
\end{aligned}
\tag{4-11}
$$

As an approximation, cosine function of a small angle may be considered equal to unity and the sine value of a small angle equal to the angle itself. Separating the term $j = k$ from the summation in the equations yields the last row of the equations.

Assuming that the voltage magnitudes are more or less 1.0 per unit,[11] the active and reactive power flows can be formulated as follows:

$$
\begin{aligned}
P_k &= |V_k|^2 G_{kk} + \sum_{\substack{j=1 \\ j \neq k}}^{N} |V_k||V_j| G_{kj} + \sum_{j=1}^{N} |V_k||V_j| B_{kj}(\theta_k - \theta_j) \\
&= \sum_{\substack{j=1 \\ j \neq k}}^{N} g_{kj}(|V_k| - |V_j|) - \sum_{j=1}^{N} b_{kj}(\theta_k - \theta_j)
\end{aligned}
\tag{4-12}
$$

$$
\begin{aligned}
Q_k &= \sum_{j=1}^{N} |V_k||V_j| G_{kj}(\theta_k - \theta_j) - |V_k|^2 B_{kk} - \sum_{\substack{j=1 \\ j \neq k}}^{N} |V_k||V_j| B_{kj} \\
&= -\sum_{j=1}^{N} g_{kj}(\theta_k - \theta_j) - b_k - \sum_{\substack{j=1 \\ j \neq k}}^{N} b_{kj}(|V_k| - |V_j|)
\end{aligned}
\tag{4-13}
$$

If compared with the decoupled power flow equations (4-8) and (4-9), the initial two terms in the active power flow equation and first term in the reactive power flow equation are added. As shown above, the suggested approach does not

[11] Observation 3)

express active power flow only with the angle difference, or reactive power flow simply with voltage magnitudes. However, of most interest in the created equations is their linearized form. Assume that the magnitudes of voltage equal to one can eliminate the squared term, and the trigonometric terms with a small angular difference are approximated as a linear form. This way, the power flow equations can be applied for the security-constrained generation scheduling that is the optimization problem denoted by MILP.

4.3 Spinning Reserve Procurement Method

One of the most important characteristics of power systems is that supply and demand are balanced at all times. An unexpected change in demand or supply results in fluctuations in the system frequency, and if the balance between generation and load is lost, it can lead to frequency deviation, a loss of synchronization between generators, or even a blackout of the entire power system. For this reason, SO should provide an operating reserve to account for unexpected fluctuations in demand or supply, or for problems that might occur in the electrical grid.

In general, operating reserves are defined as any capacity available to assist in maintaining the active power balance, which are necessary because of load forecasting errors, the unpredictable output of wind generation, and/or equipment failure [59]. Although operating reserves comprise spinning and non-spinning reserves,[12] only spinning reserves are considered in this short-term generation scheduling study.

Power system operators can procure spinning reserves from both generating units and DSR. Online units can provide spinning reserves to a system if they are not fully loaded and are ready to generate more power within an acceptable ramping capability. Because reserve requirement and classification are dependent on each electricity market's rule, no single formula and parameter value can account for the spinning reserve. In this dissertation, the following mathematical equation is used to represent the spinning reserve contributed by each generator i

[12] Non-spinning reserve indicates the generating reserve not synchronized to the power system but available to serve demand in case of need. Fast starting generators are categorized into this group.

during time period t. Equations (4-14a) and (4-14b) represent up-spinning and down-spinning reserves, respectively.

$$SR_{G,i,t}^{up} = \min(P_{G,i}^{\max} - P_{G,i,t}, RR_i^U \cdot T_{lead}) \tag{4-14a}$$

$$SR_{G,i,t}^{down} = \min(P_{G,i,t} - P_{G,i}^{\min}, RR_i^D \cdot T_{lead}) \tag{4-14b}$$

As shown in the formulas, a spinning reserve is constrained by both the level of generating output $P_{G,i,t}$ and ramp rate capability RR_i^U of each unit. The former value is time-variant, whereas the latter is constant to time. T_{lead} is the spinning reserve market lead-time, and it represents the reserve responsive time.

Loads that can be interrupted for a given time are also regarded as spinning reserves. An interruptible load is one with a prior customer agreement for reducing the load at peak demand times or at any time in requests of SO. When customers sign an interruptible load contract, they are rewarded with capacity payment incentives, and they receive an additional reward for actual load reduction in the manner of energy cost.

Much has been written about interruptible loads as spinning reserves because it is much more economical to include demand-side reserves instead of only considering supply-side reserves [23, 24, 60]. Spinning reserves obtained from generators can be expensive because additional generating units are required, and the output of other units might be forced to deviate from the most optimal point. Hence, operating costs increase significantly if power SO provides spinning reserves only from dispatched generators. In light of the above deliberations, it is quite reasonable to consider demand-side participation, especially when there are increased operating reserve needs. Accordingly, in this dissertation, it is assumed that SO can procure spinning reserves both from interruptible loads and generators.

In order for SO to prepare a secure and flexible operation, spinning reserve provision with wind farms can be considered as well. Wind power generators, for the most part, are operated in the manner of maximum power point tracking (MPPT). The rotor speed is changed with the varying speed of the wind so that the wind energy can be efficiently harvested, whereas the deloaded control of wind power can provide the inertial primary and secondary response (AGC) for the power system [25, 46, 61, 62]. The motivations for deloaded control are to improve frequency regulation through wind power as the proportion of wind energy in power systems increases (from SO perspective), and to increase the profitability of wind power (from the perspective of the wind power owners).

The deloaded control, also called “delta control” or “active power control,” ensures that a specific portion of available wind power is kept low. There are two possible methods for wind power generators to supply spinning reserve. The first is using a pitch controller that can operate wind turbines with various degrees of pitch angles. The second is to alter the rotor speed with the purpose of procuring a reserve. This is illustrated in Figure 4.1 [63]. As shown in the figure, the active power of a deloading power curve is lower than that of the MPPT curve, and the difference in volume can be translated into a spinning reserve. From the perspective of generation scheduling, the deloaded control operation can be compared with MPPT operation as exemplified in Figure 4.2. The figure shows a situation where the active power control is scheduled during hours 1 and 3, whereas MPPT operation is arranged to be performed for hour 2.

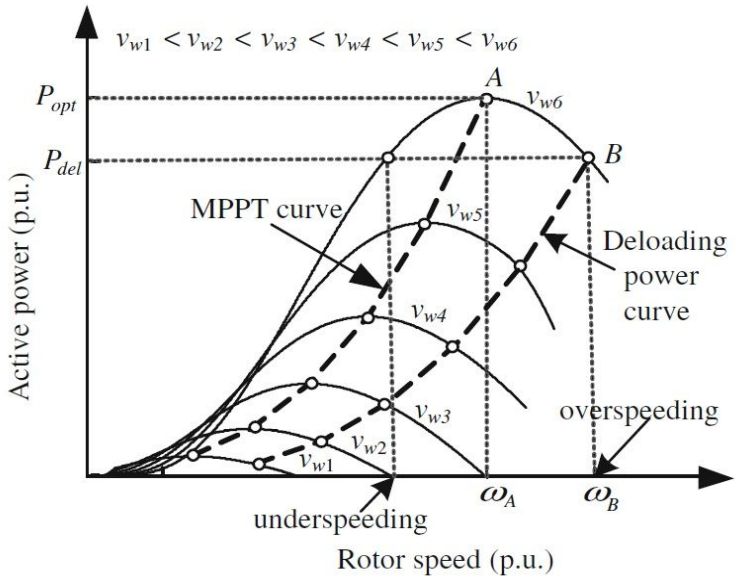

Figure 4.1 Comparison of deloading power curve and MPPT power curve [63]

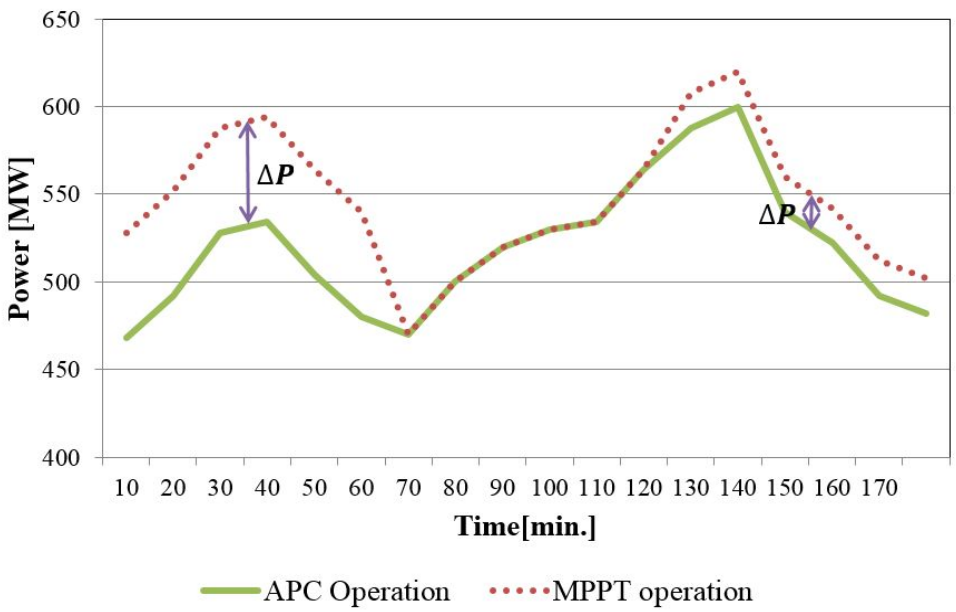

Figure 4.2 Power output difference in deloaded control and MPPT operations

4.4 Generation Scheduling Formulation for Dissertation

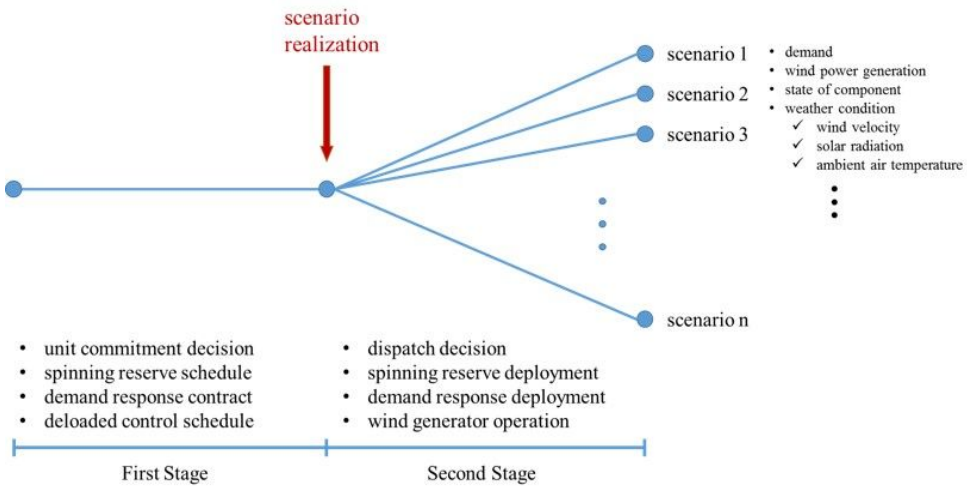

Figure 4.3 Two-stage decision model of generation scheduling problem

One of the possible methods for reflecting the stochastic nature of power systems is the two-stage decision model proposed in Figure 4.3. This approach has received much attention since the mid-1990s thanks to advanced computing capability [20, 60, 64]. In the two-stage model, decision variables for minimizing the expected operating cost are divided into first and second stage variables.

Before the realization of the scenarios, in the first stage, SO determines which generating units to turn on/off, as well as the spinning reserve contribution of each conventional unit. Sufficient generators should be turned on to exceed the expected demand plus spinning reserve. The required amount of DSR that should be contracted is also computed and then signed up. If required, the specific volume of WPG is scheduled to be deloaded in order to provide a spinning reserve. Because uncertain factors are not realized in this step, all first stage variables are identically exercised for all realized scenarios.

Thereafter, the scenarios are recognized and the system network security and

volume of load shedding are monitored. The second stage variables that vary based on the scenarios are the dispatch volume of generators and deployed spinning reserve from all prepared resources. If the scheduled reserves are insufficient, it leads to supply inadequacy and thus the increase of the expected load shedding cost. Accordingly, this case generates a signal for the first stage so that the appropriate amount of reserve is procured in advance. A detailed description in connection with decision variables is given hereinafter with the use of a mathematical formulation.

4.4.1 Objective Function

$$Obj = \min_{\substack{\mathbf{u},\mathbf{P_G},\mathbf{Q_G},\overline{\mathbf{P}}_{\mathbf{G}},\overline{\mathbf{Q}}_{\mathbf{G}},\\ \mathbf{P_{DR}},\mathbf{P_{Wgen}},\mathbf{P_{Wcur}}}} \left\{ \begin{aligned} &\sum_{s=1}^{NS}\pi_s \sum_{t=1}^{NT}\sum_{i=1}^{NG} C_{G,i}(P_{G,i,t}^{s}, u_{i,t}) \\ &\quad + \sum_{i=1}^{NG} C_{SU,i}(u_{i,1},...,u_{i,NT}) + \sum_{i=1}^{NG} C_{SD,i}(u_{i,1},...,u_{i,NT}) \\ &\quad + \sum_{t=1}^{NT}\sum_{d=1}^{ND} C_{DR^C,d,t}(P_{DR^C,d,t}) + \sum_{s=1}^{NS}\pi_s \sum_{t=1}^{NT}\sum_{d=1}^{ND} C_{DR^E,d,t}(P_{DR^E,d,t}^{s}) \\ &\quad + \sum_{s=1}^{NS}\pi_s \sum_{t=1}^{NT}\sum_{b=1}^{NB} VoLL_{b,t}\cdot LS_{b,t}^{s} \end{aligned} \right\}$$

(4-15)

The operating cost is the overall daily cost to maintain power system security, which includes the expected cost of all conventional generators (e.g., the generation cost), the expected cost related to procuring the generating reserves, and the expected cost of outages (e.g., the load shedding cost).

The overall operating cost can be divided into costs with regard to the first and second stages. For example, start-up/shutdown costs $C_{SU,i}$ and $C_{SD,i}$ are only affected by the commitment states of unit $u_{i,t}$, which is constant to all scenarios.

The contract cost of DSR, $C_{DR^C,d,t}$, especially the capacity cost that provides a spinning reserve by demand-side, is also categorized in this cost type. It is worth noting that the probability of scenario π_s is irrelevant, independent from this type of cost. On the contrary, generation cost $C_{G,i}$, deployment cost of demand-side spinning reserve $C_{DR^E,d,t}$, and the cost related to involuntary load shedding $VoLL_{b,t} \cdot LS_{b,t}^s$ vary based on the developed scenarios. These costs are calculated considering the weighing factor π_s, which is the probability of the scenarios occurring. Each component that comprises the operating cost is described in greater detail below.

1) Generation cost

The generation cost is the cost of conventional generators over 24 hours. The cost function of each generator is a quadratic function of the output of the generators, and it is determined by the sum of fuel cost $C_{G,i}$, which has unit cost coefficients a_i, b_i, and c_i in each generator. Although this cost function is not linear with respect to generating output $P_{G,i,t}^s$, the piecewise linearization technique simply allows the formulation to be placed into a MILP problem. Start-up $C_{SU,i}$/shutdown $C_{SD,i}$ costs are incurred when the units turn on the machine (start-up cost) or switch a generating unit off (shutdown cost). Consequently, the start-up/shutdown cost is a function of states of unit $u_{i,t}$, completely independent from the amount of generation.

Because demand is satisfied by both conventional and wind power generators,

the generation cost decreases as the wind power penetration increases. However, the cost savings by using WPG have inherent limitations because a larger wind curtailment tends to occur when a quite high penetration of wind power is integrated in the system. Wind power spillage can be markedly reduced with DLR that can induce efficient use of the network assets. The means for securing a spinning reserve through WPG also helps maximize wind power utilization. Benefits from these two approaches are verified with a numerical simulation in Chapter 5.

2) Spinning reserve and DSR costs

Only in the objective function does a spinning reserve cost related to DSR exist. However, it should be indicated that the aforementioned generation cost is the cost that already includes the spinning reserve contribution. In simplified terms, the spinning reserve constraint forces the conventional generators to be sufficiently committed, and to maintain the output below a certain level for the purpose of providing a spinning reserve. Consequently, the generation cost is increased indirectly as a result of the spinning reserve; as it were, the generation cost encompasses the spinning reserve cost. This interpretation can be also extended to the wind power generator. If some wind power generators were planned to provide the spinning reserve to the system, overall generating cost would increase because other generators would compensate for the corresponding amount of spinning reserve by raising their power output.

Participation of the demand-side in power systems offers flexibility and efficiency in generation scheduling and system operation. There are two costs

linked to DSR: one is capacity allocation cost $C_{DR^C,d,t}$ that concerns the sign-up for the spinning reserve support, and the other is energy cost $C_{DR^E,d,t}$ that occurs only if the contracted volumes are actually deployed. Whether DSR deployment is required varies with the scenarios, as does the actual volume deployed; therefore, the energy cost of DSR is calculated based on the probability of the scenarios, π_s.

3) Load shedding cost

When an imbalance occurs between demand and supply, SO should perform load shedding in order to maintain system frequency. Those customers affected by load shedding cannot use electricity, and monetary penalties result. The load shedding cost is the expected sum of these monetary penalties, and it increases as more load shedding occurs. This involuntary load curtailment is determined by the spinning reserve and the error in the forecast error in demand, generation outage, and difference in forecast and actual WPG. In other words, load shedding occurs when demand exceeds the sum of the supply and the spinning reserve margin.

The load shedding cost can be calculated as the product of the volume of load shedding $LS^s_{b,t}$, the value of lost load $VoLL_{b,t}$, and probability of the corresponding load shedding scenario occurring, π_s. This can be formulated as the last row in the objective function $\sum_{s=1}^{NS}\pi_s\sum_{t=1}^{NT}\sum_{b=1}^{NB}VoLL_{b,t}\cdot LS^s_{b,t}$. Because load shedding decreases as the spinning reserve margin increases, the load shedding cost also decreases.[13] It follows that the load shedding cost has an inverse relationship

[13] Meanwhile, spinning reserve cost is expected to increase.

with the short-term reliability of balance.

4.4.2 Constraints

As illustrated in Figure 4.3 (two-stage decision model of generation scheduling problem), the constraints of the stochastic security-constrained generation scheduling problem can be divided into the first and the second stage constraints.

First stage constraints:

$$\sum_{i=1}^{NG_b} P_{G,i,t} + P_{WG,t} - P_{b,t}^{D} = \sum_{k=1}^{N} P_{k,t} \qquad \forall b,t \qquad (4\text{-}16)$$

$$\sum_{i=1}^{NG_b} Q_{G,i,t} - Q_{b,t}^{D} = \sum_{k=1}^{N} Q_{k,t} \qquad \forall b,t \qquad (4\text{-}17)$$

$$u_{i,t} P_{G,i}^{\min} \le P_{G,i,t} \le u_{i,t} \overline{P}_{G,i,t} \qquad \forall i,t \qquad (4\text{-}18)$$

$$0 \le \overline{P}_{G,i,t} \le u_{i,t} P_{G,i}^{\max} \qquad \forall i,t \qquad (4\text{-}19)$$

$$u_{i,t} Q_{G,i}^{\min} \le Q_{G,i,t} \le u_{i,t} Q_{G,i}^{\max} \qquad \forall i,t \qquad (4\text{-}20)$$

$$P_{WG,t} + SR_{WG,t} \le P_{WGforecast,t} \qquad \forall t \qquad (4\text{-}21)$$

$$0 \le SR_{G,i,t}^{up} \le P_{G,i}^{\max} - P_{G,i,t} \qquad \forall i,t \qquad (4\text{-}22)$$

$$0 \le SR_{G,i,t}^{up} \le RR_i^{U} \cdot T_{lead} \qquad \forall i,t \qquad (4\text{-}23)$$

$$0 \le SR_{G,i,t}^{down} \le P_{G,i,t} - P_{G,i}^{\min} \qquad \forall i,t \qquad (4\text{-}24)$$

$$0 \le SR_{G,i,t}^{down} \le RR_i^{D} \cdot T_{lead} \qquad \forall i,t \qquad (4\text{-}25)$$

$$(\mathbf{u}, \mathbf{P_G}, \mathbf{Q_G}, \overline{\mathbf{P_G}}, \mathbf{P_{WG}}, \mathbf{SR_{WG}}) \in F \qquad \forall i,t \qquad (4\text{-}26)$$

Same constraints as equations (2-3), (2-6), (2-8), and (2-9) $\forall l,t$ (4-27)

Same constraints as equations (4-12) and (4-13) $\forall l,t$ (4-28)

$$T_{c,l} \le T_l^{\max} \qquad \forall l,t \qquad (4\text{-}29)$$

Second stage constraints

$$\sum_{i=1}^{NG_b} v_{i,t}^s P_{G,i,t}^s + v_{WG,t}^s P_{WG,t}^s + \sum_{d=1}^{ND_b} P_{DR^E,d,t}^s + LS_{b,t}^s - P_{b,t}^{D,s} = \sum_{k=1}^{N} P_{k,t}^s \qquad \forall s,b,t \qquad (4\text{-}30)$$

$$\sum_{i=1}^{NG_b} v_{i,t}^s Q_{G,i,t}^s - Q_{b,t}^{D,s} = \sum_{j=1}^{N} Q_{k,t}^s \qquad \forall s,b,t \qquad (4\text{-}31)$$

$$P_{G,i,t}^s = P_{G,i,t} + sr_{G,i,t}^{up,s} - sr_{G,i,t}^{down,s} \qquad \forall s,i,t \qquad (4\text{-}32)$$

$$P_{WG,t}^s = P_{WG,t} + sr_{WG,t}^s + \sigma_{WG,t}^s \qquad \forall s,t \qquad (4\text{-}33)$$

$$P_{WG,t}^s \le P_{WGforecast,t} + \sigma_{WG,t}^s \qquad \forall s,t \qquad (4\text{-}34)$$

$$0 \le sr_{G,i,t}^{up,s} \le v_{i,t}^s SR_{G,i,t}^{up} \qquad \forall s,i,t \qquad (4\text{-}35)$$

$$0 \le sr_{G,i,t}^{down,s} \le v_{i,t}^s SR_{G,i,t}^{down} \qquad \forall s,i,t \qquad (4\text{-}36)$$

$$0 \le sr_{WG,i,t}^{up,s} \le v_{WG,t}^s SR_{WG,i,t}^{up} \qquad \forall s,t \qquad (4\text{-}37)$$

$$0 \le P_{DR^E,d,t}^s \le P_{DR^C,d,t} \qquad \forall s,d,t \qquad (4\text{-}38)$$

$$(\mathbf{P_G^s}, \mathbf{Q_G^s}, \overline{\mathbf{P_G^s}}, \mathbf{P_{WG}^s}) \in F \qquad \forall s,i,t \qquad (4\text{-}39)$$

Same constraints as equations (2-3), (2-6), (2-8), and (2-9) $\forall s,l,t$ (4-40)

Same constraints as equations (4-12) and (4-13) $\forall s,l,t$ (4-41)

$$T_{c,l} \le T_l^{\max} \qquad \forall s,b,t \qquad (4\text{-}42)$$

The active and reactive power balances at each bus b are represented by the constraints shown in equations (4-16) and (4-17). At each bus, the active and reactive powers injected in the transmission system are defined as $P_{k,t}$ and $Q_{k,t}$, respectively. The sum of active powers injected in the connected bus is equal to the net power generation (sum of conventional generation power and wind power minus load power). Subscript k is used for the buses that are linked from bus b. The reactive power is formulated similarly. The power flow equations between two buses are developed in subchapter 4.2 with approximations, and the equations are imposed as equation (4-28). It should be remembered that the power flow equations are formulated at a snapshot in time; that is to say, such equations are independent of time. However, in the formulation of generation scheduling, the power flow constraints should be enforced hour by hour.

The constraints in inequalities (4-18) and (4-19) are intended to represent the actual maximum generation of units limited by the ramping constraints. $\overline{P}_{G,i,t}$ is explicitly introduced with the intention of formulating the constraint into the MILP model suggested in [54]. Similar to the active power, the reactive power output is confined by binary variables $u_{i,t}$ as imposed in equation (4-20). The 0-1 variables $u_{i,t}$ are the decision variables for SO to optimize the scheduling problem, and they should not be confused with index $v_{i,t}^{k,s}$, which is the binary value that indicates the operation conditions of the facilities.

The generation scheduling problem is subject to the spinning reserve inequalities (4-21) to (4-25). The uppercase SR means the procured spinning reserve in the scheduling process, whereas the lowercase sr represents the

deployed spinning reserve in the system operation. The constraints shown in inequalities (4-22) to (4-25) account for the same design as equation (4-14), but they are expressed in the linear equations at this stage. The constraint shown in equation (4-26) is a concise form that considers other constraints, such as ramping, minimum up and down time, and another type of reserve constraints [20].

All the constraints related to the heat balance equation are included in equation (4-27). The temperature of each transmission line $T_{c,l}$ is determined through the heat balance equation at every hour, and it is limited by allowable maximum temperature $T_l^{\max}$. A key point worth noting about this constraint condition is Joule heating, also called "resistive heating" and "ohmic heating term," $I^2R(T_{avg})$. Unlike the other components—convective heat loss, radiated heat loss, and solar radiation heat gain—Joule heating is affected by electrical conditions, that is, the electric current flow in the transmission line. When more transmitted power exists, a conductor releases more heat, causing the conductor temperature to increase. In conclusion, this increased temperature should be restricted by the predetermined acceptable limit, as expressed in equation (4-29).

In the second stage, all the constraints are implemented for each scenario. The power balance equations (4-30) and (4-31) are analogous to the first stage constrains shown in equations (4-16) and (4-17). In second stage, index $v_{i,t}^{k,s}$ is introduced to represent the generator states. If a machine cannot support electricity to the grid because of outages, the corresponding machine index is set to 0 in order to limit the active and reactive power output from that generating unit. The most important manifestation is the load shedding component included in the constraint. When this forced load shedding occurs, obviously the balance between supply and

demand can be satisfied; however, it levies a considerable cost on SO, which is the value of lost load $VoLL_{b,t}$.

The power generation in each scenario is adjusted with the reserve variable in comparison with the baseline scenario considered in the first stage. This is expressed in the equality constraint shown in equations (4-32) and (4-33). In the constraint shown in equation (4-34), the forecast error in WPG is added to the expected WPG, and this constrains the active power from the wind power generator in the scenarios.

The constraints shown in inequalities (4-35) to (4-38) demonstrate the relationship between the procured spinning reserve in the first stage and the deployed spinning reserve in the second stage. DSR participation in generation scheduling and its implementation are considered in the constraint shown in inequality (4-38). As specified in the constraints, the scheduled spinning reserve should be well secured in order to prevent a situation where the reserve is insufficient, thus leading to the resultant load curtailment. Similar to power generation, the spinning reserve can be provided only by the generating units in the healthy state. The last constraints shown in equations (4-39) to (4-42) are designed similarly to those of the first stage constraints shown in equations (4-26) to (4-29).

Chapter 5 Case Study

In this dissertation, two different generation schedulings are assessed: a conventional method that considers the static power flow limit and the proposed method that uses DLR. In order to analyze these policies, the expected total operating cost and unsupplied energy were calculated by applying a Monte Carlo simulation approach. Although the Monte Carlo approach imposes a computational burden, it can readily accommodate a wide range of probability distributions [65].

All factors that determines the transmission line rating, such as solar radiation and ambient air temperature, can be considered in the stochastic problem formulated in Chapter 4. Scenarios that cover the uncertain characteristics of the components can be generated. However, in this case study, the only the uncertainty in wind speed is considered owing to the computational complexity. The reason for selecting the wind speed as a representative factor is that wind speed is the most influential and uncertain value when determining the rating.

As described in Chapter 3, it was assumed that the uncertainty of wind speed follows an ARMA (p, q) model, in which p = 3 and q = 2. The autoregressive order p was set to 1.7901, 0.9087, and 0.0948, and the MA term q was set to 1.0929 and 0.2892. These parameters were obtained from [45]. The ARIMA (2, 1, 0) model represented load uncertainty; the values of ϕ for the integrated UL_t used in the model were 0.9342 and –0.3558. The constant term was set to 11.1705.[14] This uncertainty term was added to the expected load to calculate the actual load. Based

[14] It seems unreasonable for the constant term to exist in uncertainty modeling, but this is because the PJM load is extremely high. In other words, 11.1705 MW is very small compared with the PJM data where the peak value is more than 100,000 MW.

on these forecasted error models of the demand and WPG, 2000 scheduling scenarios were generated using Monte Carlo simulations. The GAMS/SCENRED function that implemented the scenario reduction technique in [66] was used to select the representative scenarios from the scheduling scenarios.

The specifications of the wind turbines considered are the following: rated power of 5 MW, cut-in speed of 3 m/s, rated speed of 11.4 m/s, cut-out speed of 25 m/s, rotor diameter of 112 m, and hub height of 90 m. The other details can be found in [47]. When solving the generation scheduling problem, the ramp rate and minimum on/off time are dependent on the test system. Here, all units were assumed to be free from must-run or must-not-run statuses at all times. The scheduling horizon for the problem was assumed to be 24 h.

The optimization problems were solved using GAMS/CPLEX software on a PC with a 2.40 GHz Intel Core i7-5500U CPU, 8 GB of RAM, and a 64-bit Windows 7 operating system. The relative gap of GAMS/CPLEX was set to 0.1%. The overall procedure for the simulation is summarized below.

Step 1. Generate the scenarios of uncertainty in load and wind speed with a probabilistic model using MATLAB.

Step 2. Generate the scenarios that represent the states of conventional generators and transmission lines using MATLAB software.[15]

Step 3. Select the representative scenarios generated from the previous steps to ease the computational process. This is performed through the GAMS/SCENRED tool.

[15] Failure of wind power generator is not considered. It is assumed that exclusion of the output of one wind power generator is a negligible quantity. The wind farms comprise 15 wind power generators.

Step 4. Solve the generation scheduling problem based on the representative scenarios with GAMS/CPLEX. Two different methods—SLR and DLR—are applied separately to the optimization problem. These scenarios contain both the states of components and the uncertainties of load and wind speed.[16]

Step 5. Determine the generation scheduling and compare the results of the two methods.

[16] WPG uncertainty is also reflected because wind speed is different in each scenario.

5.1 Six-Bus System

5.1.1 Simulation Settings

To closely monitor the effects of DLR on the system, a simple six-bus system was used for the generation scheduling problem. Although three generators supply the six-bus system in common, it was assumed in this dissertation that an additional generator is located in bus 2 because three generating units are insufficient in the case of the *N*–1 contingency incident. Wind farms were also introduced to satisfy the demand located in buses 1 and 5. The system has three loads and seven transmission lines. All facilities were placed as shown in Figure 5.1.

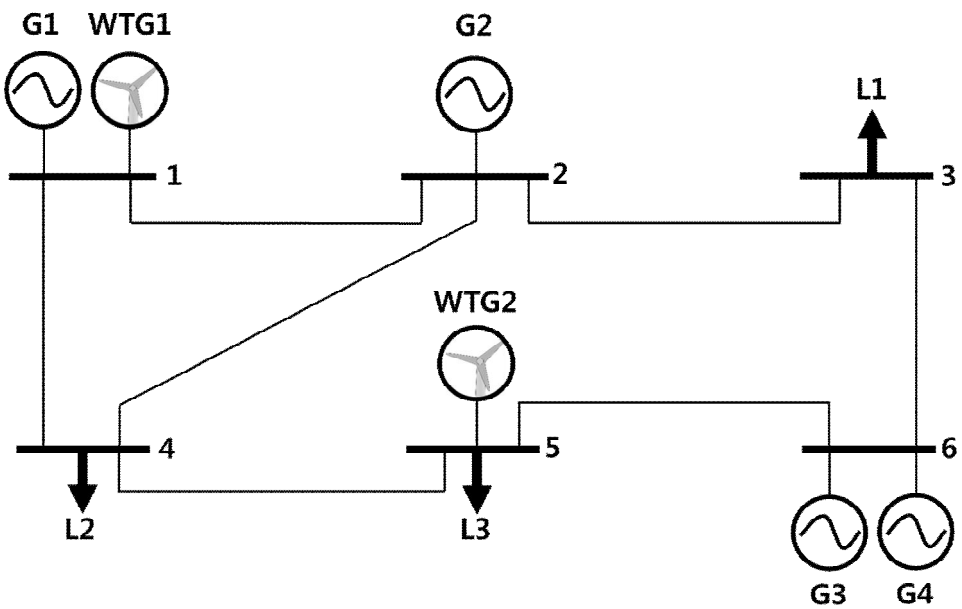

Figure 5.1 One-line diagram for six-bus system

The generator and transmission line data for the six-bus system are listed in Tables 5.1 and 5.2, respectively.

Table 5.1 Generator data for six-bus system

Gen No.	Bus No.	a [MBtu]	b [MBtu/ MWh]	c [MBtu/ MW^2h]	Pmax [MW]	Pmin [MW]	Qmax [MVar]	Qmin [MVar]	Init Hour [h]	Min Off [h]	Min On [h]	Ramp [MW/ h]	Start Up [MBtu]	Fuel Price [$/MBtu]	Mean Up [h]	Mean Down [h]
1	1	176.95	13.51	0.00045	240	100	300	-300	4	4	4	80	200	1.2469	23.6	0.4
2	2	129.97	32.63	0.0001	135	30	70	-13	2	3	2	60	100	1.2461	23.7	0.3
3	6	129.97	32.63	0.0001	135	30	70	-13	2	3	2	60	100	1.2461	23.8	0.2
4	6	137.41	18.69	0.003	60	10	300	-300	1	1	1	30	0	1.2462	23.8	0.2

Table 5.2 Transmission line data for six-bus system

Line No.	From	To	R [pu]	X [pu]	C [pu]	Rate [MVA]	Mean Up [h]	Mean Down [h]
1	1	2	0.005	0.17	0.0254	275.4	23.5	0.5
2	2	3	0.001	0.037	0.01082	137.7	23.7	0.3
3	1	4	0.003	0.258	0.0021	137.7	23.6	0.4
4	2	4	0.007	0.197	0.0284	137.7	23.6	0.4
5	4	5	0.001	0.037	0.01426	137.7	23.7	0.3
6	5	6	0.002	0.14	0.0055	137.7	23.6	0.4
7	3	6	0.0005	0.018	0.01	137.7	23.8	0.2

The forecasted load and wind speeds for 24 h are listed in Table 5.3. The forecasted wind speeds are based on the historical wind data given by the United States Bureau of Reclamation.[17] For the sake of simplicity, it is assumed that the forecasted wind speed closely resembles the average value of historical wind speed at each hour.

Table 5.3 Forecasted load and wind speed for six-bus system

Hour [h]	Demand [MW]	Wind Speed [m/s]
1	210	4.0956
2	198	4.1277
3	174	4.0665
4	120	4.1453
5	150	4.0894
6	180	4.2028
7	210	4.1654
8	234	4.1420
9	246	3.9139
10	264	3.8928
11	267	3.9273
12	252	4.1856
13	240	4.3195
14	228	4.5317
15	264	4.7597
16	270	5.2038
17	255	5.4515
18	267	5.6418
19	282	5.5059
20	294	5.0796
21	300	4.6573
22	270	4.3370

[17] The United States Bureau of Reclamation is the largest wholesaler of water and the second largest producer of hydroelectric power in the United States.

23	261	3.9530
24	246	3.8731

Before determining generation scheduling, various scenarios must be generated in advance for the purpose of representing possible operation conditions. The uncertainty of wind speed and system load was produced using Monte Carlo simulations, as shown in Figures 5.2 and 5.3. WPG scenarios were calculated according to wind speed. In the figures, the black bold line represents the mean value of uncertainty at each hour, whereas the grey thin lines indicate each generated scenario. It can be seen easily that the mean of uncertainty is zero in system load and WPG both, as expected. However, the overall shape of the generated scenarios is slightly different because load uncertainty was designed with the ARIMA model (for a non-stationary model), whereas wind speed uncertainty was designed with the ARMA model (for a stationary model).

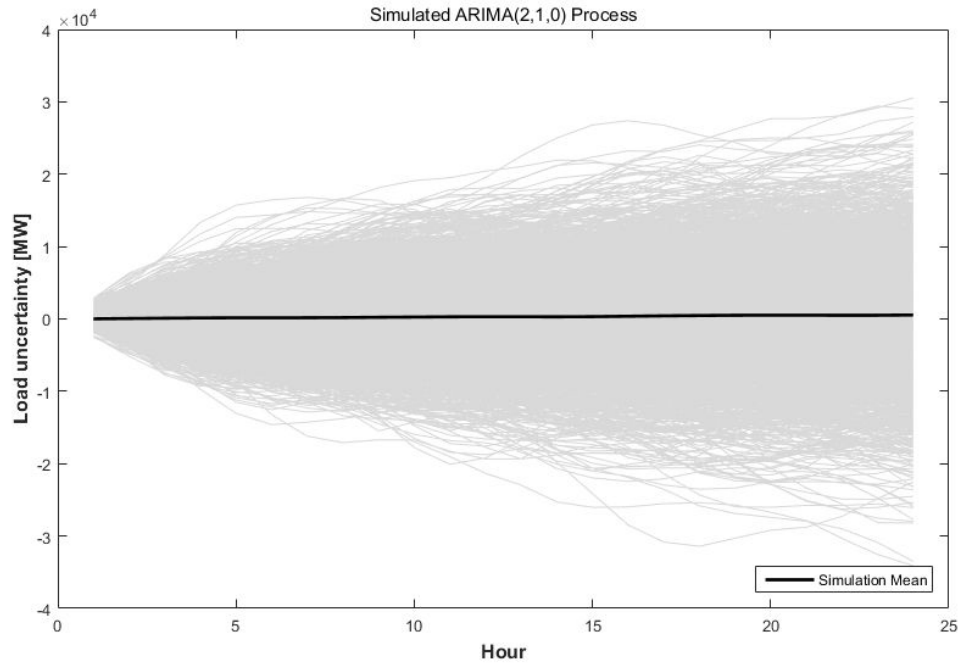

Figure 5.2 2000 scenarios of system load uncertainty[18]

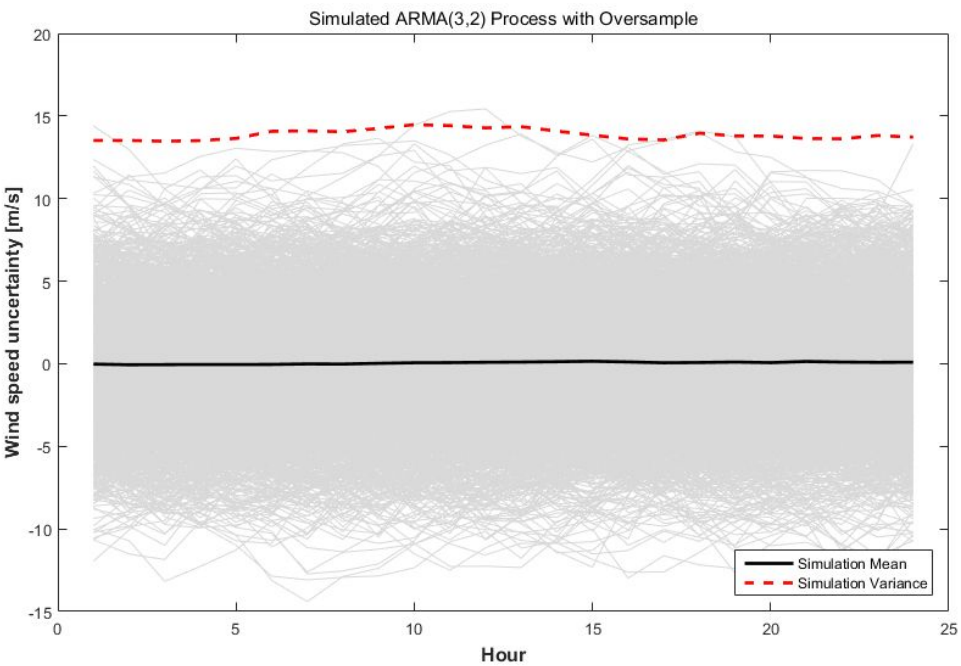

Figure 5.3 2000 scenarios of wind speed uncertainty

[18] These scenarios are based on the PJM metered load data, and their range is much larger than that of the six-bus system. Accordingly, the scenarios for this study were employed after scaling down the data.

As shown in Figure 5.3, the variance in the uncertainty of the wind speed model is stationary. These scenarios should be generated carefully because transient effects could arise that lead to non-constant variance. To avoid this issue, an oversampling technique is used, and this process is detailed in the Appendix.

Similar to the uncertainty of demand and wind speed, the operating conditions for the components were simulated using the Monte Carlo approach. The probability distribution model of the generator and transmission line was derived using FOR, which can be calculated from the mean up/down time in Tables 5.1 and 5.2. As mentioned before, it is assumed that the failed components cannot be repaired or replaced because the operation period considered in this study is too short. Multiple component failure and sequential outages are not considered for problem simplification.

After making 2000 probable scenarios with stochastic processes, scenario reduction algorithms were employed. Because of the computational complexity and time limitations, it was necessary to determine a scenario subset and allot the proper probabilities for each of the scenarios in the subset, rather than use all 2000 possible scenarios. Scenario reduction algorithms delete scenarios that are closely related or have a lower probability, and then update the new probability for the remaining scenarios. These preserved scenarios are closest to the original set of scenarios.

Based on this scenario reduction technique given by GAMS/SCENRED, ten scenarios for the uncertainty of the load and WPG were selected. The numerical value of each scenario and its probability are found in the Appendix, and the plots of each scenario are shown in Figure 5.4. Among the group, the bold long dash line

(series 5) is the most probable.[19] The entire uncertainty shown in the scenarios are biased towards negative values because of the unique uncertainty nature of WPG. WPG can increase to its rated output, while its output can only be decreased no less than zero; that is, the capacity to decline is confined.

In contrast with the load and WPG uncertainties, 12 scenarios for the operating conditions of the components were determined to represent all N-1 contingency scenarios, and they are listed in Table 5.4. Each of the scenarios from 2 to 12 implies a breakdown of the component in the six-bus system that comprises four generators and seven transmission lines.

[19] Its probability is 34.4%. The probabilities of the other scenarios are indicated in the Appendix.

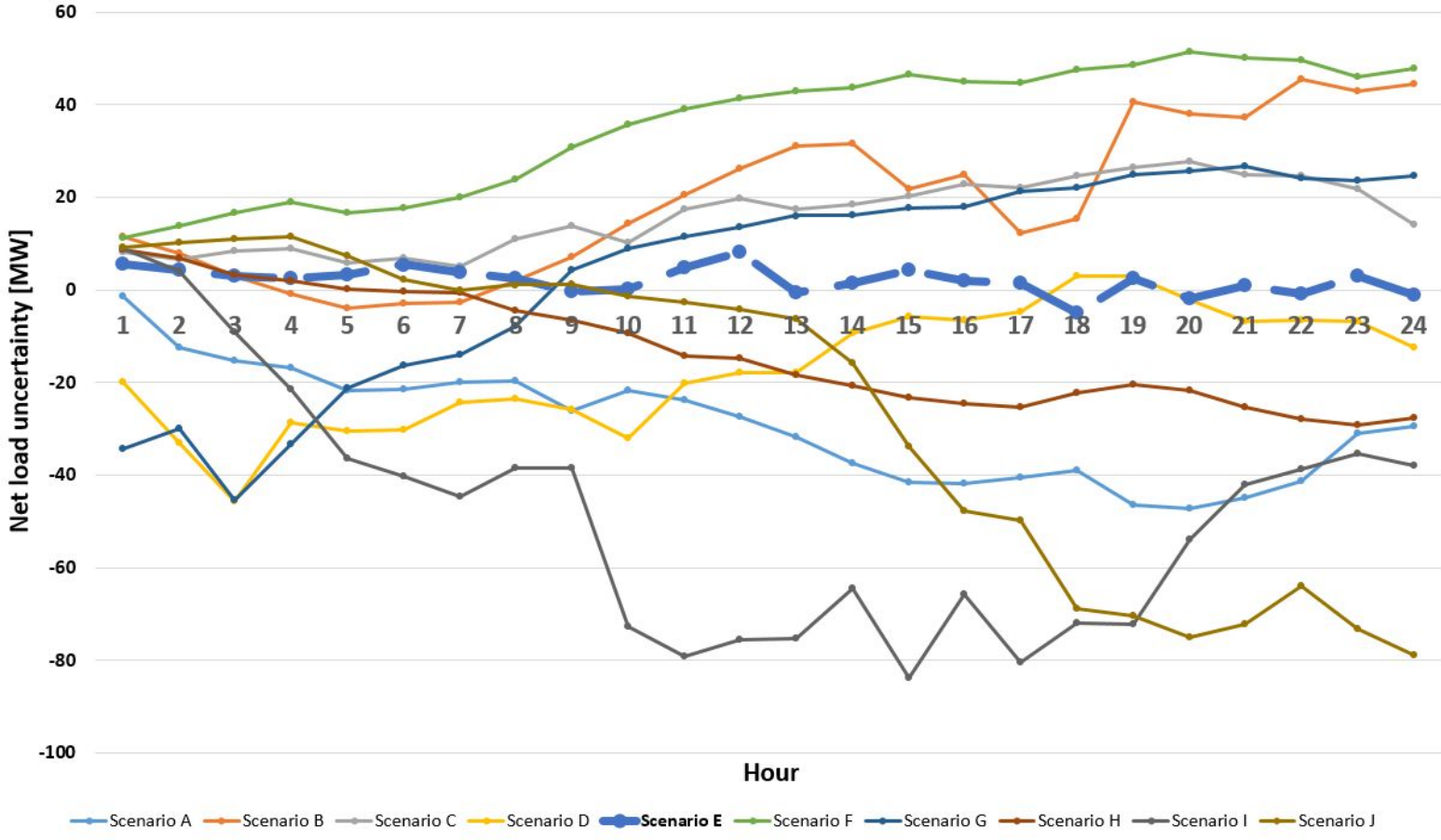

Figure 5.4 Ten representative scenarios of net load uncertainty

Table 5.4 Scenarios for operating conditions of components in the six-bus system[20]

	Gen. 1	Gen. 2	Gen. 3	Gen. 4	Tr. 1	Tr. 2	Tr. 3	Tr. 4	Tr. 5	Tr. 6	Tr. 7	Probability
Scenario 1	1	1	1	1	1	1	1	1	1	1	1	0.8605
Scenario 2	0	1	1	1	1	1	1	1	1	1	1	0.016
Scenario 3	1	0	1	1	1	1	1	1	1	1	1	0.014
Scenario 4	1	1	0	1	1	1	1	1	1	1	1	0.007
Scenario 5	1	1	1	0	1	1	1	1	1	1	1	0.008
Scenario 6	1	1	1	1	0	1	1	1	1	1	1	0.0235
Scenario 7	1	1	1	1	1	0	1	1	1	1	1	0.0125
Scenario 8	1	1	1	1	1	1	0	1	1	1	1	0.0135
Scenario 9	1	1	1	1	1	1	1	0	1	1	1	0.014
Scenario 10	1	1	1	1	1	1	1	1	0	1	1	0.0085
Scenario 11	1	1	1	1	1	1	1	1	1	0	1	0.0145
Scenario 12	1	1	1	1	1	1	1	1	1	1	0	0.008
Sum												1

[20] Zero in the table indicates that the component failed. For example, in the first row, Scenario 1 means that all the facilities are in healthy states.

5.1.2 Simulation Results

At first, the expected operating cost[21] is calculated for both SLR and DLR cases using the same procedure except for the transmission line rating, and the results of both approaches are compared. For each case, the optimization simulation is conducted based on the 120 total scenarios with 12 scenarios for state of components and 10 scenarios for varying load, wind speed and WPG. That is, in each scenario for states of components, 10 scenarios are generated to cover the uncertainties of other factors. Table 5.5 shows the resulting expected operating cost. Here, the operating cost comprises generation cost, spinning reserve cost and load shedding cost, as defined in subchapter 4.4.

Table 5.5 Comparison of DLR with SLR in generation scheduling (value of lost load = $1,000/MWh)

	Generation scheduling w/ DLR	Generation scheduling w/ SLR
Expected operating cost [$]	153,358.7	153,600.4
Cost savings [$]	241.7 (0.16%)	

In order to scrutinize the difference in the results between two approaches, the comparative study is conducted with the most probable scenario[22] (Scenario E) among normal conditions (Scenario 1). The dispatched volume of all generators after scenario realization are listed in Table 5.6 for DLR and Table 5.7 for SLR.

[21] This is the objective function of the generation scheduling optimization problem.

[22] The probability that this scenario occurs among all 120 scenarios is 0.296.

Table 5.6 Dispatched volume of generators with DLR for Scenario 1-E (MW)

	Hour 1	Hour 2	Hour 3	Hour 4	Hour 5	Hour 6	Hour 7	Hour 8	Hour 9	Hour 10	Hour 11	Hour 12
Gen 1	160.0	151.3	120.0	0	0	0	0	120.0	164.9	173.7	174.9	194.9
Gen 2	0	0	0	0	40.8	57.3	71.0	30.0	30.0	30.0	30.0	30.0
Gen 3	30.0	30.0	30.0	51.3	41.6	56.6	71.4	30.0	30.0	30.0	30.0	0
Gen 4	14.6	10.0	16.4	60.0	60.0	60.0	60.0	45.0	10.0	19.7	25.9	23.1
	Hour 13	Hour 14	Hour 15	Hour 16	Hour 17	Hour 18	Hour 19	Hour 20	Hour 21	Hour 22	Hour 23	Hour 24
Gen 1	182.1	169.4	174.6	177.4	167.8	173.2	177.5	183.6	190.4	180.9	173.3	164.1
Gen 2	30.0	30.0	30.0	30.0	30.0	30.0	30.0	30.0	30.0	30.0	30.0	30.0
Gen 3	0	0	30.0	30.0	30.0	30.0	30.0	30.0	30.0	30.0	30.0	30.0
Gen 4	14.5	16.5	19.1	18.0	11.3	10.0	28.8	32.4	36.4	15.6	19.7	10.0

Table 5.7 Dispatched volume of generators with SLR for Scenario 1-E (MW)

	Hour 1	Hour 2	Hour 3	Hour 4	Hour 5	Hour 6	Hour 7	Hour 8	Hour 9	Hour 10	Hour 11	Hour 12
Gen 1	134.6	120.0	0	0	0	0	120.0	177.5	190.3	173.7	174.9	194.9
Gen 2	30.0	30.0	53.3	30.0	41.6	57.3	0	0	0	30.0	30.0	0
Gen 3	30.0	30.0	53.1	30.0	40.8	56.6	30.0	30.0	30.0	30.0	30.0	30.0
Gen 4	10.0	11.3	60.0	51.3	60.0	60.0	52.3	17.5	14.6	19.7	25.9	23.1
	Hour 13	Hour 14	Hour 15	Hour 16	Hour 17	Hour 18	Hour 19	Hour 20	Hour 21	Hour 22	Hour 23	Hour 24
Gen 1	182.1	169.4	173.7	177.1	167.8	173.2	177.5	183.6	189.7	180.9	173.3	164.1
Gen 2	0	0	30.0	30.0	30.0	30.0	30.0	30.0	30.0	30.0	30.0	30.0
Gen 3	30.0	30.0	30.0	30.0	30.0	30.0	30.0	30.0	30.0	30.0	30.0	30.0
Gen 4	14.5	16.5	19.9	18.3	11.3	10.0	28.8	32.4	37.1	15.6	19.7	10.0

As revealed in the tables, it can be seen that the proposed DLR method made greater use of the cost-effective generating unit 1, whereas the outputs of the more expensive unit 2 and 3, were reduced at hours 15, 16, and 21.[23] These results can yield cost savings, especially in generation costs.[24] If the value of lost load is assumed to be $5,000/MWh, cost savings are increased, in other words; it can be confirmed that the suggested method is more effective. This is summarized in Table 5.8.

Table 5.8 Comparison of DLR with SLR in generation scheduling (value of lost load = $5,000/MWh)

	Generation scheduling w/ DLR	Generation scheduling w/ SLR
Expected operating cost [$]	160,610.2	161,538.4
Cost savings [$]	978.2 (0.61%)	

It is found that the total number of committed generators is reduced if DLR is applied to the generation scheduling. As shown in Table 5.6 and 5.7, the number of turned-on generators has not changed significantly. However, if considering only four generators are installed in this example, it can be expected that much difference would be shown in real power system with large number of generators installed.

The apparent power flow in the transmission lines when transmission line 3

[23] At hours 1–9, the UC result is different, and consequently, dispatched volumes are also different. Hence, only the rest of the hour is compared.
[24] In the normal condition—that is, if all components are heathy—load-shedding event is not triggered although there is uncertainties in the load and WPG.

fails in Scenario E (Scenario 8-E) is investigated by hour from 15 to 21 and included in Table 5.9 and Table 5.10 for the DLR and SLR cases, respectively.

Table 5.9 Apparent power flow in transmission lines with DLR for Scenario 8-E (MVA)

	Hour 15	Hour 16	Hour 17	Hour 18	Hour 19	Hour 20	Hour 21
Tr. 1	192.1	196.8	192.1	202.9	199.2	204.5	205.4
Tr. 2	133.7	128.3	135.4	141.8	135.7	137.9	137.5
Tr. 3	0	0	0	0	0	0	0
Tr. 4	105.7	109.7	103.3	107.6	111.7	115.1	116.7
Tr. 5	19.8	16.9	19.5	20.0	20.7	21.1	21.2
Tr. 6	121.1	122.6	116.8	120.7	129.3	133.5	136.2
Tr. 7	107.2	92.3	108.5	112.6	108.2	109.5	109.2

Table 5.10 Apparent power flow in transmission lines with SLR for Scenario 8-E (MVA)

	Hour 15	Hour 16	Hour 17	Hour 18	Hour 19	Hour 20	Hour 21
Tr. 1	186.4	195.7	187.2	198.2	194.6	200.1	186.4
Tr. 2	113.4	118.0	116.3	123.2	115.9	118.1	113.4
Tr. 3	0	0	0	0	0	0	0
Tr. 4	108.4	111.2	106.0	110.4	114.6	118.1	108.4
Tr. 5	7.2	9.9	7.0	7.3	8.2	8.4	7.2
Tr. 6	115.8	119.7	111.4	115.1	123.8	128.0	115.8
Tr. 7	58.1	64.9	62.4	67.0	56.8	57.1	58.1

It can be clearly shown that the power transfer limit in the DLR is extended compared to that of SLR, whose value is 267.4 MVA for transmission line 1 and 133.7 MVA for lines 2–7.[25] In other words, if the wind blows as anticipated[26], more power can be transferred via the transmission lines in reality. This is the most important characteristic of the DLR method.

[25] The power transfer limit is summarized in Table 5.2. The power transfer limit is calculated based on heat balance equation, of which parameter values are indicated in Appendix A.

[26] In scenario E, the actual wind speed closely follows as expected wind speed. The load level is also moderate in scenario E.

Next, the load shedding cost related to the expected energy not served in the system is examined for the comparison of DLR and SLR. Table 5.11 summarizes the result of the expected load shedding cost. This can be calculated by the product of the volume of load shedding $LS_{b,t}^{s}$, the value of lost load $VoLL_{b,t}$, and the probability of the corresponding load shedding scenario occurring. To indicate the reliability aspects, the expected volume of energy not served is also included in the second row of the table.

Table 5.11 comparison of load shedding cost and corresponding expected energy not served between DLR case and SLR case

	Generation scheduling w/ DLR	Generation scheduling w/ SLR
Expected load shedding cost [$]	6696.2	7158.3
Expected energy not served [MWh]	6.696	7.158

As shown in Table 5.11, the total volume of load shedding is expected to grow when SLR is applied to generation scheduling. The result seems reasonable because DLR allows more power to flow through the transmission line. The values in Table 5.11 correspond to the totaled UC outcomes of 24 hours. The reducing effect on expected energy not served brought by DLR cannot be distinguished from the anticipated decrease in expected energy not served attributed to different UC outcomes between DLR and SLR. Therefore, the expected energy not served in the case of DLR and SLR are investigated hour by hour as stated in Table 5.12.

Table 5.12 Volume of expected energy not served in generation scheduling (MW)[27]

	Hour 1	Hour 2	Hour 3	Hour 4	Hour 5	Hour 6	Hour 7	Hour 8	Hour 9	Hour 10	Hour 11	Hour 12
EENS w/ DLR	0.472	0.434	0.412	0.340	0.002	0.014	0.183	0.002	0.012	0.055	0.139	1.101
EENS w/ SLR	0	0	0.008	0	0	0.131	0.510	0.679	0.900	0.055	0.112	1.109
Difference	0.472	0.434	0.403	0.340	0.002	-0.117	-0.327	-0.677	-0.888	0.000	0.027	-0.008
	Hour 13	Hour 14	Hour 15	Hour 16	Hour 17	Hour 18	Hour 19	Hour 20	Hour 21	Hour 22	Hour 23	Hour 24
EENS w/ DLR	0.823	0.636	0.130	0.175	0.064	0.140	0.251	0.330	0.504	0.238	0.159	0.081
EENS w/ SLR	0.823	0.620	0.125	0.173	0.064	0.140	0.264	0.404	0.558	0.243	0.159	0.081
Difference	0	0.017	0.005	0.002	0	0	-0.013	-0.074	-0.055	-0.004	0	0

[27] It is expected that no load shedding occurs at hours 1, 2, 4 and 5 in SLR method.

Although more power can be transferred through the line in the DLR approach, the expected energy not served increases during hours 1–5. This contradictory result emanates from the different UC results between DLR and SLR case. However, load shedding arises more frequently in DLR than in SLR even in the periods of hour 11 and hours 15–16, when the UC results are exactly the same in DLR and SLR case. The reason for this unexpected result is due to the discrepancy in wind speed between the worst scenario determined with SLR (the wind speed of the worst scenario is assumed to be 0.5 m/s) and the realized scenarios. In the realized scenarios, scenarios with severe operating conditions such as harsh wind condition where wind speed is close to 0 m/s are included, whereas these conditions and resulting load shedding costs are mostly neglected in the SLR case. Hence, it should be noted that existing generation scheduling with consideration of SLR can overestimate the flow limit and overlook the probability of load shedding, which may incur erroneous costs and lead to a non-optimal solution.

To verify that SLR may bring overestimation of the line capacity, the corresponding case is examined by calculating the transmission line temperature with the heat balance equation. The changes in the temperature of the transmission lines are depicted in Figures 5.5–5.7.[28] The horizontal dashed line in each figure indicates the maximum allowable temperature $T_l^{\max}$, which is set to 100°C in this study. As seen in the figures, the line temperature exceeds the limit when generation scheduling is performed based on SLR.

[28] Line temperature especially increases when one of the component in the system fails and the wind speed is low. The Scenarios 4-A and 7-B come under this category.

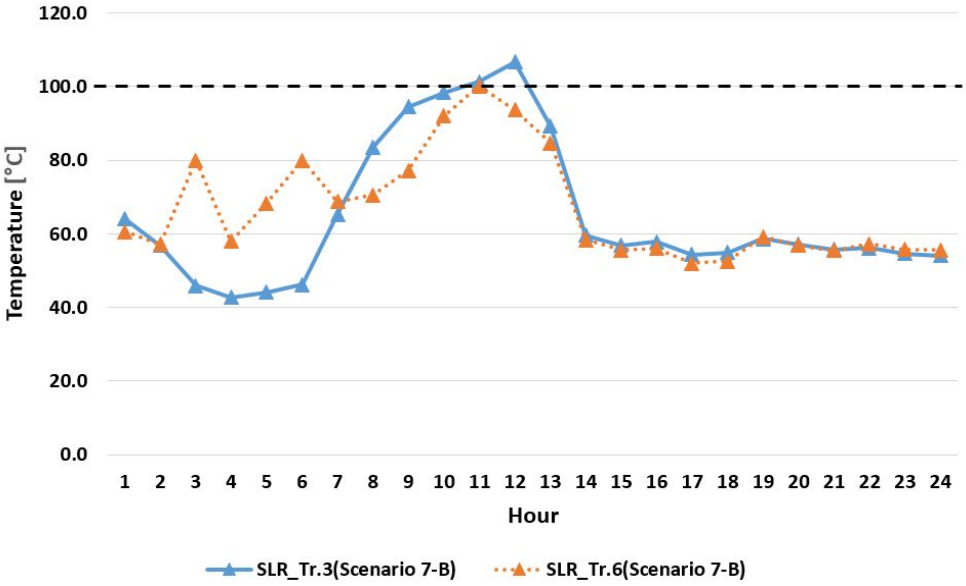

Figure 5.5 Hourly transmission line temperature (SLR Case)[29]

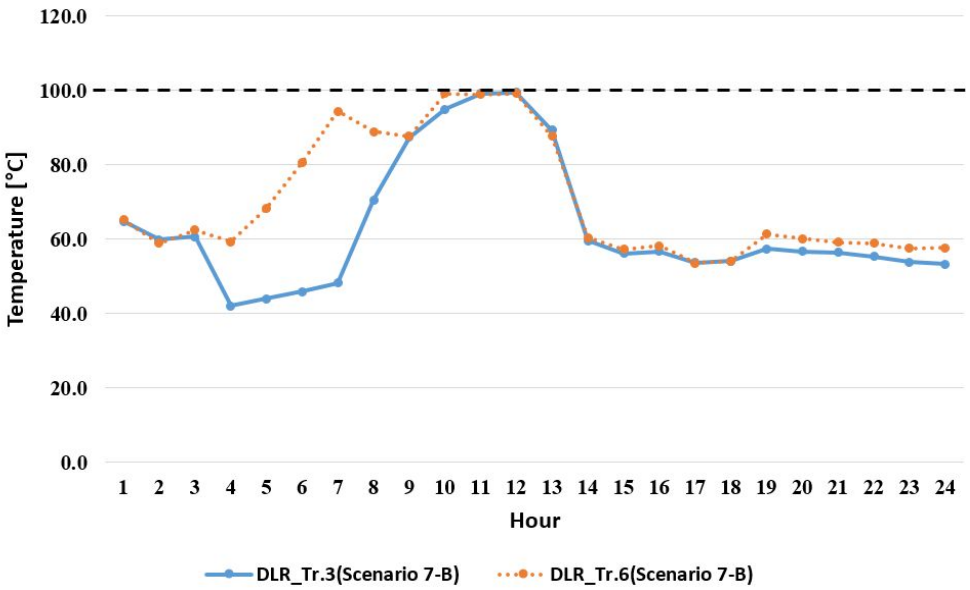

Figure 5.6 Hourly transmission line temperature (DLR Case)

[29] The exact temperature of transmission 6 at hour 11 for the SLR case(dotted line) is 100.2°C, which is beyond the thermal limit.

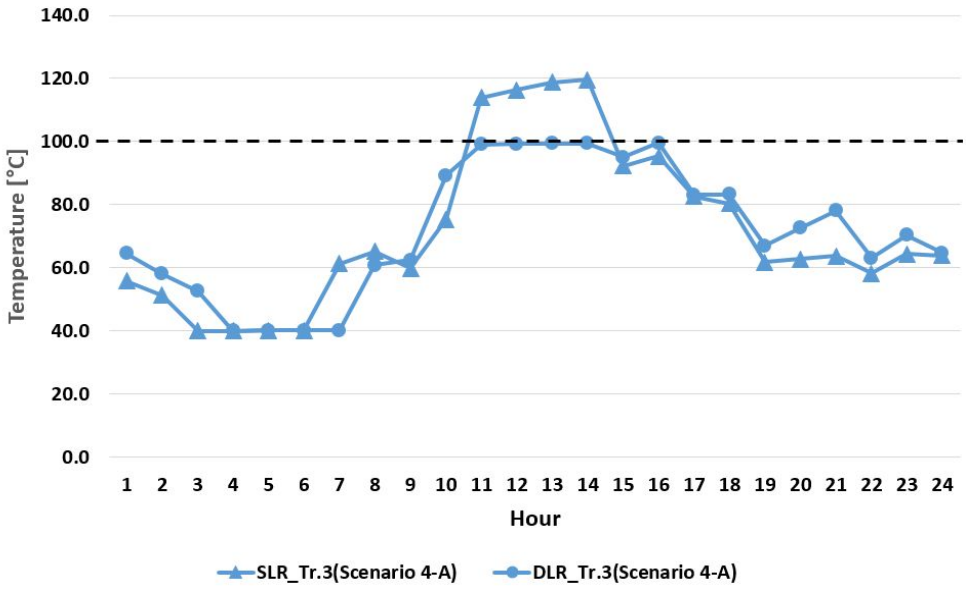

Figure 5.7 Comparison of hourly transmission line temperature (Scenario 4-A)

In contrast to the SLR cases, it can be confirmed that the temperature of the transmission lines in the DLR cases is kept below the maximum allowable bound at all times. In other words, load shedding and/or generation dispatch are conducted in accordance with the temperature limit in DLR cases, but not in SLR cases. This large point of difference induces a difference in the volume of expected energy not served, as mentioned in Table 5.11.

To analyze the effect of overestimation of SLR, the transfer limit of the line is recalculated assuming a condition where natural convection—instead of forced convection—cools the line at the wind speed is 0 m/s. The limit calculated with this new assumption is 214 MVA for line 1, and 107 MVA for the other lines which are much less than previous values specified in Table 5.2.[30] The result of operating

[30] The transfer limit is recalculated based on the parameters same as those used in the SLR case except for the wind speed.

system cost is listed in Table 5.13.

Table 5.13 Expected cost for six-bus system operation

	Operating cost [$]	Generation cost [$]	Startup cost[$]	Load shedding cost [$]
Generation scheduling w/ DLR	153,358.7	146,262.5	400	6,696.2
Generation scheduling w/ SLR*	164,299.4	148,584.4	300	15,415.0
Cost savings [$]	10,940.8 (7.13%)			

SLR*: transfer limit is recalculated based on the 0 m/s of wind speed

As revealed in Table 5.13, applying the DLR method in generation scheduling can cut down the operating cost, especially in load shedding cost. This advantage comes from fully utilizing the capacity of network resources, which leads to reduced volume of expected energy not served and to greater use of the cost-effective generating units. However, the startup cost increases slightly in the proposed approach, due to the frequent changes in states of generating units. On the other hand, most of the generators are unceasingly turned on in SLR*, and thus, start-up events are hardly discovered.

In addition to the comparison of the conventional generation cost, the actually used volume of WPG in the entire scheduling time is examined. This result is summarized in Table 5.14 and total used volume during the entire day in the system is shown in Table 5.15.

Table 5.14 Actually used WPG in entire scheduling time (MW)

	Hour 1	Hour 2	Hour 3	Hour 4	Hour 5	Hour 6	Hour 7	Hour 8	Hour 9	Hour 10	Hour 11	Hour 12
WPG w/ DLR	5.89	6.35	3.87	4.28	4.39	3.05	2.98	1.98	3.50	6.18	4.49	3.45
WPG w/ SLR*	5.67	5.04	5.84	4.28	4.39	3.05	2.96	1.97	3.49	6.15	4.47	3.33
Difference	0.22	1.32	-1.98	0.00	0.00	0.00	0.02	0.01	0.01	0.03	0.02	0.12
	Hour 13	Hour 14	Hour 15	Hour 16	Hour 17	Hour 18	Hour 19	Hour 20	Hour 21	Hour 22	Hour 23	Hour 24
WPG w/ DLR	7.18	6.87	9.02	11.32	13.51	16.74	11.19	10.33	8.13	6.41	3.11	3.30
WPG w/ SLR*	6.78	6.46	8.95	11.20	13.35	16.52	11.07	10.22	8.06	6.38	3.08	3.28
Difference	0.39	0.42	0.08	0.12	0.16	0.22	0.12	0.11	0.07	0.04	0.02	0.02

Table 5.15 Actually used WPG during a scheduling time (MW)

	Hour 1 – Hour 24
WPG w/ DLR	157.52
WPG w/ SLR*	155.97
Difference	1.55

The result in the tables demonstrates that the higher volume of WPG effectively supplies the system in the DLR case; that is, wind spillage can be reduced.[31] The reason for this is that when there is more wind energy, there is also more convective heat loss which enhances the capacity of the transmission line. This advantageous effect can be reflected only in the DLR.

Next, the simulation is conducted to analyze the effects of DSR in the generation scheduling. The cost of energy for DSR, which is the energy cost of the interruptible load was assumed to be $100/MWh, and the contract cost for was set to $10/MWh. This demand-side energy cost is roughly three times higher than that of the generating units. It is assumed that no more than 30% of the expected total load is available to take part as DSR in the system operation. Table 5.16 summarizes the changes in the expected operating cost and the total number of committed units with the participation of DSR. The contracted volume of DSR at bus 4 is shown in Figure 5.8.

Table 5.16 Expected operating cost with consideration of DSR

	Expected operating cost [$]	Total number of committed generators			
Generation scheduling w/ DSR	151,529.8	1~6 h	7~12 h	13~18 h	19~24 h
		332233	333333	333333	333333
Generation scheduling w/o DSR	153,358.7	1~6 h	7~12 h	13~18 h	19~24 h
		443333	333443	334444	444443
Cost savings [$]	1,828.9 (1.21 %)				

[31] This result was not applicable at hour 3 when the different types of generating units were turned on. In the DLR case, WPG had to be curtailed because of the minimum output constraint of conventional generators.

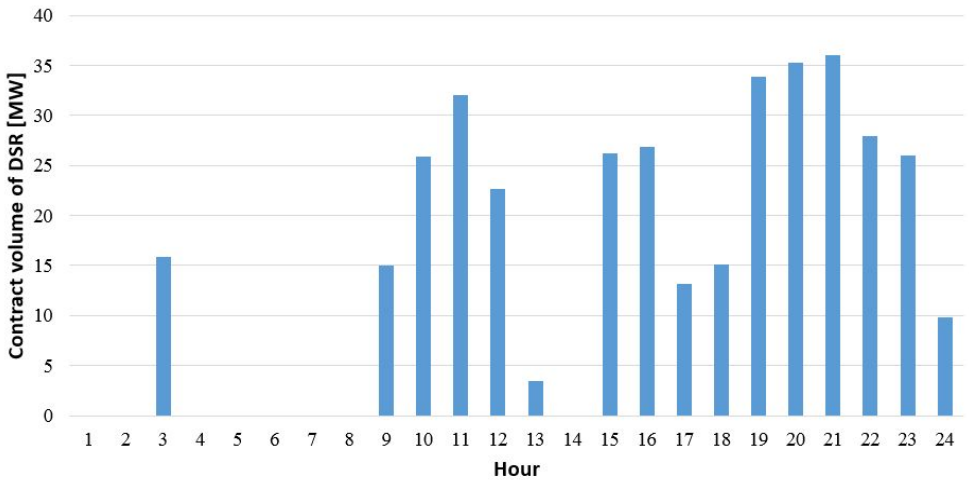

Figure 5.8 Contracted volume of DSR at bus 4

It can be confirmed that few units were turned off after considering DSR in generation scheduling, especially in the peak load. As shown in the Figure 5.8, the awarded volume of DSR is very different from hour to hour. This is one of the main advantages in which the tailored and required volume can be procured through DSR in contrast to conventional generators constrained by physical properties. The dispatched output of each generator in the first stage[32] was also altered to minimize the operating costs. Because the spinning reserve from online generators was exhausted before the interruptible load was utilized, DSR was barely used in actual operation. Therefore, DSR energy cost hardly affected the total expected operating cost.

Finally, optimal generation scheduling is found considering the deloaded control of wind power. The available deloaded volume is set as 10% of its expected WPG given the physical limitation of the machine. The results are depicted in

[32] This volume affects the spinning reserve contribution of each generators.

Figure 5.9 and Table 5.17.

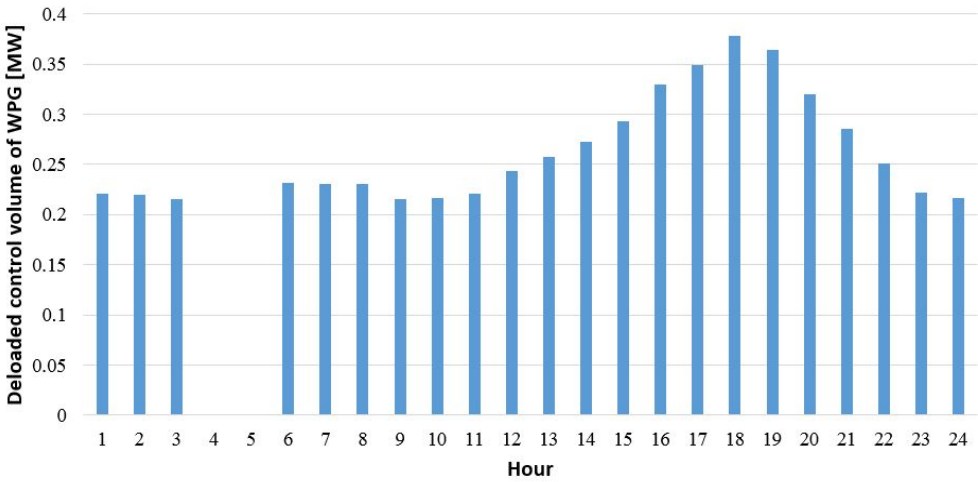

Figure 5.9 Deloaded control volume of WPG at bus 5

Table 5.17 Expected operating cost with consideration of WPG reserve

	Expected operating cost[$] -DLR case	Expected operating cost[$] -SLR case
Generation scheduling w/ WPG reserve	153,076.9	153,145.1
Generation scheduling w/o WPG reserve	153,358.7	153,600.4

Similar to the characteristic of DSR, the desirable level of the reserve from wind power can be decided independently from the sequence of time steps. It should be noted that most of the time, it is useful to procure the reserve from wind power in spite of the fact that the conventional generators must make up for the deloaded amount. The reason for this is that this study contemplates the uncertainty such as N–1 contingency, forecast error in the load and WPG where great emphasis

is placed on the reserve procurement. With this new type of reserve resource, SO can schedule differently compared to the existing approach, and make provision for the unexpected condition.

5.2 Modified IEEE 118-Bus System

5.2.1 Simulation Settings

In this subchapter, to test the scalability of this dissertation's approach, the generation scheduling problem is performed based on the modified IEEE 118-bus system. The entire procedure is similar to that in previous chapter but for the test system. The IEEE 118-bus test system consists of 54 generators and 186 branches, with a peak load of 6000 MW occurring at hour 21. All of these facilities are placed as shown in Figure 5.10. The specific data of units, branches, and demand are included in the Appendix.

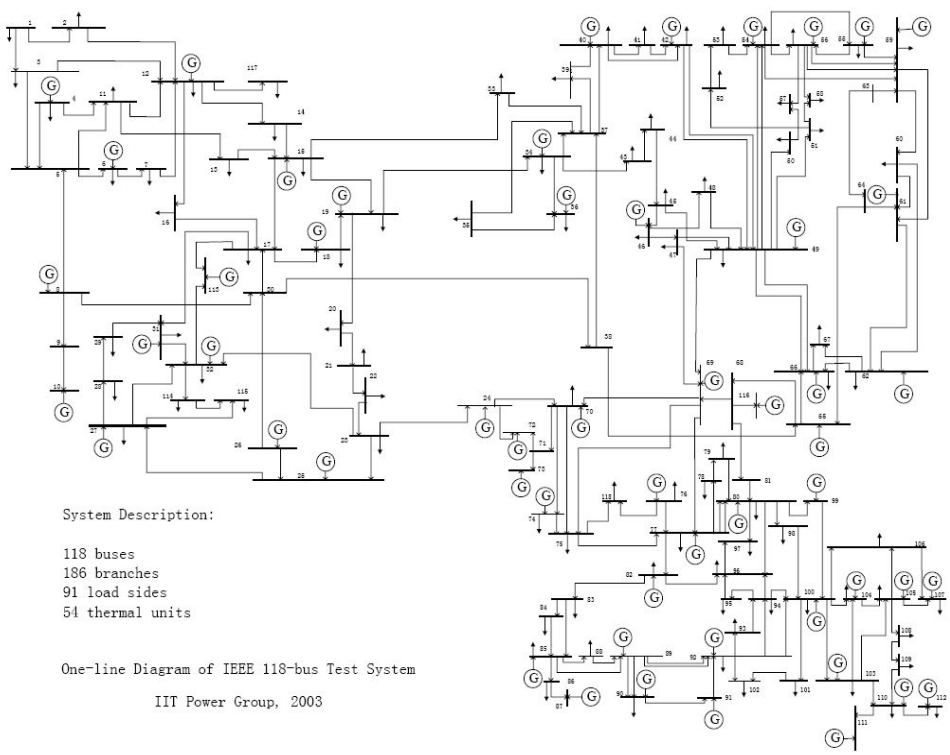

Figure 5.10 One-line diagram for IEEE 118-bus system

In contrast to the original IEEE 118-bus system where it comprises only conventional generators, wind power generators are installed in the system in this dissertation. The installed capacity is set to 1500MW, in which the proportions of 50%, 30%, and 20% of the WPG are distributed at buses of 15, 54, and 80, respectively. It is assumed that the forecasted wind speed is the same as that of the six-bus system.

Similar to the six-bus case, the uncertainties of the wind speed and system load are produced using the Monte Carlo method, and then WPG is calculated according to the generated wind speed. The scenario reduction technique is also used for reducing the computational complexity and the representative scenarios are chosen. The power transfer limit in the SLR and DLR are determined through the same approach used in the six-bus system case.

However, when simulating this large power system, the two transmission lines in the largest current loading condition are selected to be tripped out to test the security of the system operation.[33] In the normal condition, because transmission lines 128 and 159 are heavily loaded, these two components are subject to be tripped out. In addition, rather than testing the reliability of the system by means of load shedding cost[34], the volume of the expected energy not served is constrained to be zero to secure the robustness of system operation; in other words, no load shedding is allowable in this 118-bus system.

[33] In the case of six-bus system, all N-1 contingency scenarios are considered.

[34] In reliability aspects, the load shedding cost is compared to show the effectiveness of the proposed method in the six-bus system case.

5.2.2 Simulation Result

The expected operating cost is calculated for the SLR and DLR cases through the same procedure used in the previous six-bus system. Table 5.18 shows the resultant expected operating cost and the corresponding cost savings.

Table 5.18 Comparison of DLR with SLR in generation scheduling

	Generation scheduling w/ DLR	Generation scheduling w/ SLR
Expected operating cost [$]	1,552,459.5	1,554,403.8
Cost savings [$]	1,944.3 (0.13%)	

As shown in Table 5.18, the expected operating cost can be reduced if generation scheduling is determined with consideration of DLR. However, contrary to the six-bus system case, SO can create major cost savings by fully utilizing cost-effective units and making good use of WPG.[35] The detailed result of the UC and dispatch volume of generators are included in the Appendix.

Finally, the computational time required to solve the generation scheduling problem via each of the two approaches was evaluated. To avoid considerable variation in computational time depending on the relation between multiple scenarios, the computational time is measured and compared based on only one scenario. Table 5.19 lists the computational times for the different methods.

[35] The main contribution of cost savings in the six-bus test system is reduced load shedding costs.

Table 5.19 Comparison of the computational time

	Generation scheduling w/ DLR	Generation scheduling w/ SLR
Computational time [s]	63.220	49.626

The elapsed time for solving the optimization problem indicates that the computational burdens are slightly increased if generation scheduling is conducted with DLR. This is due to the additionally included constraints regarding heat balance equations and allowable temperature limits. However, the increases in computational times is not excessive thanks to the reduced non-linearity of the mathematical formulation.

Although, in this dissertation, all transmission lines in the power system are investigated whether the line temperature is above the threshold, it is also possible to select a specific line and check the selected line temperature. This method can greatly relieve the computational burdens while sustaining the economic advantages and operating the power system reliably.

Chapter 6 Conclusions and Future Works

6.1 Conclusions

This dissertation proposed daily generation scheduling that utilizes DSR and wind power as reserves to manage increased uncertainty. Conventionally SLR is used for the network constraint when optimizing the scheduling process. However, a constant line rating across time may dissipate network resources, especially under conditions where heat can be easily dispersed: abundant wind, low ambient temperature, and low solar radiations. Therefore, DLR was considered as the power flow limit for the transmission line in this dissertation. Newly introduced uncertainty that originates from DLR was also properly managed by the suggested stochastic generation scheduling problem. The uncertainty in load forecast was expressed using the time series model after analyzing real metered data in-depth. The wind speed forecast error was also designed as a time series model in order to reflect the tendency of time sequential change. Equipment failures were modeled via a Markov chain.

The performance of the proposed generation scheduling was verified using a six-bus system and modified IEEE 118-bus system integrated with wind power units. All the constraints and objective functions were converted to mixed integer linear forms in order to solve the optimization problem by applying the MILP problem generally adopted in practical system operation. The expected operating costs that comprise the generation, reserve, DSR, and load-shedding costs were minimized in the optimization problem. The expected energy not supplied was also compared to analyze reliability. The simulation results clearly demonstrated that with DLR, SO could reduce the expected operating costs significantly. This

advantage stems from sufficient utilization of the existing transmission line, which leads to optimal commitment of the generating units and dispatched volume. The expected energy not served was also drastically decreased by incorporating DLR.

The simulation results showed that additional cost savings can be achieved with demand-side participation and deloaded control of WPG. It can be interpreted that DSR and reserve from wind power are capable of managing the increased uncertainty due to wind power integration with desired reliability.

The generation scheduling suggested in this dissertation can be practically used in power system operations. It is plain that incorporating DLR in generation scheduling can result in computational complexity. Moreover, using DLR has a demerit in a sense that securing a predetermined margin in the transmission rating is more difficult, which may lead to reliability problem. However, the process of selecting the specific line and testing the temperature of the only selected line, can relieve the computational burdens. Also the concerns that SO could not manage the risk, which is the inherent disadvantage of stochastic processes, can be alleviated. The detailed description on this relieving technique and other future extensions related to this dissertation follows in the next subchapter.

6.2 Future Works

The proposed strategies indeed enhance the flexibility of transmission operations and reduce operating costs as verified in the case study from the previous Chapter 5. However, there remain further questions, and future works will be required to develop a better approach.

Flow Limit-Constrained Dynamic Line Rating

Incorporating DLR into generation scheduling results in an indefinite flow limit for system operation. Although refined scenarios that consider various unexpected conditions are recognized in the generation scheduling problem, it is difficult for SO to ensure that a desired level of margin is secured from stochastic generation scheduling. One way to answer this question is to insert a minimum flow limit into the stochastic problem. This type of flow limit should not be confused with SLR. While SLR is the only constraint that restricts power flow for stable transmission operation, inserting a minimum flow limit aims to complement DLR in order to prevent too "incautiously" calculated ratings.

More Refined Stochastic Generation Scheduling and Congestion Management Related to Dynamic Line Rating

When generating scenarios to be used as an input to the stochastic generation scheduling, the operating conditions of the power system are not reflected. In other words, the scenarios based on FOR for the generator alone cannot capture the results of generator commitment. The demand varies as a function of time and the committed state of the generators also varies, whereas FOR for generators is

constant with time. Similar to the method described in Figure 6.1 [67], recursive generation scheduling can overcome this potential limitation.

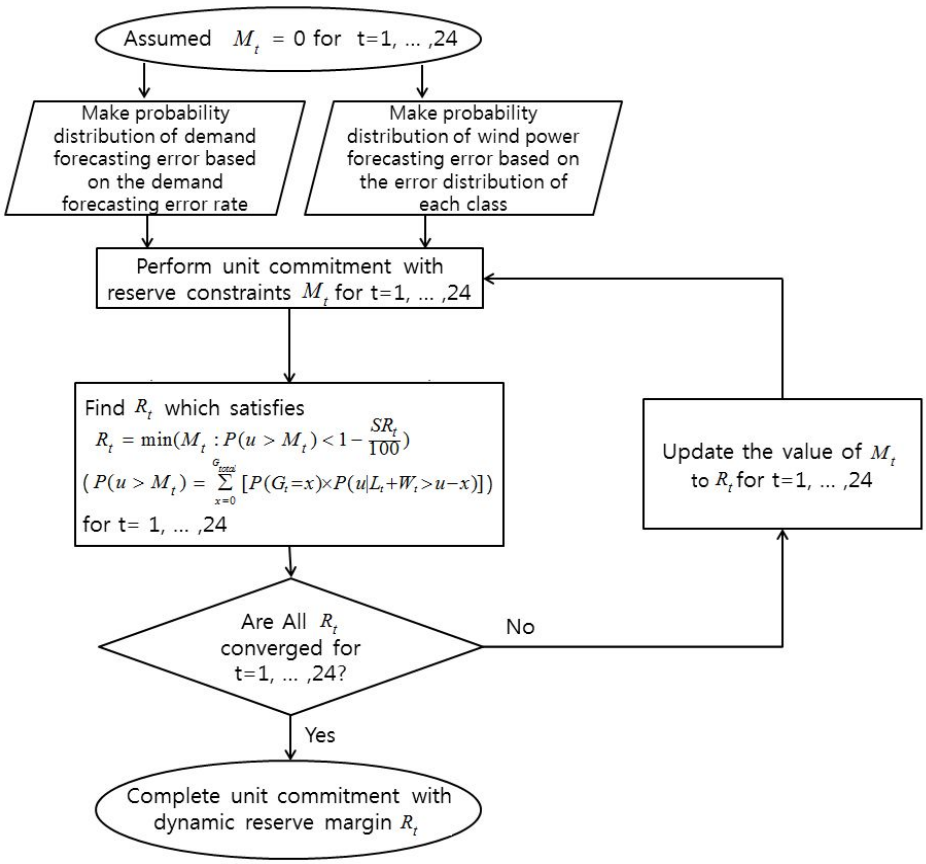

Figure 6.1 Recursive method for determining hourly spinning reserve margin

On the other hand, the congestion management scheme might change if generation scheduling is conducted with DLR. This is because the transmission line where the congestion mainly occurred can be changed because of the introduction of new approaches. Hence, the effect of DLR on congestion management strategies should be investigated.

Stability Limit on Generation Scheduling

As mentioned in Chapter 2, transmitting power from one point to another is confined not only by the thermal limit, which is mainly considered in this dissertation, but also by the voltage and stability limits. Although voltage can be controlled by various locally installed facilities and it is not critical to the power flow constraint, a stability limit study still should be conducted for the power flow limit, especially for the case where the transmission line is very long. For instance, all the lines placed in South Korea can be considered to be governed by the thermal limit because the lines are sufficiently short. However, for the case of other power system with long lines involved, stability limit should be essentially checked for reliable operation.

Reserved-Constrained Stochastic Unit Commitment

The stochastic UC method is advantageous in terms of expected cost, but it is insufficient in terms of the reliability associated with load shedding. An increase in the number of representative scenarios can improve reliability; however, such an increase is difficult to achieve on account of the computational problem. Instead, a procedure that comprises multiple stages can be proposed. This can be constructed as follows: first, obtain the base stochastic UC solution using the same small number of representative scenarios. Subsequently, modify the initial solution with consideration of the required operating reserve. The amount of required reserve can be computed to satisfy the target reliability level. This final solution is more reliable in terms of a reduced load-shedding amount and more economical with regard to a reduced expected operating cost compared with the solution from the basic stochastic UC method.

Bibliography

[1] B. Hamilton, "U.S. Wind Market Outlook - Pathways to Competitiveness," AWEA WINDPOWER 2015, 2015.

[2] E. Martinez-Cesena and J. Mutale, "Impact of wind speed uncertainty and variability on the planning and design of wind power projects in a smart grid environment," in Innovative Smart Grid Technologies (ISGT Europe), 2011 2nd IEEE PES International Conference and Exhibition on, 2011, pp. 1-8.

[3] M. Simms and L. Meegahapola, "Comparative analysis of dynamic line rating models and feasibility to minimise energy losses in wind rich power networks," Energy Conversion and Management, vol. 75, pp. 11-20, 2013.

[4] T. Ringelband, M. Lange, M. Dietrich, and H.-J. Haubrich, "Potential of improved wind integration by dynamic thermal rating of overhead lines," in PowerTech, 2009 IEEE Bucharest, 2009, pp. 1-5.

[5] B. Banerjee, D. Jayaweera, and S. Islam, "Impact of wind forecasting and probabilistic line rating on reserve requirement," in Power System Technology (POWERCON), 2012 IEEE International Conference on, 2012, pp. 1-6.

[6] A. K. Kazerooni, J. Mutale, M. Perry, S. Venkatesan, and D. Morrice, "Dynamic thermal rating application to facilitate wind energy integration," in PowerTech, 2011 IEEE Trondheim, 2011, pp. 1-7.

[7] L. Xie, P. M. Carvalho, L. A. Ferreira, J. Liu, B. H. Krogh, N. Popli, et al., "Wind integration in power systems: Operational challenges and possible solutions," Proceedings of the IEEE, vol. 99, pp. 214-232, 2011.

[8] J. MacDowell, S. Dutta, M. Richwine, S. Achilles, and N. Miller, "Serving the Future: Advanced Wind Generation Technology Supports Ancillary Services," Power and Energy Magazine, IEEE, vol. 13, pp. 22-30, 2015.

[9] J. DeCesaro, K. Porter, and M. Milligan, "Wind energy and power system operations: A review of wind integration studies to date," The Electricity Journal, vol. 22, pp. 34-43, 2009.

[10] M. Albadi and E. El-Saadany, "Overview of wind power intermittency impacts on power systems," Electric Power Systems Research, vol. 80, pp. 627-632, 2010.

[11] J. Wang, A. Botterud, R. Bessa, H. Keko, L. Carvalho, D. Issicaba, et al., "Wind power forecasting uncertainty and unit commitment," Applied Energy, vol. 88, pp. 4014-4023, 2011.

[12] H. Gooi, D. Mendes, K. Bell, and D. Kirschen, "Optimal scheduling of spinning reserve," Power Systems, IEEE Transactions on, vol. 14, pp. 1485-1492, 1999.

[13] F. Bouffard and F. D. Galiana, "An electricity market with a probabilistic spinning reserve criterion," Power Systems, IEEE Transactions on, vol. 19, pp. 300-307, 2004.

[14] M. A. Ortega-Vazquez and D. S. Kirschen, "Optimizing the spinning reserve requirements using a cost/benefit analysis," Power Systems, IEEE Transactions on, vol. 22, pp. 24-33, 2007.

[15] D. Pozo and J. Contreras, "A chance-constrained unit commitment with an security criterion and significant wind generation," Power Systems, IEEE Transactions on, vol. 28, pp. 2842-2851, 2013.

[16] J. M. Morales, A. J. Conejo, and J. Pérez-Ruiz, "Economic valuation of

reserves in power systems with high penetration of wind power," Power Systems, IEEE Transactions on, vol. 24, pp. 900-910, 2009.

[17] M. A. Ortega-Vazquez and D. S. Kirschen, "Estimating the spinning reserve requirements in systems with significant wind power generation penetration," Power Systems, IEEE Transactions on, vol. 24, pp. 114-124, 2009.

[18] A. Botterud, Z. Zhou, J. Wang, J. Valenzuela, J. Sumaili, R. Bessa, et al., "Unit commitment and operating reserves with probabilistic wind power forecasts," in PowerTech, 2011 IEEE Trondheim, 2011, pp. 1-7.

[19] P. Carpentier, G. Gohen, J.-C. Culioli, and A. Renaud, "Stochastic optimization of unit commitment: a new decomposition framework," Power Systems, IEEE Transactions on, vol. 11, pp. 1067-1073, 1996.

[20] P. A. Ruiz, C. R. Philbrick, E. Zak, K. W. Cheung, and P. W. Sauer, "Uncertainty management in the unit commitment problem," Power Systems, IEEE Transactions on, vol. 24, pp. 642-651, 2009.

[21] A. Tuohy, P. Meibom, E. Denny, and M. O'Malley, "Unit commitment for systems with significant wind penetration," Power Systems, IEEE Transactions on, vol. 24, pp. 592-601, 2009.

[22] A. Papavasiliou, S. S. Oren, and R. P. O'Neill, "Reserve requirements for wind power integration: A scenario-based stochastic programming framework," Power Systems, IEEE Transactions on, vol. 26, pp. 2197-2206, 2011.

[23] H.-G. Park, J.-K. Lyu, Y. Kang, and J.-K. Park, "Unit Commitment Considering Interruptible Load for Power System Operation with Wind Power," Energies, vol. 7, pp. 4281-4299, 2014.

[24] F. Aminifar, M. Fotuhi-Firuzabad, and M. Shahidehpour, "Unit commitment with probabilistic spinning reserve and interruptible load considerations," Power Systems, IEEE Transactions on, vol. 24, pp. 388-397, 2009.

[25] L.-R. Chang-Chien, C.-C. Sun, and Y.-J. Yeh, "Modeling of wind farm participation in AGC," Power Systems, IEEE Transactions on, vol. 29, pp. 1204-1211, 2014.

[26] K. De Vos and J. Driesen, "Active participation of wind power in operating reserves," Renewable Power Generation, IET, vol. 9, pp. 566-575, 2015.

[27] X. Tang, B. Fox, and K. Li, "Reserve from wind power potential in system economic loading," Renewable Power Generation, IET, vol. 8, pp. 558-568, 2014.

[28] J. Heckenbergerova and J. Hosek, "Dynamic thermal rating of power transmission lines related to wind energy integration," in Environment and Electrical Engineering (EEEIC), 2012 11th International Conference on, 2012, pp. 798-801.

[29] H. Banakar, N. Alguacil, and F. D. Galiana, "Electrothermal coordination part I: Theory and implementation schemes," Power Systems, IEEE Transactions on, vol. 20, pp. 798-805, 2005.

[30] N. Alguacil, M. H. Banakar, and F. D. Galiana, "Electrothermal coordination part II: Case studies," Power Systems, IEEE Transactions on, vol. 20, pp. 1738-1745, 2005.

[31] M. Nick, O. Alizadeh-Mousavi, R. Cherkaoui, and M. Paolone, "Security Constrained Unit Commitment<? Pub _newline?> With Dynamic Thermal Line Rating," 2015.

[32] O. I. Elgerd, "Electric energy systems theory: an introduction," 1982.

[33] P. Kundur, N. J. Balu, and M. G. Lauby, Power system stability and control vol. 7: McGraw-hill New York, 1994.

[34] A. R. Bergen, Power systems analysis: Pearson Education India, 2009.

[35] I. S. 738-2012, "IEEE Standard for Calculating the Current-Temperature Relationship of Bare Overhead Conductors," Transmission and Distribution Committee of the IEEE Power Engineering Society, 2013.

[36] "The thermal behavior of overhead line conductors," Cigre Working Group 22., 12. 1992.

[37] A. Arroyo, P. Castro, R. Martinez, M. Manana, A. Madrazo, R. Lecuna, et al., "Comparison between IEEE and CIGRE Thermal Behaviour Standards and Measured Temperature on a 132-kV Overhead Power Line," Energies, vol. 8, pp. 13660-13671, 2015.

[38] L. Staszewski and W. Rebizant, "The differences between IEEE and CIGRE heat balance concepts for line ampacity considerations," in Modern Electric Power Systems (MEPS), 2010 Proceedings of the International Symposium, 2010, pp. 1-4.

[39] 조종만, "송전선로의 동적송전용량 산정과 합리적 운영방안에 관한 연구-A Study on the Dynamic Line Rating and the Operation of Transmission Lines," Hanyang University Doctoral Thesis, 2006. 8.

[40] F. Bouffard and M. Ortega-Vazquez, "The value of operational flexibility in power systems with significant wind power generation," in Power and Energy Society General Meeting, 2011 IEEE, 2011, pp. 1-5.

[41] J. Aghaei and M.-I. Alizadeh, "Demand response in smart electricity grids

equipped with renewable energy sources: A review," Renewable and Sustainable Energy Reviews, vol. 18, pp. 64-72, 2013.

[42] O. Ekren and B. Y. Ekren, Size optimization of a solar-wind hybrid energy system using two simulation based optimization techniques: INTECH Open Access Publisher, 2011.

[43] R. H. Shumway and D. S. Stoffer, Time series analysis and its applications: with R examples: Springer Science & Business Media, 2010.

[44] A. Naimo, "A Novel Approach to Generate Synthetic Wind Data," Procedia-Social and Behavioral Sciences, vol. 108, pp. 187-196, 2014.

[45] R. Billinton, H. Chen, and R. Ghajar, "Time-series models for reliability evaluation of power systems including wind energy," Microelectronics Reliability, vol. 36, pp. 1253-1261, 1996.

[46] J. Aho, A. Buckspan, J. Laks, P. Fleming, Y. Jeong, F. Dunne, et al., "A tutorial of wind turbine control for supporting grid frequency through active power control," in American Control Conference (ACC), 2012, 2012, pp. 3120-3131.

[47] J. M. Jonkman, S. Butterfield, W. Musial, and G. Scott, "Definition of a 5-MW reference wind turbine for offshore system development," ed: National Renewable Energy Laboratory Golden, CO, USA, 2009.

[48] R. Allan, Reliability evaluation of power systems: Springer Science & Business Media, 2013.

[49] R. Billinton and R. N. Allan, Reliability evaluation of engineering systems: Springer, 1992.

[50] J. A. Muckstadt and S. A. Koenig, "An application of Lagrangian relaxation to scheduling in power-generation systems," Operations research,

vol. 25, pp. 387-403, 1977.

[51] C.-L. Chen and S.-C. Wang, "Branch-and-bound scheduling for thermal generating units," Energy Conversion, IEEE Transactions on, vol. 8, pp. 184-189, 1993.

[52] W. L. Snyder Jr, H. D. Powell Jr, and J. C. Rayburn, "Dynamic programming approach to unit commitment," Power Systems, IEEE Transactions on, vol. 2, pp. 339-348, 1987.

[53] S. Virmani, E. C. Adrian, K. Imhof, and S. Mukherjee, "Implementation of a Lagrangian relaxation based unit commitment problem," Power Systems, IEEE Transactions on, vol. 4, pp. 1373-1380, 1989.

[54] M. Carrión and J. M. Arroyo, "A computationally efficient mixed-integer linear formulation for the thermal unit commitment problem," Power Systems, IEEE Transactions on, vol. 21, pp. 1371-1378, 2006.

[55] X. Guan, Q. Zhai, and A. Papalexopoulos, "Optimization based methods for unit commitment: Lagrangian relaxation versus general mixed integer programming," in Power Engineering Society General Meeting, 2003, IEEE, 2003.

[56] D. Das, D. Kothari, and A. Kalam, "Simple and efficient method for load flow solution of radial distribution networks," International Journal of Electrical Power & Energy Systems, vol. 17, pp. 335-346, 1995.

[57] H. Brown, G. Carter, H. Happ, and C. Person, "Power flow solution by impedance matrix iterative method," Power Apparatus and Systems, IEEE Transactions on, vol. 82, pp. 1-10, 1963.

[58] N. M. Peterson, W. F. Tinney, and D. W. Bree Jr, "Iterative linear AC power flow solution for fast approximate outage studies," Power Apparatus

and Systems, IEEE Transactions on, pp. 2048-2056, 1972.

[59] N. NERC, "Operating Manual,“Glossary of Terms Used in Reliability Standards”,[en línea]," ed.

[60] M. Parvania and M. Fotuhi-Firuzabad, "Demand response scheduling by stochastic SCUC," Smart Grid, IEEE Transactions on, vol. 1, pp. 89-98, 2010.

[61] E. Muljadi, M. Singh, and V. Gevorgian, "Fixed-speed and variable-slip wind turbines providing spinning reserves to the grid," in IEEE Power and Energy Society General Meeting, Vancouver, Canada, 2013.

[62] E. Muljadi, V. Gevorgian, M. Singh, and S. Santoso, Understanding inertial and frequency response of wind power plants: IEEE, 2012.

[63] C. Pradhan and C. Bhende, "Adaptive deloading of stand-alone wind farm for primary frequency control," Energy Systems, vol. 6, pp. 109-127, 2015.

[64] F. D. Galiana, F. Bouffard, J. M. Arroyo, and J. F. Restrepo, "Scheduling and pricing of coupled energy and primary, secondary, and tertiary reserves," Proceedings of the IEEE, vol. 93, pp. 1970-1983, 2005.

[65] S.-J. Deng and L. Xu, "Mean-risk efficient portfolio analysis of demand response and supply resources," Energy, vol. 34, pp. 1523-1529, 2009.

[66] J. Dupačová, N. Gröwe-Kuska, and W. Römisch, "Scenario reduction in stochastic programming," Mathematical programming, vol. 95, pp. 493-511, 2003.

[67] K.-B. Kwon, H.-G. Park, J.-K. Lyu, Y.-C. Kim, and J.-K. Park, "Dynamic Reserve Estimating Method with Consideration of Uncertainties in Supply and Demand," The Transactions of The Korean Institute of Electrical Engineers, vol. 62, pp. 1495-1504, 2013.

[68] H. Park, J. Kim, J. Yi, and J.-K. Park, "Impact of dynamic thermal line rating on generation scheduling," Energy Systems Conference, 2016.

Appendix A. Heat Balance Equations and Simulation Conditions for Case Study

The values of wind direction factor (K_{angle}), air density (ρ_f), absolute viscosity (μ_f), and thermal conductivity of air (k_f) must be known to calculate the convective heat loss (q_c). In Appendix A, equations are defined for these parameters. At first, K_{angle} can be determined as follows:

$$K_{angle} = 1.194 - \cos(\phi) + 0.194 \cdot \cos(2\phi) + 0.368 \cdot \sin(2\phi) \quad \text{(A-1)}$$

where ϕ represents the angle between the transmission line axis and wind direction. The complement of the angle ϕ, expressed as β[36], can be used to express the wind direction factor as well. In this case, K_{angle} is given by

$$K_{angle} = 1.194 - \sin(\beta) - 0.194 \cdot \cos(2\beta) + 0.368 \cdot \sin(2\beta) \quad \text{(A-2)}$$

On the other hand, air properties such as ρ_f, μ_f and k_f can be defined and calculated with the following equations.

$$\rho_f = \frac{1.293 - 1.525 \cdot 10^{-4} \cdot H_e + 6.379 \cdot 10^{-9} \cdot H_e^2}{1 + 0.00367 \cdot T_{film}} \quad \text{(A-3)}$$

$$H_c = \arcsin[\cos(Lat) \cdot \cos(\delta') \cdot \cos(\omega) + \sin(Lat) \cdot \sin(\delta')] \quad \text{(A-4)}$$

$$\delta' = 23.46 \cdot \sin\left[\frac{284 + N_{days}}{365} \cdot 360\right] \quad \text{(A-5)}$$

$$\mu_f = \frac{1.458 \cdot 10^{-6} \cdot (T_{film} + 273)^{1.5}}{T_{film} + 383.4} \quad \text{(A-6)}$$

[36] β represents the angle between the perpendicular to the line axis and wind direction.

$$k_f = 2.424 \cdot 10^{-2} + 7.477 \cdot 10^{-5} \cdot T_{film} - 4.407 \cdot 10^{-9} \cdot T_{film}^2 \quad \text{(A-7)}$$

$$T_{film} = \frac{T_c + T_a}{2} \quad \text{(A-8)}$$

where, H_c represents the solar altitude and is given by equation (A-4). In the equation (A-4), w and Lat represent the hour angle relative to noon and the degrees of latitude, respectively. δ' is solar declination, which can be calculated by means of equation (A-5)[37]. Both μ_f and k_f depend on the temperature of the boundary layer (T_{film}) and they can be calculated as shown in equation (A-6) and (A-7).

For the calculation of the solar heat gain (q_s), the effective angle of incidence of the sun's rays (θ') should be determined as shown in the (A-8).

$$\theta' = \arccos[\cos(H_c) \cdot \cos(Z_c - Z_l)] \quad \text{(A-8)}$$

As seen in (A-8), the azimuth of the line (Z_l), azimuth of the sun (Z_c) and related solar azimuth variable χ are used to find the effective angle of the sun's rays.

$$Z_c = C + \arctan(\chi) \quad \text{(A-9)}$$

$$\chi = \frac{\sin(\omega)}{\sin(Lat) \cdot \cos(\omega) - \cos(Lat) - \tan(\delta')} \quad \text{(A-10)}$$

The solar heat intensity (Q_s) may be adjusted to reflect the elevation effects. In this case, the solar altitude correction factor (K_{solar}) is multiplied by Q_s, to determine the solar heat intensity corrected value(Q_{se}). This can be represented as

[37] N_{days} is the day of the year. For example, February 26 = 57

follows:

$$Q_{se} = K_{solar} Q_s \tag{A-11}$$

Table A.1 Identification of letter symbols and simulation conditions for case study[35]

Symbol	Description	SI units	Used value for case study
$R(T_{avg})$	Resistance of conductor at temperature, T_{avg}	Ω/m	–
D_0	Outside diameter of conductor	m	0.0281
ρ_f	Air density	kg/m^3	1.029
s_t	Wind velocity	m/s	SLR: 0.5m/s SLR*: 0m/s
μ_f	Absolute viscosity of air	kg/m-s	2.04E-05
K_{angle}	Wind direction factor	–	1
k_f	Thermal conductivity of air	W/(m·°C)	0.0295
T_c	Conductor temperature	°C	–
T_a	Ambient air temperature	°C	40
ε	Emissivity	–	0.8
α	Absorptivity	–	0.8
Q_{se}	Heat flux density corrected for the elevation	W/m^2	**
Q_s	Heat flux density	W/m^2	**
θ'	Effective angle of incidence of the sun's ray	deg	**
A'	Projected area of the conductor	m^2/linear m	0.0281
$R(T_{high})$	Resistance of conductor at high average temperature, T_{high}	Ω/m	8.69E-08
$R(T_{low})$	Resistance of conductor at low average temperature, T_{low}	Ω/m	7.28E-08

ϕ	Angle between the transmission line axis and wind direction	deg	**
β	Angle between the perpendicular to the line axis and wind direction	deg	**
H_e	Elevation of conductor above sea level	m	**
T_{film}	Temperature of the boundary layer	°C	**
H_c	Solar altitude	Deg	**
w	Hour angle relative to noon	Deg	**
Lat	Degrees of Latitude	Deg	**
δ'	Solar Declination	deg	**
Z_l	Azimuth of the line	deg	**
Z_c	Azimuth of the sun	deg	**
χ	Solar azimuth variable	–	**
K_{solar}	Solar altitude correction factor	–	**
N_{days}	Day of the year	–	**

*: Transfer limit is recalculated based on the 0 m/s of wind speed. (Refer p82)

**: When calculating the solar heat gain, the peak values in the historical data of year 2015 are used for case study. This data can be downloaded from the United States Bureau of Reclamation website.

Appendix B. Stationary Scenarios Simulation

In Appendix B, the method of stationary process simulation without presample observations is included. As described in Chapter 3, wind speed uncertainty is represented by the ARMA (3, 2) model. Figure B.1 represents the 2000 scenarios from the ARMA (3, 2) model whose parameters are the same values used in the case study.

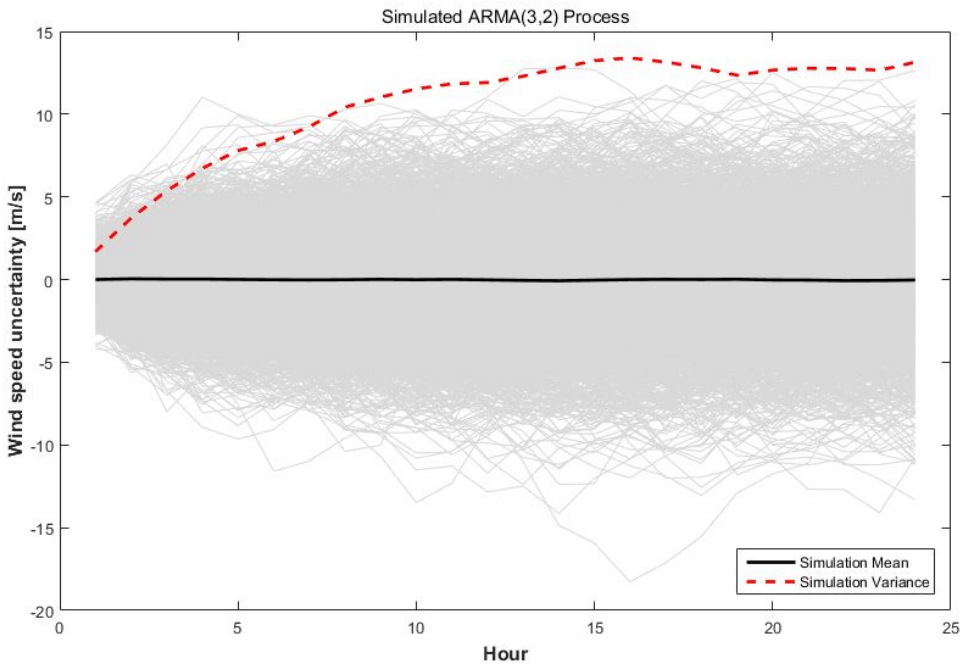

Figure B.1 2000 scenarios of wind speed uncertainty

As shown in the figure, the simulation mean is constant over time. This result satisfies the characteristics of a stationary model, but simulation variance is not constant over time. Generating scenarios without presample observations induces transient effects, and the non-constant variance issue arises. To nullify the transient

effects, an oversampling technique is adopted in this dissertation. More specifically, more than 24 scenarios are generated, and the first part of the samples are discarded.[38] The result of the 2000 samples of the ARMA (3, 2) process with oversampling is given in Figure B.2. As evident in the figure, it can be confirmed that generated samples with oversampling are consistent with the definition of a stationary stochastic model.

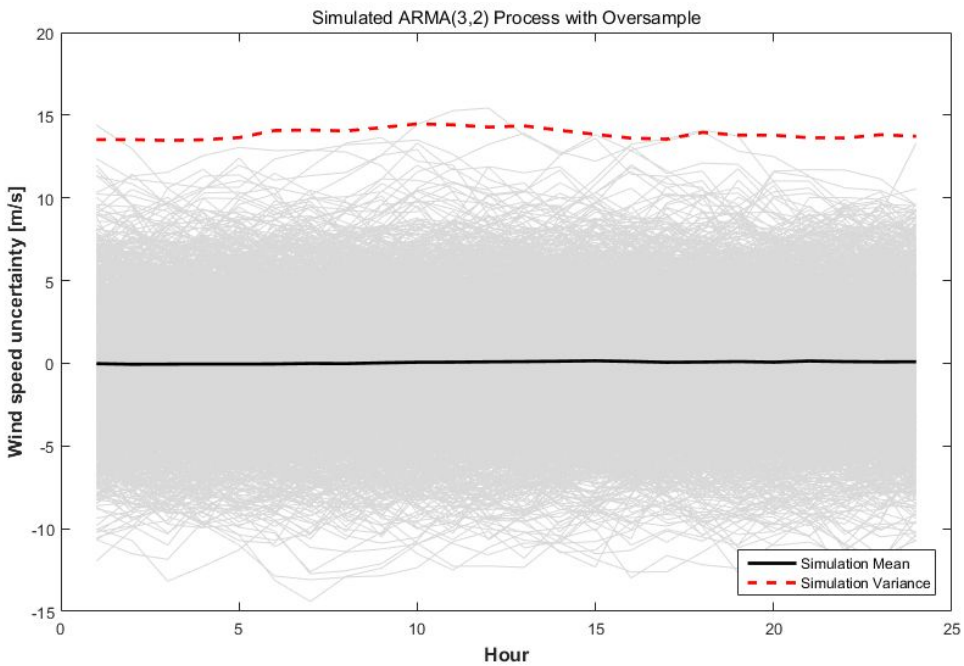

Figure B.2 2000 scenarios of wind speed uncertainty (oversample)

[38] The scheduling horizon for the problem was 24 h in this study.

Appendix C. Scenarios Representing Uncertainty of Net Load

Table C.1 Scenarios for uncertainty of net load at hour 1–12 (MW)

	Hour 1	Hour 2	Hour 3	Hour 4	Hour 5	Hour 6	Hour 7	Hour 8	Hour 9	Hour 10	Hour 11	Hour 12	Probability
Scenario A	-1.23	-12.52	-15.35	-16.88	-21.78	-21.35	-19.82	-19.65	-26.14	-21.58	-23.85	-27.31	0.0685
Scenario B	11.40	8.01	3.09	-0.79	-3.84	-2.87	-2.63	2.08	7.04	14.38	20.64	26.25	0.096
Scenario C	8.26	6.69	8.44	8.87	5.81	6.89	4.96	10.95	13.82	10.11	17.51	19.67	0.1795
Scenario D	-19.98	-33.05	-45.64	-28.68	-30.34	-30.21	-24.30	-23.61	-25.78	-31.98	-20.24	-17.75	0.0555
Scenario E	5.70	4.25	3.09	2.40	3.24	5.46	3.89	2.54	-0.39	0.30	4.93	8.10	0.344
Scenario F	11.21	13.76	16.58	18.92	16.59	17.60	20.10	23.78	30.89	35.69	39.00	41.30	0.041
Scenario G	-34.26	-29.92	-45.47	-33.16	-21.16	-16.37	-13.86	-7.75	4.27	8.96	11.52	13.70	0.0355
Scenario H	8.78	6.97	3.36	1.90	0.27	-0.25	-0.68	-4.36	-6.40	-9.40	-14.33	-14.67	0.14
Scenario I	8.86	4.03	-8.99	-21.37	-36.33	-40.21	-44.60	-38.34	-38.49	-72.75	-79.05	-75.46	0.02
Scenario J	9.20	10.23	11.10	11.43	7.28	2.19	-0.01	1.09	1.20	-1.24	-2.65	-4.25	0.02
Sum													1

Table C.2 Scenarios for uncertainty of net load at hour 13–24 (MW)

	Hour 13	Hour 14	Hour 15	Hour 16	Hour 17	Hour 18	Hour 19	Hour 20	Hour 21	Hour 22	Hour 23	Hour 24	Probability
Scenario A	-31.62	-37.35	-41.49	-41.86	-40.45	-38.98	-46.31	-47.07	-44.91	-41.29	-30.89	-29.45	0.0685
Scenario B	31.08	31.49	21.74	24.94	12.21	15.27	40.62	38.11	37.35	45.41	42.80	44.44	0.096
Scenario C	17.48	18.39	20.24	22.74	22.14	24.56	26.36	27.82	24.79	24.68	21.73	14.12	0.1795
Scenario D	-17.76	-9.41	-5.62	-6.45	-4.77	3.14	2.96	-2.06	-6.70	-6.53	-6.65	-12.34	0.0555
Scenario E	-0.51	1.46	4.33	1.90	1.53	-4.94	2.50	-1.98	1.06	-0.93	3.06	-1.09	0.344
Scenario F	42.80	43.67	46.52	44.95	44.59	47.57	48.56	51.37	50.06	49.61	45.94	47.90	0.041
Scenario G	16.02	16.07	17.67	17.92	21.18	22.03	24.90	25.62	26.81	24.22	23.51	24.56	0.0355
Scenario H	-18.31	-20.56	-23.31	-24.51	-25.26	-22.20	-20.37	-21.82	-25.38	-27.98	-29.07	-27.61	0.14
Scenario I	-75.33	-64.32	-83.67	-65.78	-80.44	-71.93	-72.10	-53.82	-42.01	-38.57	-35.26	-37.99	0.02
Scenario J	-6.20	-15.78	-33.77	-47.61	-49.68	-68.71	-70.35	-74.91	-72.17	-63.87	-73.16	-78.92	0.02
Sum													1

Appendix D. IEEE 118-bus System Data

Table D.1 Forecasted load and wind speed for IEEE 118-bus system

Hour [h]	Demand [MW]	Wind Speed [m/s]
1	4200	4.0956
2	3960	4.1277
3	3480	4.0665
4	2400	4.1453
5	3000	4.0894
6	3600	4.2028
7	4200	4.1654
8	4680	4.1420
9	4920	3.9139
10	5280	3.8928
11	5340	3.9273
12	5040	4.1856
13	4800	4.3195
14	4560	4.5317
15	5280	4.7597
16	5400	5.2038
17	5100	5.4515
18	5340	5.6418
19	5640	5.5059
20	5880	5.0796
21	6000	4.6573
22	5400	4.3370
23	5220	3.9530
24	4920	3.8731

Table D.2 Generator data for IEEE 118-bus system

Gen No.	Bus No.	a [MBtu]	b [MBtu/ MWh]	c [MBtu/ MW^2h]	Pmax [MW]	Pmin [MW]	Qmax [MVar]	Qmin [MVar]	Init Hour [h]	Min Off [h]	Min On [h]	Ramp [MW/h]	Start Up [MBtu]	Fuel Price [$/MBtu]
1	4	31.67	26.2438	0.069663	30	5	300	-300	1	1	1	15	40	1
2	6	31.67	26.2438	0.069663	30	5	50	-13	1	1	1	15	40	1
3	8	31.67	26.2438	0.069663	30	5	300	-300	1	1	1	15	40	1
4	10	6.78	12.8875	0.010875	300	150	200	-147	8	8	8	150	440	1
5	12	6.78	12.8875	0.010875	300	100	120	-35	8	8	8	150	110	1
6	15	31.67	26.2438	0.069663	30	10	30	-10	1	1	1	15	40	1
7	18	10.15	17.82	0.0128	100	25	50	-16	5	5	5	50	50	1
8	19	31.67	26.2438	0.069663	30	5	24	-8	1	1	1	15	40	1
9	24	31.67	26.2438	0.069663	30	5	300	-300	1	1	1	15	40	1
10	25	6.78	12.8875	0.010875	300	100	140	-47	8	8	8	150	100	1
11	26	32.96	10.76	0.003	350	100	1000	-1000	8	8	8	175	100	1
12	27	31.67	26.2438	0.069663	30	8	300	-300	1	1	1	15	40	1
13	31	31.67	26.2438	0.069663	30	8	300	-300	1	1	1	15	40	1
14	32	10.15	17.82	0.0128	100	25	42	-14	5	5	5	50	50	1
15	34	31.67	26.2438	0.069663	30	8	24	-8	1	1	1	15	40	1
16	36	10.15	17.82	0.0128	100	25	24	-8	5	5	5	50	50	1
17	40	31.67	26.2438	0.069663	30	8	300	-300	1	1	1	15	40	1

18	42	31.67	26.2438	0.069663	30	8	300	-300	1	1	1	15	40	1
19	46	10.15	17.82	0.0128	100	25	100	-100	5	5	5	50	59	1
20	49	28	12.3299	0.002401	250	50	210	-85	8	8	8	125	100	1
21	54	28	12.3299	0.002401	250	50	300	-300	8	8	8	125	100	1
22	55	10.15	17.82	0.0128	100	25	23	-8	5	5	5	50	50	1
23	56	10.15	17.82	0.0128	100	25	15	-8	5	5	5	50	50	1
24	59	39	13.29	0.0044	200	50	180	-60	10	8	8	100	100	1
25	61	39	13.29	0.0044	200	50	300	-100	10	8	8	100	100	1
26	62	10.15	17.82	0.0128	100	25	20	-20	5	5	5	50	50	1
27	65	64.16	8.3391	0.01059	420	100	200	-67	10	10	10	210	250	1
28	66	64.16	8.3391	0.01059	420	100	200	-67	10	10	10	210	250	1
29	69	6.78	12.8875	0.010875	300	80	99999	-99999	10	8	8	150	100	1
30	70	74.33	15.4708	0.045923	80	30	32	-10	4	4	4	40	45	1
31	72	31.67	26.2438	0.069663	30	10	100	-100	1	1	1	15	40	1
32	73	31.67	26.2438	0.069663	30	5	100	-100	1	1	1	15	40	1
33	74	17.95	37.6968	0.028302	20	5	9	-6	1	1	1	10	30	1
34	76	10.15	17.82	0.0128	100	25	23	-8	5	5	5	50	50	1
35	77	10.15	17.82	0.0128	100	25	70	-20	5	5	5	50	50	1
36	80	6.78	12.8875	0.010875	300	150	280	-165	10	8	8	150	440	1
37	82	10.15	17.82	0.0128	100	25	9900	-9900	5	5	5	50	50	1

38	85	31.67	26.2438	0.069663	30	10	23	-8	1	1	1	15	40	1
39	87	32.96	10.76	0.003	300	100	1000	-100	10	8	8	150	440	1
40	89	6.78	12.8875	0.010875	200	50	300	-210	10	8	8	100	400	1
41	90	17.95	37.6968	0.028302	20	8	300	-300	1	1	1	10	30	1
42	91	58.81	22.9423	0.009774	50	20	100	-100	1	1	1	25	45	1
43	92	6.78	12.8875	0.010875	300	100	9	-3	8	8	8	150	100	1
44	99	6.78	12.8875	0.010875	300	100	100	-100	8	8	8	150	100	1
45	100	6.78	12.8875	0.010875	300	100	155	-50	8	8	8	150	110	1
46	103	17.95	37.6968	0.028302	20	8	40	-15	1	1	1	10	30	1
47	104	10.15	17.82	0.0128	100	25	23	-8	5	5	5	50	50	1
48	105	10.15	17.82	0.0128	100	25	23	-8	5	5	5	50	50	1
49	107	17.95	37.6968	0.028302	20	8	200	-200	1	1	1	10	30	1
50	110	58.81	22.9423	0.009774	50	25	23	-8	2	2	2	25	45	1
51	111	10.15	17.82	0.0128	100	25	1000	-100	5	5	5	50	50	1
52	112	10.15	17.82	0.0128	100	25	1000	-100	5	5	5	50	50	1
53	113	10.15	17.82	0.0128	100	25	200	-100	5	5	5	50	50	1
54	116	58.81	22.9423	0.009774	50	25	1000	-1000	2	2	2	25	45	1

Table D.3 Load data for IEEE 118-bus system

Bus No.	Ratio	Bus No.	Ratio
1	0.0145	2	0.0057
3	0.0111	4	0.0085
6	0.0148	7	0.0054
11	0.0199	12	0.0134
13	0.0097	14	0.0040
15	0.0256	16	0.0071
17	0.0031	18	0.0171
19	0.0128	20	0.0051
21	0.0040	22	0.0028
23	0.0020	27	0.0176
28	0.0048	29	0.0068
31	0.0122	32	0.0168
33	0.0065	34	0.0168
35	0.0094	36	0.0088
39	0.0072	40	0.0054
41	0.0099	42	0.0099
43	0.0048	44	0.0043
45	0.0142	46	0.0075
47	0.0091	48	0.0054
49	0.0233	50	0.0046
51	0.0046	52	0.0048
53	0.0062	54	0.0303
55	0.0169	56	0.0225
57	0.0032	58	0.0032
59	0.0742	60	0.0209
62	0.0206	66	0.0104
67	0.0075	70	0.0177
74	0.0182	75	0.0126
76	0.0182	77	0.0163
78	0.0190	79	0.0104
80	0.0348	82	0.0145
83	0.0054	84	0.0029
85	0.0064	86	0.0056
88	0.0129	90	0.0209
92	0.0174	93	0.0032

94	0.0080	95	0.0113
96	0.0102	97	0.0040
98	0.0091	100	0.0099
101	0.0059	102	0.0013
103	0.0062	104	0.0102
105	0.0083	106	0.0115
107	0.0075	108	0.0005
109	0.0021	110	0.0104
112	0.0067	114	0.0023
115	0.0063	117	0.0057
118	0.0088		

Table D.4 Transmission line data for IEEE 118-bus system

Line No.	From	To	R [pu]	X [pu]	C [pu]	Rate [MVA]
1	1	2	0.0303	0.0999	0.0254	133.7
2	1	3	0.0129	0.0424	0.01082	133.7
3	4	5	0.00176	0.00798	0.0021	668.5
4	3	5	0.0241	0.108	0.0284	133.7
5	5	6	0.0119	0.054	0.01426	133.7
6	6	7	0.00459	0.0208	0.0055	133.7
7	8	9	0.00244	0.0305	1.162	668.5
8	8	5	0	0.0267	0	668.5
9	9	10	0.00258	0.0322	1.23	668.5
10	4	11	0.0209	0.0688	0.01748	133.7
11	5	11	0.0203	0.0682	0.01738	133.7
12	11	12	0.00595	0.0196	0.00502	133.7
13	2	12	0.0187	0.0616	0.01572	133.7
14	3	12	0.0484	0.16	0.0406	133.7
15	7	12	0.00862	0.034	0.00874	133.7
16	11	13	0.02225	0.0731	0.01876	133.7
17	12	14	0.0215	0.0707	0.01816	133.7
18	13	15	0.0744	0.2444	0.06268	133.7
19	14	15	0.0595	0.195	0.0502	133.7
20	12	16	0.0212	0.0834	0.0214	133.7

21	15	17	0.0132	0.0437	0.0444	668.5
22	16	17	0.0454	0.1801	0.0466	133.7
23	17	18	0.0123	0.0505	0.01298	133.7
24	18	19	0.01119	0.0493	0.01142	133.7
25	19	20	0.0252	0.117	0.0298	133.7
26	15	19	0.012	0.0394	0.0101	133.7
27	20	21	0.0183	0.0849	0.0216	133.7
28	21	22	0.0209	0.097	0.0246	133.7
29	22	23	0.0342	0.159	0.0404	133.7
30	23	24	0.0135	0.0492	0.0498	133.7
31	23	25	0.0156	0.08	0.0864	668.5
32	26	25	0	0.0382	0	668.5
33	25	27	0.0318	0.163	0.1764	668.5
34	27	28	0.01913	0.0855	0.0216	133.7
35	28	29	0.0237	0.0943	0.0238	133.7
36	30	17	0	0.0388	0	668.5
37	8	30	0.00431	0.0504	0.514	133.7
38	26	30	0.00799	0.086	0.908	668.5
39	17	31	0.0474	0.1563	0.0399	133.7
40	29	31	0.0108	0.0331	0.0083	133.7
41	23	32	0.0317	0.1153	0.1173	133.7
42	31	32	0.0298	0.0985	0.0251	133.7
43	27	32	0.0229	0.0755	0.01926	133.7
44	15	33	0.038	0.1244	0.03194	133.7
45	19	34	0.0752	0.247	0.0632	133.7
46	35	36	0.00224	0.0102	0.00268	133.7
47	35	37	0.011	0.0497	0.01318	133.7
48	33	37	0.0415	0.142	0.0366	133.7
49	34	36	0.00871	0.0268	0.00568	133.7
50	34	37	0.00256	0.0094	0.00984	668.5
51	38	37	0	0.0375	0	668.5
52	37	39	0.0321	0.106	0.027	133.7
53	37	40	0.0593	0.168	0.042	133.7
54	30	38	0.00464	0.054	0.422	133.7
55	39	40	0.0184	0.0605	0.01552	133.7
56	40	41	0.0145	0.0487	0.01222	133.7
57	40	42	0.0555	0.183	0.0466	133.7

58	41	42	0.041	0.135	0.0344	133.7
59	43	44	0.0608	0.2454	0.06068	133.7
60	34	43	0.0413	0.1681	0.04226	133.7
61	44	45	0.0224	0.0901	0.0224	133.7
62	45	46	0.04	0.1356	0.0332	133.7
63	46	47	0.038	0.127	0.0316	133.7
64	46	48	0.0601	0.189	0.0472	133.7
65	47	49	0.0191	0.0625	0.01604	133.7
66	42	49	0.0715	0.323	0.086	133.7
67	42	49	0.0715	0.323	0.086	133.7
68	45	49	0.0684	0.186	0.0444	133.7
69	48	49	0.0179	0.0505	0.01258	133.7
70	49	50	0.0267	0.0752	0.01874	133.7
71	49	51	0.0486	0.137	0.0342	133.7
72	51	52	0.0203	0.0588	0.01396	133.7
73	52	53	0.0405	0.1635	0.04058	133.7
74	53	54	0.0263	0.122	0.031	133.7
75	49	54	0.073	0.289	0.0738	133.7
76	49	54	0.0869	0.291	0.073	133.7
77	54	55	0.0169	0.0707	0.0202	133.7
78	54	56	0.00275	0.00955	0.00732	133.7
79	55	56	0.00488	0.0151	0.00374	133.7
80	56	57	0.0343	0.0966	0.0242	133.7
81	50	57	0.0474	0.134	0.0332	133.7
82	56	58	0.0343	0.0966	0.0242	133.7
83	51	58	0.0255	0.0719	0.01788	133.7
84	54	59	0.0503	0.2293	0.0598	133.7
85	56	59	0.0825	0.251	0.0569	133.7
86	56	59	0.0803	0.239	0.0536	133.7
87	55	59	0.04739	0.2158	0.05646	133.7
88	59	60	0.0317	0.145	0.0376	133.7
89	59	61	0.0328	0.15	0.0388	133.7
90	60	61	0.00264	0.0135	0.01456	668.5
91	60	62	0.0123	0.0561	0.01468	133.7
92	61	62	0.00824	0.0376	0.0098	133.7
93	63	59	0	0.0386	0	668.5
94	63	64	0.00172	0.02	0.216	668.5

95	64	61	0	0.0268	0	668.5
96	38	65	0.00901	0.0986	1.046	668.5
97	64	65	0.00269	0.0302	0.38	668.5
98	49	66	0.018	0.0919	0.0248	668.5
99	49	66	0.018	0.0919	0.0248	668.5
100	62	66	0.0482	0.218	0.0578	133.7
101	62	67	0.0258	0.117	0.031	133.7
102	65	66	0	0.037	0	668.5
103	66	67	0.0224	0.1015	0.02682	133.7
104	65	68	0.00138	0.016	0.638	668.5
105	47	69	0.0844	0.2778	0.07092	133.7
106	49	69	0.0985	0.324	0.0828	133.7
107	68	69	0	0.037	0	668.5
108	69	70	0.03	0.127	0.122	668.5
109	24	70	0.00221	0.4115	0.10198	133.7
110	70	71	0.00882	0.0355	0.00878	133.7
111	24	72	0.0488	0.196	0.0488	133.7
112	71	72	0.0446	0.18	0.04444	133.7
113	71	73	0.00866	0.0454	0.01178	133.7
114	70	74	0.0401	0.1323	0.03368	133.7
115	70	75	0.0428	0.141	0.036	133.7
116	69	75	0.0405	0.122	0.124	668.5
117	74	75	0.0123	0.0406	0.01034	133.7
118	76	77	0.0444	0.148	0.0368	133.7
119	69	77	0.0309	0.101	0.1038	133.7
120	75	77	0.0601	0.1999	0.04978	133.7
121	77	78	0.00376	0.0124	0.01264	133.7
122	78	79	0.00546	0.0244	0.00648	133.7
123	77	80	0.017	0.0485	0.0472	668.5
124	77	80	0.0294	0.105	0.0228	668.5
125	79	80	0.0156	0.0704	0.0187	133.7
126	68	81	0.00175	0.0202	0.808	668.5
127	81	80	0	0.037	0	668.5
128	77	82	0.0298	0.0853	0.08174	133.7
129	82	83	0.0112	0.03665	0.03796	133.7
130	83	84	0.0625	0.132	0.0258	133.7
131	83	85	0.043	0.148	0.0348	133.7

132	84	85	0.0302	0.0641	0.01234	133.7
133	85	86	0.035	0.123	0.0276	668.5
134	86	87	0.02828	0.2074	0.0445	668.5
135	85	88	0.02	0.102	0.0276	133.7
136	85	89	0.0239	0.173	0.047	133.7
137	88	89	0.0139	0.0712	0.01934	668.5
138	89	90	0.0518	0.188	0.0528	668.5
139	89	90	0.0238	0.0997	0.106	668.5
140	90	91	0.0254	0.0836	0.0214	133.7
141	89	92	0.0099	0.0505	0.0548	668.5
142	89	92	0.0393	0.1581	0.0414	668.5
143	91	92	0.0387	0.1272	0.03268	133.7
144	92	93	0.0258	0.0848	0.0218	133.7
145	92	94	0.0481	0.158	0.0406	133.7
146	93	94	0.0223	0.0732	0.01876	133.7
147	94	95	0.0132	0.0434	0.0111	133.7
148	80	96	0.0356	0.182	0.0494	133.7
149	82	96	0.0162	0.053	0.0544	133.7
150	94	96	0.0269	0.0869	0.023	133.7
151	80	97	0.0183	0.0934	0.0254	133.7
152	80	98	0.0238	0.108	0.0286	133.7
153	80	99	0.0454	0.206	0.0546	133.7
154	92	100	0.0648	0.295	0.0472	133.7
155	94	100	0.0178	0.058	0.0604	133.7
156	95	96	0.0171	0.0547	0.01474	133.7
157	96	97	0.0173	0.0885	0.024	133.7
158	98	100	0.0397	0.179	0.0476	133.7
159	99	100	0.018	0.0813	0.0216	133.7
160	100	101	0.0277	0.1262	0.0328	133.7
161	92	102	0.0123	0.0559	0.01464	133.7
162	101	102	0.0246	0.112	0.0294	133.7
163	100	103	0.016	0.0525	0.0536	668.5
164	100	104	0.0451	0.204	0.0541	133.7
165	103	104	0.0466	0.1584	0.0407	133.7
166	103	105	0.0535	0.1625	0.0408	133.7
167	100	106	0.0605	0.229	0.062	133.7
168	104	105	0.00994	0.0378	0.00986	133.7

169	105	106	0.014	0.0547	0.01434	133.7
170	105	107	0.053	0.183	0.0472	133.7
171	105	108	0.0261	0.0703	0.01844	133.7
172	106	107	0.053	0.183	0.0472	133.7
173	108	109	0.0105	0.0288	0.0076	133.7
174	103	110	0.03906	0.1813	0.0461	133.7
175	109	110	0.0278	0.0762	0.0202	133.7
176	110	111	0.022	0.0755	0.02	133.7
177	110	112	0.0247	0.064	0.062	133.7
178	17	113	0.00913	0.0301	0.00768	133.7
179	32	113	0.0615	0.203	0.0518	668.5
180	32	114	0.0135	0.0612	0.01628	133.7
181	27	115	0.0164	0.0741	0.01972	133.7
182	114	115	0.0023	0.0104	0.00276	133.7
183	68	116	0.00034	0.00405	0.164	668.5
184	12	117	0.0329	0.14	0.0358	133.7
185	75	118	0.0145	0.0481	0.01198	133.7
186	76	118	0.0164	0.0544	0.01356	133.7

Appendix E. Economic Dispatch Result of Modified 118-bus System

Table E.1 Dispatched volumes of generators with DLR (MW)

Units	Hours 1-24																							
	1	**2**	**3**	**4**	**5**	**6**	**7**	**8**	**9**	**10**	**11**	**12**	**13**	**14**	**15**	**16**	**17**	**18**	**19**	**20**	**21**	**22**	**23**	**24**
1	0	0	0	0	0	0	0	0	0	0	0	0	0	0	0	0	0	0	13	20	5	0	0	0
2	0	0	0	0	0	0	0	0	0	0	0	0	0	0	0	0	0	0	13	20	12	0	0	0
3	0	0	0	0	0	0	0	0	0	0	0	0	0	0	0	0	0	0	13	20	5	0	0	0
4	225	165	150	150	150	150	207	225	225	225	225	225	225	225	225	225	225	225	225	225	225	225	225	225
5	145	105	120	100	100	120	175	215	225	225	225	205	205	185	225	225	195	205	225	225	225	225	225	205
6	0	0	0	0	0	0	0	0	0	0	0	0	0	0	0	0	0	0	15	22	10	0	0	0
7	0	0	0	0	0	0	50	58	61	50	0	0	50	50	65	58	50	50	58	73	75	50	50	50
8	0	0	0	0	0	0	0	0	0	0	0	0	0	0	0	0	0	0	13	20	13	0	0	0
9	0	0	0	0	0	0	0	0	0	0	0	0	0	0	0	0	0	0	13	20	13	0	0	0
10	159	151	122	100	100	120	175	215	235	225	225	205	205	185	225	225	195	205	225	225	225	225	225	205
11	263	263	263	188	263	263	263	263	263	350	350	350	350	282	350	350	350	350	350	350	350	263	350	350
12	0	0	0	0	0	0	0	0	0	0	0	0	0	0	0	0	0	0	15	22	15	0	0	0
13	0	0	0	0	0	0	0	0	0	0	0	0	0	0	0	0	0	0	15	22	15	0	0	0
14	0	0	0	0	0	0	50	65	50	0	0	0	50	50	65	57.5	50	50	58	73	75	50	50	50
15	0	0	0	0	0	0	0	0	0	0	0	0	0	0	0	0	0	0	15	22	8	0	0	0

16	0	0	0	0	0	0	50	58	50	0	0	0	50	50	65	57.5	50	50	58	73	75	50	50	50
17	0	0	0	0	0	0	0	0	0	0	0	0	0	0	0	0	0	0	15	20	15	0	0	0
18	0	0	0	0	0	0	0	0	0	0	0	0	0	0	0	0	0	0	15	20	15	0	0	0
19	0	0	0	0	0	0	50	58	50	0	0	0	50	50	61	58	50	50	58	73	75	50	50	50
20	250	250	213	113	188	216	250	250	250	250	250	250	250	250	250	250	250	250	250	250	250	250	250	250
21	250	250	188	113	188	188	250	250	250	250	250	250	250	250	250	250	250	250	250	250	250	250	250	250
22	0	0	0	0	0	0	50	58	50	0	0	0	50	50	65	58	50	50	58	73	75	50	50	50
23	0	0	0	0	0	0	50	58	50	0	0	0	50	50	65	58	50	50	58	73	75	50	50	50
24	200	200	120	50	100	150	200	200	200	200	200	200	150	150	167	200	160	200	200	172	200	200	197	150
25	200	200	120	50	100	150	200	200	200	200	200	200	150	150	175	200	169	200	200	175	200	200	200	150
26	0	0	0	0	0	0	50	58	50	0	0	0	50	50	65	58	50	50	60	73	75	50	50	50
27	420	387	333	155	219	325	397	409	420	420	420	415	374	333	397	404	397	414	406	397	419	397	397	361
28	420	420	333	196	237	333	397	420	420	420	420	420	397	333	397	420	397	420	420	397	420	397	397	365
29	177	155	155	80	80	155	155	221	229	225	225	211	203	181	225	225	203	203	225	225	225	223	225	203
30	0	0	0	0	0	0	0	0	0	0	0	0	0	0	0	0	0	0	40	56	60	40	0	0
31	0	0	0	0	0	0	0	0	0	0	0	0	0	0	0	0	0	0	15	22	15	0	0	0
32	0	0	0	0	0	0	0	0	0	0	0	0	0	0	0	0	0	0	13	23	13	0	0	0
33	0	0	0	0	0	0	0	0	0	0	0	0	0	0	0	0	0	0	10	0	0	0	0	0
34	0	0	0	0	0	0	25	50	58	65	50	0	50	50	65	58	50	50	58	73	75	50	50	50
35	0	0	0	0	0	0	50	50	58	65	50	0	50	50	65	59	50	50	65	73	75	50	50	50
36	225	225	225	225	225	225	225	225	225	225	225	225	225	225	225	225	225	225	225	225	225	225	225	225
37	0	0	0	0	0	0	33	50	58	65	50	0	50	50	65	65	50	50	65	73	75	50	50	50

38	300	300	300	193	248	300	300	300	300	300	300	300	300	300	300	300	300	300	300	300	300	300	300	300
39	160	145	100	50	60	100	150	170	200	166	187	150	150	150	150	150	150	150	150	150	150	150	150	150
40	0	0	0	0	0	0	0	0	0	0	0	0	0	0	0	0	0	0	0	0	0	0	0	0
41	0	0	0	0	0	0	0	0	0	0	0	0	0	0	0	0	0	0	0	0	0	0	0	0
42	0	0	0	0	0	0	0	0	0	0	0	0	0	0	0	0	0	0	0	0	0	0	0	0
43	195	175	175	100	175	175	175	215	235	225	225	205	185	177	225	225	195	205	225	225	225	225	215	205
44	195	175	175	141	175	175	175	199	193	190	186	182	178	177	215	215	195	205	225	225	197	201	205	205
45	195	175	175	175	175	175	175	215	235	225	225	205	195	185	225	225	195	206	225	225	225	225	212	205
46	0	0	0	0	0	0	0	0	0	0	0	0	0	0	0	0	0	0	0	0	0	0	0	0
47	0	0	0	0	0	0	50	50	50	58	50	0	50	0	0	0	0	0	65	65	50	50	50	50
48	50	0	0	0	0	0	50	50	50	50	0	0	50	50	50	0	0	0	65	65	50	50	50	50
49	0	0	0	0	0	0	0	0	0	0	0	0	0	0	0	0	0	0	0	0	0	0	0	0
50	0	0	0	0	0	0	0	0	0	0	0	0	0	0	0	0	0	0	0	0	0	0	0	0
51	0	0	0	0	0	0	50	50	50	55	50	0	50	50	0	0	0	0	65	65	50	50	50	0
52	0	0	0	0	0	0	0	0	0	0	0	0	50	65	50	50	0	0	65	65	51	50	50	50
53	0	0	0	0	0	0	50	58	65	50	0	0	50	50	65	58	50	50	58	73	75	50	50	50
54	0	0	0	0	0	0	0	0	0	0	0	0	0	0	0	0	0	0	25	38	25	0	0	0

Table E.2 Dispatched volumes of generators with SLR (MW)

Units	Hours 1-24																							
	1	**2**	**3**	**4**	**5**	**6**	**7**	**8**	**9**	**10**	**11**	**12**	**13**	**14**	**15**	**16**	**17**	**18**	**19**	**20**	**21**	**22**	**23**	**24**
1	0	0	0	0	0	0	0	0	0	0	0	0	0	0	0	0	0	0	13	20	13	0	0	0
2	0	0	0	0	0	0	0	0	0	0	0	0	0	0	0	0	0	0	13	20	5	0	0	0
3	0	0	0	0	0	0	0	0	0	0	0	0	0	0	0	0	0	0	13	20	8	0	0	0
4	196	180	150	150	150	150	216	225	225	225	225	225	225	225	225	225	225	225	225	225	225	225	225	225
5	145	105	100	100	100	120		213	225	225	225	187	195	185	225	225	197	225	225	225	225	225	225	225
6	0	0	0	0	0	0	0	0	0	0	0	0	0	0	0	0	0	0	15	18	18	10	0	0
7	0	0	0	0	0	0	50	73	50	0	0	0	50	48	65	58	50	50	73	75	75	50	65	58
8	0	0	0	0	0	0	0	0	0	0	0	0	0	0	0	0	0	0	13	23	23	13	0	0
9	0	0	0	0	0	0	0	0	0	0	0	0	0	0	0	0	0	0	13	20	13	0	0	0
10	180	125	139	100	100	136	175	225	235	225	225	215	195	185	225	225	205	225	225	225	225	225	225	225
11	350	350	275	188	263	263	348	350	350	350	350	350	350	272	350	350	350	350	350	350	350	350	350	350
12	0	0	0	0	0	0	0	0	0	0	0	0	0	0	0	0	0	0	15	20	15	0	0	0
13	0	0	0	0	0	0	0	0	0	0	0	0	0	0	0	0	0	0	15	20	12	0	0	0
14	0	0	0	0	0	0	25	50	65	65	50	0	50	50	58	58	50	50	65	75	75	50	50	50
15	0	0	0	0	0	0	0	0	0	0	0	0	0	0	0	0	0	0	15	20	12	0	0	0
16	0	0	0	0	0	0	25	50	65	65	50	0	50	40	58	58	50	50	65	75	75	50	50	50
17	0	0	0	0	0	0	0	0	0	0	0	0	0	0	0	0	0	0	15	20	15	0	0	0
18	0	0	0	0	0	0	0	0	0	0	0	0	0	0	0	0	0	0	15	20	8	0	0	0

19	0	0	0	0	0	0	25	65	58	50	0	0	50	50	53	58	50	50	65	75	75	50	50	50
20	250	250	188	113	188	233	250	250	250	250	250	250	213	233	250	250	250	250	250	250	250	250	250	235
21	188	188	188	113	188	215	250	250	250	188	188	188	188	188	188	188	188	188	188	188	188	188	188	188
22	0	0	0	0	0	0	25	73	73	50	0	0	50	50	65	73	50	63	73	75	75	50	58	55
23	0	0	0	0	0	0	25	50	73	73	50	0	50	50	73	75	50	75	75	75	75	50	65	58
24	200	158	150	50	100	150	200	200	200	200	200	200	200	175	200	200	200	200	200	200	200	200	200	200
25	200	172	150	50	100	150	200	200	200	200	200	200	200	150	200	200	200	200	200	200	200	200	200	200
26	0	0	0	0	0	0	30	72	65	50	0	0	50	50	58	59	50	50	65	75	75	50	50	50
27	420	414	324	155	219	324	397	420	420	420	420	420	397	365	398	420	413	404	420	420	420	420	397	397
28	420	420	329	155	224	333	397	420	420	420	420	420	365	348	397	420	397	420	405	399	420	397	384	365
29	199	177	155	80	155	155	177	221	225	225	225	221	203	181	225	225	203	225	225	225	225	225	225	225
30	0	0	0	0	0	0	0	0	0	0	0	0	40	0	0	0	0	0	55	60	60	50	40	0
31	0	0	0	0	0	0	0	0	0	0	0	0	0	0	0	0	0	0	15	22	20	15	0	0
32	0	0	0	0	0	0	0	0	0	0	0	0	0	0	0	0	0	0	13	20	20	13	0	0
33	0	0	0	0	0	0	0	0	0	0	0	0	0	0	0	0	0	0	10	0	0	0	0	0
34	0	0	0	0	0	0	40	73	65	50	0	0	50	50	58	58	50	50	65	75	75	50	50	50
35	0	0	0	0	0	0	50	65	50	0	0	0	50	50	58	58	50	50	65	75	75	50	50	50
36	225	225	225	225	225	225	225	225	225	225	238	225	225	225	225	225	225	225	225	225	225	225	225	225
37	0	0	0	0	0	0	50	56	75	67	50	0	50	50	58	65	50	50	73	75	75	50	62	50
38	300	300	300	193	248	300	300	300	300	300	300	300	300	300	300	300	300	300	300	300	300	300	300	300
39	225	281	268	193	229	290	300	283	282	300	300	300	300	300	300	300	300	300	300	300	300	300	300	300
40	174	150	100	50	65	100	143	200	200	199	200	175	150	144	150	169	150	150	150	160	200	150	150	150

41	0	0	0	0	0	0	0	0	0	0	0	0	0	0	0	0	0	0	0	0	0	0	0	0
42	0	0	0	0	0	0	0	0	0	0	0	0	0	0	0	0	0	0	0	0	0	0	0	0
43	192	175	175	175	175	175	175	215	235	225	235	195	175	175	225	205	175	203	205	225	230	205	210	225
44	200	180	175	106	127	175	175	202	202	202	202	202	175	175	180	195	178	180	180	180	202	180	180	175
45	215	191	175	175	175	175	175	224	235	225	235	225	188	175	225	225	195	215	225	225	235	210	225	225
46	0	0	0	0	0	0	0	0	0	0	0	0	0	0	0	0	0	0	0	0	0	0	0	0
47	0	0	0	0	0	0	0	0	0	0	0	0	50	50	50	50	0	0	50	53	53	50	50	0
48	0	0	0	0	0	0	50	58	50	0	0	0	50	50	50	50	50	50	50	53	53	50	50	0
49	0	0	0	0	0	0	0	0	0	0	0	0	0	0	0	0	0	0	0	0	0	0	0	0
50	0	0	0	0	0	0	0	0	0	0	0	0	0	0	0	0	0	0	0	0	0	0	0	0
51	0	0	0	0	0	0	0	0	0	0	0	0	50	50	50	50	0	0	50	53	57	50	50	0
52	0	0	0	0	0	0	0	0	0	0	0	0	0	0	0	0	0	0	50	53	53	50	50	0
53	0	0	0	0	0	0	50	58	50	0	0	0	50	50	50	58	50	50	61	75	75	50	50	50
54	0	0	0	0	0	0	0	0	0	0	0	0	0	0	0	0	0	0	25	38	38	25	0	0

Appendix F. Case Study-Impact of Using TACSR

Recently, rather than Aluminum Conductor Steel Reinforced (ACSR), the application of new overhead lines, such as Thermal Resistant Aluminum Alloy Conductors Steel Reinforced (TACSR), is considered in power system planning. TACSR is very similar to a conventional ACSR, but zirconium is doped to aluminum alloy, which enables the line to maintain its electrical and mechanical properties above 150°C. Hence, SO can achieve stable operation at elevated temperatures. Table F.1 shows the expected operating cost of generation scheduling when TACSR is installed in the six-bus test system. The overall procedure for calculating the operating cost is identical to the procedure used in subchapter 5.1.

Table F.1 Comparison of DLR with SLR in generation scheduling (TACSR)

	Generation scheduling w/ DLR	Generation scheduling w/ SLR
Expected operating cost [$]	150,016.6	150,389.5
Cost savings [$]	626.5 (0.41%)	

As indicated in Table F.1, it can be confirmed that applying DLR into the generation scheduling can reduce the expected operating costs in the situation when TACSR replaces conventional ACSR. Although detailed and comprehensive work should be further conducted for the impact of TACSR on generation scheduling with DLR, it is plain that DLR can bring economic advantages regardless of the transmission line type.

Appendix G. Case Study-Impact of Wind Power Penetration Level

In order to analyze the impact of the wind power penetration level on the proposed method, the operating cost is calculated by varying the installed wind power generator capacity.[39] Because the purpose of this case study is to examine the relationship between wind power capacity and expected cost savings, only the results are summarized in Table G.1–Table G.3 [68].

Table G.1 Comparison of DLR with SLR in generation scheduling (no wind case)

	Generation scheduling w/ DLR	Generation scheduling w/ SLR
Expected operating cost [$]	150,284.0	150,499.5
Cost savings [$]	215.5 (0.14%)	

Table G.2 Comparison of DLR with SLR in generation scheduling (WPPL = 25%)

	Generation scheduling w/ DLR	Generation scheduling w/ SLR
Expected operating cost [$]	143,229.6	143,477.6
Cost savings [$]	248.0 (0.17%)	

[39] The result of this case study was presented at the "Energy Systems Conference" held in Westminster, London, UK on 14–15 June 2016.

Table G.3 Comparison of DLR with SLR in generation scheduling (WPPL = 50%)

	Generation scheduling w/ DLR	Generation scheduling w/ SLR
Expected operating cost [$]	136,150.3	136,472.1
Cost savings [$]	321.8 (0.23%)	

As indicated in the tables, in all cases, the expected operating cost apparently decreases if generation scheduling is conducted based on the DLR approach. It is interesting to note that the cost-effectiveness of the proposed method is more significant when high wind capacity penetrates the power system. The reason for this is that wind power spillage is definitely reduced in the DLR case, and accordingly, this impact is enhanced for higher wind power penetration levels.

초 록

풍력발전을 포함한 계통에서 동적송전용량을 고려한 확률론적 발전계획 수립 방안

박 현 곤
전기·컴퓨터공학부
공과대학원
서울대학교

친환경적으로 에너지를 생산 할 수 있는 신재생 발전자원의 도입이 전세계적으로 활발히 이루어지고 있다. 하지만, 풍력발전과 같은 신재생 발전자원은 출력의 정확한 예측이 어렵고, 이는 전력계통 운영에 있어 단기적인 공급력 부족을 초래할 수 있다. 또한, 지속적인 부하의 증가와 충분치 못한 송전설비는 송전 혼잡, 발전기의 재급전, 풍력발전량의 강제적 감축 등의 새로운 문제를 야기한다. 이러한 이유로 전력계통의 신뢰도를 적정한 수준으로 유지시킬 수 있는 운영 예비력 양을 산정하는 것과 더불어 기존의 송전설비를 충분하게 활용하는 것의 중요성이 대두되고 있다.

본 학위논문에서는 수요자원과 풍력발전의 deloaded control을 예

비력 자원으로 고려하여 전일 발전계획을 수립하는 방법을 제안한다. 전일 발전계획 수립 시, 송전선로에 최대로 흐를 수 있는 용량은 정적송전용량(Static Line Rating)이 아닌 동적송전용량(Dynamic Line Rating)을 기준으로 하여 계산하였다. 이와 같은 동적송전용량을 통한 전일 발전계획의 수립 시 계통운영자는 동적송전용량의 산정에 수반되는 새로운 불확실성 문제에 직면한다. 본 논문에서는 확률론적 최적화 기법을 활용하여 이러한 문제점을 해결하였다.

부하의 불확실성은 실제 과거자료를 분석한 후에 시계열 모형을 이용하여 모델링을 하였다. 한 시점의 값이 그 이전 시점의 결과로부터 영향을 받을 경우 자기회귀모형(AR: Auto-Regressive Model) 혹은 자기회귀이동평균모형(ARMA: Auto-Regressive Moving Average Model)을 이용하여 표현할 수 있는데, 본 학위논문에서는 차분을 한 자기회귀이동평균모형(ARIMA)을 이용하여 부하의 불확실성을 모델링 하였다. 추정된 모델의 정확성을 검증하기 위하여 Q-Q plot, 자기상관계수 함수, 부분 자기상관계수 함수를 이용하였다. 풍속의 불확실성 또한 시계열 모형인 자기회귀이동평균모형(ARMA)을 이용하여 모델링을 하였다. 전력계통의 발전기 고장과 송전선로 탈락은 마르코브 체인 모델로 표현하였다.

실제 전력계통에서 기동정지계획(unit commitment)을 포함한 발전계획 최적화 문제를 풀 때 사용하는 방법은 혼합 정수 선형 프로그래밍(mixed integer linear programming)이다. 본 학위논문에서도 혼합 정수 선형 프로그래밍을 이용하여 최적화 문제를 풀었는데, 동적송전용량

산정시 필요한 열평형 방정식(heat balance equation)과 조류 계산식(power flow equation)을 모두 선형화하여 최적화 문제를 정식화하였다. 한편, 기존의 연구에서 주로 사용하던 decoupled 조류 계산식은 동적송전용량을 고려한 발전계획 문제에 적용할 수 없기 때문에 조류 계산식을 선형화하는 새로운 방법을 제안하였다.

최적화 문제는 2단계로 구성된 모델(two-stage model)로 정식화하였다. 목적함수는 발전 비용, 예비력 비용, 수요자원 확보 비용과 부하차단비용의 합이며 발전기의 기동정지상태(on/off state)와 예비력 확보량, 수요자원 계약량 등을 결정변수로 갖는다. 이 때, 각 발전기들의 제약조건(증감발율 제약, 최소기동/정지 시간 제약, 출력제약)과 전력계통 제약조건(유효전력과 무효전력의 수급균형 제약, 예비력 제약, 조류 제약)을 모두 고려하여 최적화 문제를 구성하였다. 또한, 전력계통의 신뢰도를 평가하기 위하여 각 모선의 공급지장전력량 기대치(expected energy not served)를 산출하였다.

제안하는 발전계획 방법의 적용가능성을 검증하기 위하여 대규모 풍력단지를 포함시킨 6 모선 계통과 수정된 IEEE 118 모선 계통을 대상으로 사례연구를 수행하였다. 사례연구 결과는 동적송전용량을 고려한 발전계획을 통하여 계통운영자가 기대운영비용 감소를 기대할 수 있음을 보여준다. 이러한 기대운영비용 감소는 송전설비를 충분하게 활용을 하여 비용 효율적인 발전기를 더 많이 사용하고, 연료비용이 발생하지 않는 풍력발전을 효과적으로 사용하였기 때문이라고 해석할 수 있다. 또한, 제안하는 발전계획 방법을 통하여 공급지장전력량 기대치가 감소하였고,

이는 동적송전용량의 사용으로 계통운영자가 더 큰 신뢰도 수준 하에서 계통운영을 할 수 있음을 나타낸다.

수요자원과 풍력발전의 deloaded control을 예비력 확보 방안으로 고려하여 발전계획을 수행한 사례연구는 기대운영비용을 추가적으로 감소시킬 수 있다는 것을 보여준다. 즉, 불확실성과 변동성이 큰 풍력발전이 대규모로 계통에 도입될 경우 전력계통 운영에 필요한 예비력 확보량이 증가하는데 일부 예비력을 수요자원이나 풍력발전을 통하여 확보하는 것이 효과적임을 확인 할 수 있다. 이러한 효과는 특히 풍력발전의 계통 수용률이 높을 경우에 더 큰 것을 확인 할 수 있다. 동적송전용량을 고려한 발전계획의 경우 새롭게 추가되는 제약조건과 더 복잡해진 조류 계산식으로 인하여 계산수행시간이 증가하지만, 그 증가분은 크지 않았다. 이는 기존의 혼합 정수 선형 프로그래밍 방법을 활용하여 최적화를 하였기 때문이라고 볼 수 있다.

주요어: 동적송전용량, 발전계획, 운영 예비력, 풍력발전, 불확실성, 전력시스템 운영
학 번: 2011-20848